

INEEL/EXT-01-00763

Revision 0

December 21, 2000

**Final Report
Column Tests to Study
the Transport of Plutonium
and Other Radioanuclides
in Sedimentary Interbed
at INEEL**

*Idaho National Engineering and Environmental Laboratory
Bechtel BWXT Idaho, LLC*



**Final Report
Column Tests to Study the Transport
of Plutonium and Other Radionuclides
in Sedimentary Interbed at INEEL**

**Robert J. Fjeld
John T. Coates
Alan W. Elzerman**

**Department of Environmental Engineering and Science
Clemson University**

Published December 21, 2000

**Idaho National Engineering and Environmental Laboratory
Environmental Restoration Program
Idaho Falls, Idaho 83415**

**Prepared under Subcontract No. K99-181044
for the
U.S. Department of Energy
Assistant Secretary for Environmental Management
Under DOE Idaho Operations Office
Contract DE-AC07-99ID13727**

Note: This document was produced for the Idaho National Engineering and Environmental Laboratory (INEEL) by an external subcontractor, and may not have been technically reviewed or edited to meet the INEEL publications standard.

FINAL REPORT

**COLUMN TESTS TO STUDY THE TRANSPORT OF PLUTONIUM AND OTHER
RADIONUCLIDES IN SEDIMENTARY INTERBED AT INEEL**

submitted by

**Robert A. Fjeld, John T. Coates, and Alan W. Elzerman
Department of Environmental Engineering and Science
Clemson University**

to

Idaho National Engineering and Environmental Laboratory

December 21, 2000

Technical Contact:

**Robert A. Fjeld
864-656-5569 (voice)
864-656-0672 (fax)
e-mail: fjeld@clemson.edu**

TABLE OF CONTENTS

SUMMARY	v
ACKNOWLEDGEMENTS	x
1. INTRODUCTION	1
2. BACKGROUND	3
Overview	3
Relevant Laboratory and Field Data	3
Actinide Chemistry	5
3. MATERIALS AND METHODS	12
Water Simulants	12
Sedimentary Interbed	12
Radionuclide Preparations	15
Mobility Studies	15
Procedures	17
4. COLUMN TEST VERIFICATION STUDIES	21
Tritium	21
Strontium	21
Mean Linear Velocity	25
Background Radiation	27
5. RADIONUCLIDE MOBILITIES	29
Americium	29
Thorium and Plutonium(IV)	32
Neptunium and Plutonium(V)	39
Uranium	50
6. CONCLUSIONS	57
REFERENCES	62
APPENDICES	66

LIST OF TABLES

3.1	Composition of SRPA Groundwater and the Perched Water Simulants Used in this Study	13
3.2	Particle Size Distribution for the M6S and M7S Borehole Samples	14
3.3	Summary of Chemical and Physical Properties of Composite Interbed used in Batch and Column Studies	16
4.1.	Tritium Recoveries and Retardation Factors	23
4.2	Strontium Recoveries and Retardation Factors	26
5.1	Recoveries and Retardation Factors for the Americium Intermediate Mobility Component	30
5.2	Recoveries for the Americium High Mobility Component	31
5.3	Recoveries and Retardation Factors for the Thorium Intermediate Mobility Component	35
5.4	Recoveries for the Thorium High Mobility Component	36
5.5	Recoveries and Retardation Factors for the Plutonium(IV) Intermediate Mobility Component	40
5.6	Recoveries for the Plutonium(IV) High Mobility Component	41
5.7	Retardation Factors and Recoveries for Neptunium	48
5.8	Retardation Factors and Recoveries for Neptunium under Oxidizing Conditions	49
5.9	Plutonium(V) Recoveries for Discrete Time Periods	51
5.10	Uranium Recoveries and Retardation Factors	56
5.11	Speciation Modeling Results for Uranium	56
6.1	Summary of Hypothesized Physical/Chemical Form (in the Absence of EDTA)	58

LIST OF FIGURES

3.1	Experimental apparatus for column studies	16
4.1	Tritium breakthrough curves	22
4.2	Tritium breakthrough curve exhibiting channeling	22
4.3	Strontium breakthrough curves	24
4.4	Retardation factor as a function of mean linear velocity for strontium, uranium, and neptunium	26
4.5	Intrinsic background	28
5.1	Americium breakthrough curves	30
5.2	Expanded view of high mobility time period for americium	31
5.3	Americium high mobility component for an elevated C_0 – unfiltered and filtered (> 3 nm) analyses	33
5.4	Particulate fraction as a function of aging time for americium	33
5.5	Thorium breakthrough curves	35
5.6	Expanded view of high mobility time period for thorium	36
5.7	Thorium high mobility component for an elevated C_0 – unfiltered and filtered (> 3 nm) analyses	37
5.8	Particulate fraction as a function of aging time for thorium	37
5.9	Plutonium(IV) breakthrough curves	38
5.10	Expanded view of high mobility time period for plutonium(IV) for the PWS	40
5.11	Expanded view of high mobility time period for plutonium(IV) for the MPWS	41
5.12	Plutonium(IV) high mobility component for an elevated C_0 – unfiltered and filtered (> 12 nm) analyses	42
5.13	Particulate fraction as a function of aging time for plutonium(IV).	42
5.14	Neptunium breakthrough curves	43
5.15	Effect of removing CO_3^{2-} , F^- , and SO_4^{2-} on neptunium breakthrough curves	45
5.16	Effect of removing CO_3^{2-} , CO_3^{2-} & F^- , and CO_3^{2-} & SO_4^{2-} on neptunium breakthrough curves	45
5.17	Expanded view of high mobility time period for neptunium	46
5.18	Neptunium high mobility component for an elevated C_0 – unfiltered and filtered (> 12 nm) analyses	46
5.19	Neptunium breakthrough curves under oxidizing conditions	48
5.20	Plutonium(V) breakthrough curves	49

5.21	Expanded view of high mobility time period for plutonium(V)	51
5.22	Plutonium(V) high mobility component for an elevated C_0 - unfiltered and filtered (> 12 nm) analyses	52
5.23	Plutonium(V) breakthrough curves under oxidizing conditions	52
5.24	Uranium breakthrough curves	53
5.25	Effect of removing CO_3^{2-} , F^- , and SO_4^{2-} on uranium breakthrough curves	55
5.26	Effect of removing CO_3^{2-} , CO_3^{2-} & F^- , and CO_3^{2-} & SO_4^{2-} on uranium breakthrough curves	55

SUMMARY

The purpose of this report is to document the results of laboratory studies, primarily column experiments, on the mobilities of selected radionuclides in sedimentary interbed from the Subsurface Disposal Area (SDA) at the Idaho National Engineering and Environmental Laboratory (INEEL). The work was motivated by routine environmental monitoring data which are inconsistent with predictions based on classical advection/dispersion/sorption theory in which contaminant mobility is inferred from distribution coefficients measured in batch partitioning experiments. Whereas plutonium and americium mobilities estimated through this approach are extremely low and interbed is predicted to be an effective barrier to migration, the field data suggest they may have penetrated one or more interbed layers.

There are both hydrological and chemical/geochemical mechanisms, acting either separately or in combination, that can explain these observations. This project focused on chemical/geochemical mechanisms that may affect the mobilities of various actinides, especially plutonium, in sedimentary interbed. The initial objective was to determine if high mobility forms of plutonium were possible in laboratory columns eluted with a perched water simulant. As the project progressed, the scope expanded to include uranium and americium, which are important contaminants at the SDA, as well as thorium and neptunium, which are often used as analogs for plutonium(IV) and plutonium(V), respectively. The objectives were also extended to include mechanistic explanations for the observed behaviors, which is critical for determining if the phenomena observed in the laboratory setting are relevant in the field.

Column experiments were performed using unconsolidated interbed collected from nearby cores and various ground water simulants containing elevated concentrations of potential complexing agents. The interbed sample was composited from five cores taken from different depths. Most of the experiments were conducted with the less than 250 μm size fraction, although the 106-250 μm size fraction was used in selected experiments. The ionic species in the ground water simulants were based on analyses of perched water from the site. The perched water simulant (PWS) also contained humic acid and ethylenediaminetetraacetic acid (EDTA), based on their extensive presence in natural waters and low level radioactive wastes, respectively. The modified perched wa-

ter simulant (MPWS) had the same ionic composition as the PWS, but it did not contain either humic acid or EDTA.

The experimental apparatus consisted of reservoirs for the perched water simulant and the spiked simulant, a peristaltic pump, the column packed with sedimentary interbed, and a fraction collector. The spiked simulant was introduced into the column as a finite step of approximately one pore volume in width. Following the spike, the column was eluted with anywhere from 10 to more than 1000 pore volumes of unspiked simulant. Analyses of the effluent fractions were performed with an alpha/beta discriminating liquid scintillation counter. This made it possible, in a single test, to simultaneously measure a beta emitter, such as strontium-85, and an alpha emitting actinide. The data are displayed graphically in the form of breakthrough curves, *i.e.* normalized effluent concentration (effluent concentration divided by concentration in spike) versus time (expressed as displaced pore volumes, DPV, which is the integrated volumetric flow divided by the pore volume). The breakthrough curves are quantitatively characterized by the retardation factor and the corresponding fractional recovery.

The breakthrough curves for strontium were characterized by a single peak containing, within the limits of experimental uncertainty, all of the radioactivity in the spike. The retardation factor was consistently between 200 and 300 for both the PWS and the MPWS. Uranium breakthrough was also characterized by a single peak containing all of the radioactivity in the spike. However, uranium was much more mobile than strontium, with retardation factors between 3 and 4. The breakthrough curves for the other actinides differed significantly from those for uranium. Under the influence of the PWS, the curves for americium, thorium, plutonium(IV), neptunium, and plutonium(V) were all characterized by multiple components having distinctly different mobilities. There was a small, (<<1%) high mobility component that emerged within the first few DPV; a large ($\approx 50\%$), intermediate mobility component that emerged between a few DPV and 500 DPV (not present for plutonium(V)); and a large, low mobility component that was retained in the column. For the MPWS (*i.e.* in the absence of EDTA and HA), in excess of 99% of the americium, thorium, plutonium(IV), and plutonium(V) had very low mobility ($R > 1000$).

Based on the results of the column experiments, batch filtration studies, and thermodynamic calculations, three major conclusions are drawn regarding actinide transport under the influence of the perched water simulants used in these studies. These are as follows: (1) multiple physical/chemical forms, each having distinctly different mobilities,

are possible, (2) for time scales on the order of weeks and longer, the behavior of americium, thorium, and plutonium is dominated by solid forms, and (3) high mobility forms, the physical/chemical natures of which differ among the actinides, are possible. These findings have important implications regarding the behavior of actinide contaminants below the SDA and the conceptual models used to predict their transport.

Multiple physical/chemical forms, each having distinctly different mobilities, are possible: This phenomenon, which was not observed for strontium or uranium, was most pronounced for americium, thorium, and plutonium(IV) in the presence of EDTA and for neptunium in the presence and absence of EDTA. In these tests, the mobilities were characterized by a small (<1%) high mobility component with $R < 3$, a large ($\approx 50\%$) intermediate mobility component with $3 < R < 1000$, and a large ($\approx 50\%$) low mobility component with $R > 1000$. This finding has significant implications with respect to modeling because it suggests that the traditional approach of using batch distribution coefficients (K_D) to infer contaminant mobility may not be appropriate for some contaminants in some situations. The key, of course, is identifying those situations where an alternate approach is warranted. For example, the plutonium(IV) – EDTA complex which was responsible for the intermediate mobility component in the experiments is a transient species which would only be important at the SDA in an episodic infiltration event such as a flood.

The behavior of americium, thorium, and plutonium is dominated by solid species of low mobility: In the absence of EDTA, more than 99% of the americium, thorium, and plutonium(IV) had low mobilities ($R > 1000$) in the columns. This behavior is consistent with the thermodynamic phase diagrams which predict americium to be an insoluble carbonate or hydroxy-carbonate precipitate and thorium and plutonium(IV) to either be a hydroxide or an oxy-hydroxide polymer. The behavior is also consistent with sorption to silicate precipitates as speciation modeling predicts that the groundwater simulants are oversaturated with respect to silicates. Although not obvious, the behaviors of neptunium and plutonium(V) are also likely to be dominated by solid species. The neptunium data for "oxidized" columns and for normal columns at different flow rates both suggest reduction of neptunium(V) to neptunium(IV) by the interbed. Neptunium(IV) is hydrolyzed at pH 8 and likely forms the same immobile solid species as thorium and plutonium(IV). Plutonium(V) is more easily reduced than neptunium(V), and its low mobility component was greater than 99%, both in the presence and absence of EDTA. Thus, its behavior is likely governed by its reduction to the immobile plutonium(IV). The low mo-

bility of plutonium(V) is contingent on its encountering redox active constituents in the path of migration. This seems likely below the SDA.

In the laboratory columns uranium had high mobility ($R \approx 3$) due to the soluble complexes that it forms with carbonate. While the carbonate species are likely to control transport in the short term and would be important in episodic transport scenarios, long term transport is affected by aging processes and is likely dominated by insoluble calcium and/or phosphate mineral species. Since the solubilities of these uranium mineral species are typically much lower than the uranyl carbonates, long-term uranium mobility below the SDA is likely to be much lower than suggested by the column experiments.

High mobility forms are possible: High mobility forms were observed for americium, thorium, plutonium(IV), neptunium, and plutonium(V). The physical/chemical nature of these forms differed. Effluent filtrations showed the americium and neptunium high mobility form to be smaller than 3 nm, thorium to be larger than 3 nm, and plutonium(IV) and plutonium(V) to have portions both smaller and larger than 3 nm. When combined with batch filtration data and speciation modeling predictions, hypotheses are advanced regarding the nature of these high mobility forms as follows: americium – americium carbonate or hydroxy carbonate in either a soluble or small (<3 nm) precipitate form; thorium – thorium oxy-hydroxide polymer or hydrolyzed thorium sorbed to silicate precipitates (>3 nm); plutonium(IV) - plutonium oxy-hydroxide polymer or hydrolyzed plutonium sorbed to silicate precipitates; neptunium – soluble neptunium carbonate; plutonium(V) – plutonium carbonate complexes and the same species as above for plutonium(IV), due to reduction of plutonium(V) to plutonium(IV).

Collectively, these results provide a plausible explanation for the apparent disconnect between the transport model, which predicts interbed to be an effective barrier for plutonium and americium migration, and field data, which indicate penetration of that barrier. They are consistent with the transport model in that the column tests also show interbed to be an effective geochemical barrier ($R > 1000$). They differ from the transport model however, in that the interbed was experimentally found to be effective for most of the americium and plutonium rather than all of it as predicted. The results are, at the same time, consistent with the field data. The high mobility forms appear to be at least partly colloidal, and the transport of colloidal material through the subsurface is likely to be stochastic. In fact, some of the breakthrough curves, particularly those for plutonium(V), not only had a high mobility component early in the test but also exhibited spo-

radic release of very small amounts throughout the duration of the experiment. This is consistent with the sporadic occurrence of americium and plutonium in monitoring data.

Additional findings of potential interest are the effect of mean linear velocity and the ability of the interbed matrix to attenuate colloids. Decreasing the mean linear velocity an order of magnitude below the value used in most of the tests did not affect retardation factors for any of the contaminants that were tested (neptunium, uranium, and strontium). These results provide a measure of assurance that behavior predicted by the columns may be applicable at the much lower mean linear velocities that are typical below the SDA. However, this extrapolation needs to be applied with care because there can be kinetic effects which are significant. For example, fractional recovery for neptunium declined when the flow rate was reduced because the increase in residence time provided for a greater reduction from neptunium(V) to neptunium(IV) by the soil. Similarly, the intermediate mobility fractions that resulted from EDTA complexation with americium, thorium, and plutonium(IV) were short lived. The ability of the 106 to 250 μm size fraction to attenuate colloids smaller than 20 nm was surprising and supports the findings that there is very little penetration of interbed by the colloidal forms.

ACKNOWLEDGEMENTS

The authors express their appreciation to John Hackett and Chris Grossman for their long hours of work in the laboratory, Rachael Williams for her assistance in the laboratory and in data analysis; Sandra Clipp for dealing with administrative details and preparing the final report, Tim DeVol for helping with radiation detection problems, and April Long and Claire Woelfel for assisting with the final report. Special thanks are extended to Jim Navratil, who first conceived this work while at the Idaho National Engineering and Environmental Laboratory (INEEL). Appreciation is also extended to the following individuals who provided constructive comments during periodic reviews: Greg Choppin, Sue Clark, Jess Cleveland, Ken Czerwinski, Larry Hull, and Fedor Macasek. In addition, the authors wish to acknowledge the support provided by Dirk Gombert, Bruce Becker, and Doug Jorgensen at INEEL and Alan Jines and Aran Armstrong at the Department of Energy's Idaho Operations office. This work was funded by the INEEL under contracts K97-560265, K98-564517, and K99-181044.

1. INTRODUCTION

The purpose of this report is to document the results of laboratory studies on the mobilities of selected radionuclides in sedimentary interbed from the Subsurface Disposal Area (SDA) at the Idaho National Engineering and Environmental Laboratory (INEEL). The work was conducted in support of risk analyses for the Waste Area Group 7 (WAG 7) Comprehensive Remedial Investigation and Feasibility Study. The principal exposure pathway of concern for WAG 7 involves the Snake River Plain aquifer, which lies approximately 200 m below the SDA. In the risk analyses, contaminant transport from the waste trenches to the aquifer is based on classical advection/dispersion/sorption theory in which the interaction between the contaminant and the solid phase is conceptualized as a linear, reversible, sorption process. In this approach, contaminant mobility is inferred from distribution coefficients measured in batch partitioning experiments. Plutonium and americium mobilities estimated through this approach are extremely low, and interbed is predicted to be an effective barrier to migration. However, field measurements below the SDA suggest that americium and plutonium may have penetrated one or more interbed layers.

There are a number of observations, from both field and laboratory investigations, suggesting that some contaminants of concern at Department of Energy sites can travel faster than predictions based on classical advection/dispersion/sorption models of the type used for the Interim Risk Assessment at WAG 7. There are both hydrological and chemical/geochemical mechanisms, acting either separately or in combination, that can be invoked to explain these observations. The work reported here focused on chemical/geochemical mechanisms that may affect the mobilities of various actinides, especially plutonium, in sedimentary interbed. The initial objective was to determine if high mobility forms of plutonium were possible in laboratory columns eluted with a perched water simulant. As the project progressed, the scope expanded to include uranium and americium, which are important contaminants at the SDA, as well as thorium and neptunium, which are potential analogs for plutonium(IV) and plutonium(V), respectively. The objectives were also extended to include mechanistic explanations for the observed behaviors, which are critical for determining if the phenomena observed in the laboratory setting are relevant to the field. The resulting body of data, in aggregate and in combi-

nation with thermodynamic calculations, not only yields explanations for the transport behaviors observed in the laboratory system, but also provides a basis for identifying the chemical/geochemical processes that are likely to be important under a given set of field conditions. Also included in this report are results of tests performed to examine a limited number of potential experimental artifacts that might limit or prohibit extrapolation of the laboratory findings to the field.

2. BACKGROUND

Overview

The SDA is part of the Radioactive Waste Management Complex at INEEL. It contains shallow pits, soil vaults, and trenches where a variety of low-level, mixed, and transuranic wastes are buried. The Snake River Plain aquifer is separated from the SDA by a thick (approximately 180 m) vadose zone consisting of a layered sequence of fractured volcanic rocks (primarily basalt) and sedimentary interbeds. There are at least 11 basalt layers and 10 interbed layers between the SDA and the aquifer (USGS, 1999). The modeling of contaminant transport from the SDA to the aquifer is an extremely difficult problem because of inherent complexities and uncertainties associated with both the hydrology and the geochemistry. Contributing to the hydrological complexity are questions regarding the integrity (*i.e.* the presence of fractures) and uniformity of the interbed layers, the role of past flood events on contaminant migration, and the relative importance of vertical infiltration of water from the surface versus lateral infiltration from adjacent areas. The geochemical complexity is due to the varied composition of leachate from waste trenches, the changes in chemistry that occur due to contact with the subsurface media, and the assortment of liquid and solid phase processes that may influence contaminant mobility. These processes, which include hydrolysis, precipitation, complexation, colloid formation, ion exchange, and oxidation/reduction, are discussed in detail later in this section.

Relevant Laboratory and Field Data

A key question with respect to transport modeling is whether the geochemical interactions can be adequately approximated by the traditional modeling approach, in which contaminant mobility is inferred from batch sorption experiments. An inherent assumption of the traditional approach is that the contaminant exists in a single physical/chemical form. There is a growing body of evidence suggesting that some contaminants, especially some of the actinides, can exist in multiple physical/chemical forms, each with different mobilities. Fried *et al.* (1974) observed high mobility forms of americium and plutonium in laboratory experiments with volcanic tuff from Los Alamos. They performed two types of experiments. In the first, plutonium and americium were depos-

ited in a depression on the top of a block of tuff. After several “rain-drought” cycles in which the block was showered with water and allowed to dry, cores were extracted from the block. Each core showed two zones of activity as a function of depth. There was a low mobility zone close to the site of deposition that contained the majority of the plutonium and a high mobility zone some distance away that contained less than 1% of the original activity. Small, high mobility components were also observed in column tests with crushed and washed tuff. From these experiments, it was estimated that 1% of the plutonium had a mobility that was 25,000 times higher than the bulk of the plutonium. Thompson (1989) performed column tests with crushed tuff and groundwater (“J-13”) from the Nevada Test Site. He observed some of the plutonium, americium, and neptunium to travel through the columns at approximately the same speed as tritium. For plutonium, the high mobility fraction depended on the oxidation state. It was as high as 70% for plutonium(V) and/or plutonium(VI), but it was generally less than 10% for plutonium(IV). The behavior of americium was similar to that of plutonium(IV) and the behavior of neptunium was similar to that of plutonium(V)/plutonium(VI). In previous work performed in our laboratory, column experiments were conducted with basalt and sedimentary interbed from INEEL. Cobalt, plutonium and americium were observed to have multiple mobilities, presumably due to multiple physical/chemical forms; but uranium, cesium, and strontium did not (Fjeld *et al.*, 2000).

There is also field evidence suggesting multiple mobilities. Based on an examination of field data at the Savannah River Site (SRS), Looney *et al.* (1987) incorporated high mobility fractions for selected contaminants in risk assessments of waste management activities at the site. The contaminants exhibiting evidence of high mobility transport were barium, cadmium, chromium, lead, mercury, cobalt, strontium, cesium, uranium, and plutonium. Kaplan *et al.* (1994) found varying fractions of fast moving plutonium, uranium, americium, and curium in an acidic groundwater plume at SRS. Penrose *et al.* (1990) found elevated plutonium and americium concentrations in a small aquifer at Los Alamos. Although Penrose *et al.* attributed the presence of the radionuclides to colloidal transport through the aquifer, Marty *et al.* (1997) subsequently made a case for infiltration of surface water. Buddemeier and Hunt (1988) and Kersting *et al.* (1999) observed high mobility transport of radionuclides at the Nevada Test Site. Based on field tracer experiments with lanthanides, McCarthy *et al.* (1998) concluded that high mobility forms of americium at the Oak Ridge National Laboratory were due to association with natural organic matter.

Actinide Chemistry

The actinides are heavy metal cations that can exist in the environment in several different oxidation states, and their behavior in the environment is often dictated by the oxidation state of the ion under the conditions present (Kim, 1986). Some actinides are quite stable with respect to oxidation state. For example, americium and thorium are generally only found in the III and IV oxidation states, respectively. Others may be present in multiple oxidation states. Neptunium can exist as IV and V and uranium as IV and VI. At the extreme is plutonium, which can exist in up to four oxidation states (III, IV, V, and VI) simultaneously (Cleveland, 1970). For the groundwater and perched water typical at INEEL, americium is III, thorium is IV, neptunium is V, uranium is VI, and plutonium is IV and V. Because of the similarities in atomic structure among the actinides, different elements with the same oxidation state are expected to exhibit similar chemical behavior (Silva and Nitsche, 1995). Thus, thorium (IV) should behave as plutonium(IV); neptunium(V) should behave as plutonium(V), and so on.

Due to the complex chemistry that exists under environmental conditions, it is necessary to examine several aspects of actinide chemical behavior. There are five facets of actinide chemistry that can significantly affect the migration of actinides through the subsurface - solubility, complexation, sorption, colloid formation, and redox conditions. Each process is often difficult to single out because of the influence of the others. This section provides a basic overview of these areas of actinide chemistry as they pertain to the five radionuclides studied in these experiments - americium, thorium, neptunium, uranium, and plutonium.

Solubility

Generally, the solubilities of metal ions in natural water systems are regulated by the formation of hydroxide or carbonate precipitates (Stumm and Morgan, 1981). To a lesser extent, solubilities are also affected by the presence of other ligands, such as fluoride, sulfate, silicate, and phosphate (Nitsche and Edelstein, 1985). The mobility of a metal species generally decreases with decreasing solubility because it can become trapped within the soil matrix when it precipitates out of the dissolved phase.

Due to variations in oxidation state and groundwater chemistry and the difficulty in truly reaching equilibrium, universally applicable solubility data for the actinides in natural waters do not exist. The solubility of americium, which is initially present as the Am^{3+} ion, is primarily dependent on the carbonate concentration in solution. Between pH 7

and 9 its solubility is limited by the formation of $\text{AmOHCO}_3(\text{c})$ and can fall below 10^{-8} M; above pH 9, however, further carbonate complexation actually increases its solubility (Hobart, 1990; Langmuir, 1997). These solubility predictions are also strongly influenced by the concentration of the carbonate/bicarbonate ions. At low carbonate concentrations and pH 9, the crystalline AmCO_3OH is predicted to be present.

Plutonium(IV) can hydrolyze in natural waters to form the amorphous polymer $\text{Pu}(\text{OH})_4 \times \text{H}_2\text{O}$, which has a very low solubility product, approximately 10^{-56} (Cleveland, 1970). Upon sufficient aging, this amorphous polymer can attain a crystalline structure, which increases the difficulty of dissolution (Rai and Ryan, 1982). It is also reported that plutonium(IV) solubility tends to be high in solutions in which the concentrations of carbonate and fluoride ions are also high (Nash *et al.*, 1988). Furthermore, α -radiolysis may complicate matters by creating oxidation products that oxidize the Pu^{4+} ion to the more soluble higher oxidation states. For example, it was found that, over an aging period of 1300 days, a sample of ^{238}Pu had remained in the amorphous Pu^{4+} polymer while a sample of the less radioactive ^{239}Pu achieved the crystalline form (Nitsche, 1991). However, since radiolysis generally occurs at much higher plutonium concentrations than those typically encountered in environmental settings, this process is probably not important.

Thorium, which exists primarily in the IV oxidation state in natural waters, behaves similarly to Pu^{4+} , generally having a low solubility which is limited by the formation of the $\text{Th}(\text{OH})_4$ amorphous polymer and subsequent crystalline solid. Thorium may also form complexes with sulfate, fluoride, carbonate and phosphate in natural waters, which may increase its solubility (Lieser and Hill, 1992).

In the V oxidation state, plutonium is present as PuO_2^+ , which is typically quite soluble (Watters, 1983). However, the amounts of all oxidation states of plutonium in solution are limited by the amount of $\text{Pu}(\text{OH})_4$ in solution (Choppin and Stout, 1989). Also, at concentrations above 10^{-8} M, the PuO_2^+ ion may disproportionate or be reduced to form Pu^{4+} , which can further complicate its solubility (Bagnall, 1972; Choppin, 1994b). Plutonium(V) most readily disproportionates in highly acidic conditions; however, at near-neutral pH, it is the most observed oxidation state of plutonium in natural waters (Keller, 1971).

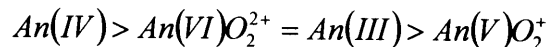
Neptunium, in its V oxidation state, also exists as an oxygenated ion, NpO_2^+ . Neptunium is quite soluble in this form. In one study it was reported that under normal geo-

chemical conditions, aqueous neptunium concentrations may be as high as 10^{-4} mol/L, which is two orders of magnitude higher than the highest soluble concentrations of the other transuranic ions (Kim, 1986). The solubility of neptunium, like that of plutonium, is also affected by the formation of $\text{Np}(\text{OH})_4$ polymer, although neptunium(IV) is much more prone to oxidation to neptunium(V) in near-surface conditions (Morse and Choppin, 1991). It has also been found that the presence of carbonate ions may increase the solubility of neptunium(V) above pH 9 (Nakayama *et al.*, 1988).

Uranium, which is present in the VI oxidation state (as the UO_2^{2+} ion), is also very soluble, as it tends to form carbonate complexes that keep it in solution (Morse and Choppin, 1991). UO_2^{2+} reacts with hydroxide to form $\text{UO}_2(\text{OH})_2 \cdot \text{H}_2\text{O}$ (the mineral Schoepite), which limits the amount of uranium in solution. Since the formation of Schoepite takes on the order of several weeks to reach equilibrium (Silva, 1992), it would not be important in the short term but it could be important in the long term. The solubility of the uranyl ion may also be affected by the presence of silicates in some environments (Choppin *et al.*, 1994a).

Complexation

Complex formation is an important aspect of actinide ion behavior in natural waters. Complexes can alter solubility, solid surface characteristics, and sorption ability, which in turn can greatly affect migration (Snoeyink and Jenkins, 1980; Jensen, 1980). Typically, actinide cations, considered hard acids, preferentially interact with hard bases such as fluoride or oxygen rather than nitrogen, sulfur, phosphorous, or other softer bases (Morse and Choppin, 1991). Furthermore, complexation behavior is mostly a function of oxidation state rather than specific element. Because actinides with the same oxidation state have similar ionic radii, it is possible to make generalizations concerning their complexation behavior. Typically, the relative affinity for actinides to form complexes follows the order:



As a result, actinides in the IV oxidation state tend to form the strongest complexes and the V actinides form the weakest (Hobart, 1990). In addition, the complexation strengths of the various ligands present in the groundwater are also an important factor in determining the complexes that are formed. The relative strengths of some common inorganic groundwater ligands are (Silva and Nitsche, 1995):



Since complex formation is dependent primarily on oxidation state and on the ligands present, it is necessary to examine the behavior of the four oxidation states (III, IV, V, and VI) that are studied in this work.

Americium, in the III oxidation state, tends to form several different carbonate complexes in a natural system. In the pH range of 7.9 to 9.1, the most prevalent soluble americium-carbonate species are $Am(CO_3)_2^{1-}$, $Am(HCO_3)_2^{1+}$, and $Am(OH)(CO_3)_2^{2-}$ (Bidoglio, 1982; Newton and Sullivan, 1985), and they are considered to be the major solution species (Silva, 1984). With the typical amounts of carbonate present in groundwater under natural conditions, americium(III) generally forms carbonate species, despite the presence of other ligands (Nitsche, 1991). It must be noted, however, that there are discrepancies in the literature regarding the complexation of americium and the specific carbonate complexes that are formed (Silva *et al.*, 1995).

As noted in the section on solubility, thorium and plutonium in the IV oxidation state generally form hydroxides under natural conditions. In a carbonate solution, it has been found that thorium(IV) can form $Th(CO_3)_4^{4-}$, $Th(CO_3)_5^{6-}$, and $Th(CO_3)_6^{8-}$ (Hobart, 1990). However, it is believed that at natural pH levels, both organic and inorganic complexes of thorium(IV) are insignificant relative to $Th(OH)_4$ (Lieser and Hill, 1992). There are uncertainties in the literature regarding the carbonate complexation of plutonium(IV) due to its variable oxidation state in natural waters. It is thought that $Pu(CO_3)_2^{2-}$, $Pu(OH)_2(CO_3)_2^{2-}$, and $Pu(OH)_4(CO_3)_4^{4-}$ are the most prevalent plutonium-carbonate species at high carbonate and bicarbonate concentrations; but, as with thorium(IV), the plutonium(IV) hydroxide is still the dominant plutonium species at natural carbonate levels (Yamaguchi *et al.*, 1994; Nitsche and Silva, 1996).

The actinides in the pentavalent oxidation state, plutonium and neptunium, are the least likely to form complexes of the elements under study here. Both PuO_2^+ and NpO_2^+ are quite resistant to hydrolysis and carbonate complexation at near neutral pH (Jensen, 1980). In carbonate solutions at high pH, pentavalent neptunium can form both hydrolysis species and mixed hydroxy-carbonate species (Neck *et al.*, 1997). However, since plutonium(V) is much more susceptible to reduction or oxidation than neptunium(V), they cannot be expected to behave similarly under all conditions.

Uranium, which occurs as UO_2^{2+} , is quite likely to form complexes with several different groundwater ligands. It has been found that uranium(VI) complexes with carbonate, forming $\text{UO}_2(\text{CO}_3)$, $\text{UO}_2(\text{CO}_3)_2^{2-}$, and $\text{UO}_2(\text{CO}_3)_3^{4-}$, which play an important role in migration (Brookins, 1989). Uranium also forms complexes with the fluoride ion, forming several species ranging from UF^{3+} to UF_6^{2-} , and also may hydrolyze to form $\text{UO}_2(\text{OH})^+$, $(\text{UO}_2)_2(\text{OH})_2^{2+}$, and subsequent polymers (Kohler *et al.*, 1996). Furthermore, under acidic conditions, uranium may complex with sulfate, producing $\text{UO}_2(\text{SO}_4)_2^{2-}$ (Brookins, 1989).

Sorption

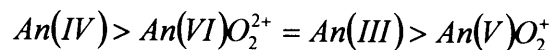
Sorption behavior is an important factor to consider when studying actinide migration. Even temporary sorption of an actinide solute onto a solid surface can significantly retard its transport (Deutsch, 1997). Typically, sorption occurs through an ion exchange process in which negatively charged minerals in clay and soils electrostatically interact with the positively charged actinide cations (Livens *et al.*, 1996). This ion exchange process is often pH dependent, and competition may occur for exchange sites between different cations. Chemisorption may also occur through a chemically driven process, in which a chemical bond is formed between the adsorbent surface and the adsorbing species. This type of sorption is basically irreversible.

Generally, the chemical parameters in a natural system that have the most significant influence on actinide sorption behavior are redox conditions (affecting the oxidation state of the actinide species), pH (affecting the amount of hydrolysis), and the presence of complexing agents (Allard *et al.*, 1982; Dozol and Hagemann, 1993). The ionic strength of the groundwater solution has also been shown to have important effects on the sorption of actinides (Kaplan *et al.*, 1998). Since the lower valence actinides (americium, plutonium, and thorium) are more likely to undergo hydrolysis and hydroxycarbonate complexation, they are also more likely to be involved in some sorption process at the soil surface. The actinides at the higher oxidation states (plutonium, neptunium, and uranium) are typically not sorbed to a large extent. However, because of chemical reduction and complexation, the higher valence actinides may be sorbed more than expected (Jensen, 1980; Choppin and Stout, 1989; McCubbin and Leonard, 1995).

Colloid Formation

The formation of colloids can play an important role in actinide migration. Both organic and inorganic colloids are ubiquitous in natural systems. Actinide colloids may be formed by polynucleation followed by agglomeration ("real" or "true" colloids), or by associating through sorption or ion exchange onto existing groundwater colloids ("associated colloids"). It is believed that natural organic colloids have the largest impact in colloidal transport, though inorganic colloids may have a significant influence as well (van Gunten and Benes, 1995).

As with sorption, the formation of actinide colloids is complex and highly dependent upon solubility, hydrolysis, complexation, and, ultimately, oxidation state of the actinide in question. The relative tendency to generate real colloids among the different actinide oxidation states is the same as the tendency for complexation and hydrolysis that was indicated above (Kim, 1991):



This suggests that plutonium and thorium, in the IV oxidation state, most readily undergo real colloid formation. The An(IV) hydroxide agglomerates into an oxy-hydroxide colloid form, which can have a high mobility if it remains suspended or a low mobility if it becomes trapped in the soil matrix. The complexation ability of An(VI) is well documented, but the colloid formation ability has not been widely investigated. The trivalent actinides also undergo hydrolysis and thus form real colloids, but those colloids are less stable than their tetravalent counterparts and are more prone to sorption onto solid surfaces. The actinides in the V oxidation state are not thought to undergo significant colloid formation (Ramsay, 1988; Nagasaki *et al.*, 1998).

The generation of associated colloids is of concern because of their potential for increased transport. Depending on the electrostatic charge of the colloid relative to the surrounding media, actinide associated colloids have the ability to move faster than the groundwater (Nagasaki *et al.* 1997). Typically, the formation of associated colloids is a function of the sorption ability of the actinide species present, which can be affected by pH, groundwater chemistry, redox potential, *etc.* For actinides in all oxidation states, associated colloid formation may be abated in the presence of a strong complexing agent, such as carbonate or an organic ligand like EDTA or humic acid (Kim, 1991).

Redox

Actinide speciation and mobility is influenced by the redox potential of the ground-water and surface-active constituents such as reduced iron and manganese of sediments (interbed soils) in contact with the groundwater. Most E_H -pH phase diagrams presented in the literature address the An—C—O—H and An—O—H systems. In many natural subsurface environments, pH values range from near neutrality to >9, and E_H values may vary between -0.1 and +0.6 volts. Phase diagrams generally reflect these ranges and may be found for the actinides studied in this investigation. Presented in this basic review are E_H -pH diagrams for the An—C—O—H system. A collection of the diagrams is presented in [E_H-pH Diagrams for Geochemistry](#) (Brookins, 1987). Excerpts from the text for americium, thorium, plutonium, neptunium and uranium are noted in the following discussion to suggest likely predominant actinide species present in groundwaters at the SDA. The perched water simulants used in this investigation were formulated from Wood and Low (1986) and contain oversaturation concentrations of several anions and cations resulting in solid phases not considered in Brookins' review. The presence of these solid phases may influence the mobility of the actinides and therefore will be discussed later in this report.

A collection of the more pertinent phase diagrams used in this investigation is included in Appendix A. These phase diagrams are presented for the An—C—O—H system and generally allow the reader to review likely solid and aqueous species in the E_H -pH range for most natural systems. Thermodynamic data used to calculate these phase regions for important actinide species are also listed in Brookins (1987).

It is interesting to note that at pH 8, within an E_H range of 0.1 to 0.4 and in the presence of carbonate, solid species for each of the actinides included in this investigation are predicted. Thermodynamic data for americium predicts $Am_2(CO_3)_3$; for plutonium, PuO_2 ; for neptunium, NpO_2 ; and for thorium, ThO_2 . However, soluble uranyl carbonate species are predicted for uranium(VI). It is generally accepted that the cation An(IV) is hydrolyzed to $An(OH)_4$, which ages to AnO_2 in most natural settings.

3. MATERIALS AND METHODS

Water Simulants

Several distinctly different chemical compositions of perched water were used for column and batch experiments as water simulants. All perched water simulants were formulated from data provided by Wood and Lowe (1986) for the Snake River Plain Aquifer. The mean, maximum, and minimum concentrations of the major cations and anions are given in Table 3.1. Compositions of the various perched water simulants used in this investigation are also listed in the table. These simulants include (1) a perched water simulant (PWS), which is formulated from all of the major cations and anions found in the Snake River Plain Aquifer and includes humic acid (HA) and ethylenediaminetetraacetic acid (EDTA); (2) a modified perched water simulant (MPWS), which is identical to the PWS but does not contain HA and EDTA; and (3) several MPWS formulations in which specific chemical constituents were removed, *e.g.* MPWS-F denotes a modified perched water simulant minus the fluoride ion. Each of the simulants was prepared using reagent grade chemicals and distilled water. Dilute hydrochloric acid and sodium hydroxide were used to adjust pH.

Sedimentary Interbed

Sedimentary interbed was collected from the M6S and M7S boreholes at different depths and composited. Interbed samples were collected from depths of 166-177, 322-338 and 386 feet from the M6S borehole and at 213-214 and 329-330 feet from the M7S borehole. Particle size distribution for the composited interbed sample is given in Table 3.2. A more detailed description of the particle size distribution for the interbed samples used to obtain the composited sample is presented in Appendix B. The composited sample was classified as a sandy loam with 17% of the total being composed of particles greater than 2 mm. Of the fraction less than 2 mm, 74% was between 0.05 and 2 mm, 22% was between 0.002 and 0.05 mm and 4% was less than 0.002 mm. Sixty-one percent of the particles less than 2 mm was smaller than 0.25 mm. The composited interbed soil was dry sieved using U. S. Standard Testing Sieves meeting ASTM E-11 specifications and the fraction less than 0.25 mm was retained. Based on USDA classification of soil texture, the <0.25-mm fraction included clays, silts, very fine sand, and fine sand. Most column and batch experiments were conducted using the <0.25-mm fraction.

Table 3.1. Composition of SRPA Groundwater and the Perched Water Simulants Used in this Study

Component	SRPA Groundwater			Perched Water Simulants						
	Mean	Max.	Min.	PWS	MPWS	MPWS (F)	MPWS (SO ₄ ²⁻)	MPWS (CO ₃ ²⁻)	MPWS (F- & CO ₃ ²⁻)	MPWS (SO ₄ ²⁻ & CO ₃ ²⁻)
	mg/L	mg/L	mg/L	mg/L	mg/L	mg/L	mg/L	mg/L	mg/L	mg/L
Ca ²⁺	51	120	5	10.5	10.5	10.5	10.5	10.5	10.5	10.4
K ¹⁺	4	12	0	10	10	10	10	0	0	0
Mg ²⁺	18	54	0.2	17.5	17.5	17.5	2.3	17.5	17.5	2.3
Na ¹⁺	26	140	3.9	570	570	566	450	316	291	174
Cl ¹⁻	28	230	1.8	220	220	218	218	218	217	217
SO ₄ ²⁻	41	218	2.7	350	350	356	NP	355	355	NP
HO ₃ ⁻	220	510	52	750	750	747	749	Trace	Trace	Trace
F ⁻	0.6	11	0.03	20	20	NP	20	20	NP	20
Si ²⁺	50	138	5.8	10	10	10	10	10	10	10
HA	NA	NA	NA	1.3	NP	NP	NP	NP	NP	NP
EDTA	NA	NA	NA	1.3	NP	NP	NP	NP	NP	NP
pH	7.8	9.1	7.0	8.2 ± 0.2	8.2 ± 0.2	8.2 ± 0.2	8.2 ± 0.2	8.2 ± 0.2	8.2 ± 0.2	8.2 ± 0.2
I	0.008	0.02	0.002	0.034	0.034	0.031	0.02	0.02	0.0085	0.019

Table 3.2. Particle Size Distribution for the M6S and M7S Borehole Samples

Sample and Texture	mm	Interbed Composite Sandy Loam
Large	>2	16.7
Small	{ 1.00-2.00 0.50-1.00 0.25-0.50 0.10-0.25 0.05-0.10	12.2
		12.2
		15.5
		20.9
		12.9
	% Total	
% Silt	0.002-0.050	22.4
% Clay	<0.002	3.9
% Total Small		100.0

A summary of the major physical and chemical characteristics of the <0.25 mm size fraction of the interbed composite sample is presented in Table 3.3. The exchangeable iron expressed as %Fe₂O₃ and manganese as ppm Mn are presented in addition to the cation exchange capacity data. The dominant minerals represent approximately 90% of the clay minerals present. Extractable iron and manganese data for the samples that were used to obtain the interbed composite sample are presented in Appendix B. A more detailed chemical analysis of the M6S and M7S borehole samples and the composite sample is also presented in Appendix B.

Radionuclide Preparations

Of primary concern to the INEEL was the mobility of plutonium, uranium, and americium through the sedimentary interbed in the vadose zone beneath the SDA. Under natural environmental conditions plutonium can exist in several oxidation states and its mobility is a function of the oxidation state and the species present. Experiments were conducted for americium, uranium, plutonium(IV) and (V) and the plutonium analogs, thorium(IV) and neptunium(V). Column spiking solutions were therefore prepared for each of the radionuclides in the various water simulants noted in Table 3.1. In addition, solutions of tritium and strontium were prepared and studied for quality control purposes.

Spiking solutions were typically prepared by adding a known activity of a radionuclide to the appropriate water simulant followed by a pH adjustment to 8.0 ± 0.2 using dilute HCl or NaOH. The target radionuclide concentration in a spiking solution was typically on the order of 300 Bq/mL. The activity and molar concentrations of americium, thorium, plutonium, neptunium, and uranium in each experiment are given in Appendix C.

Mobility Studies

Apparatus

A block diagram of the flow through column apparatus used in this study is given in Figure 3.1. The apparatus consisted of a peristaltic pump (Masterflex, Cole-Palmer Instrument Co.), column, and fraction collector (Universal Fraction Collector, Eldex Laboratories, Inc.). The columns were fabricated from Plexiglas® tubing 2.1 cm OD, 1.5 cm ID and approximately 8 cm in length. End caps were fabricated from Plexiglas® plate approximately 2.2 cm thick and cut into squares of approximately 4 cm. The center

Table 3.3. Summary of Chemical and Physical Properties of Composite Interbed Used in Batch and Column Studies

Parameter	Composite Interbed
Particle Size Used (mm)	<0.25
Dithionite-Citrate Buffer (DCB) Extractable Fe ₂ O ₃ (%)	1.77
NH ₄ Oac Extractable Mn (ppm)	1.90
Total Cation Exchange Capacity (meq/100g)	17.39
Dominant Minerals	Montmorillonite, Muscovite and Biotite, Vermiculite

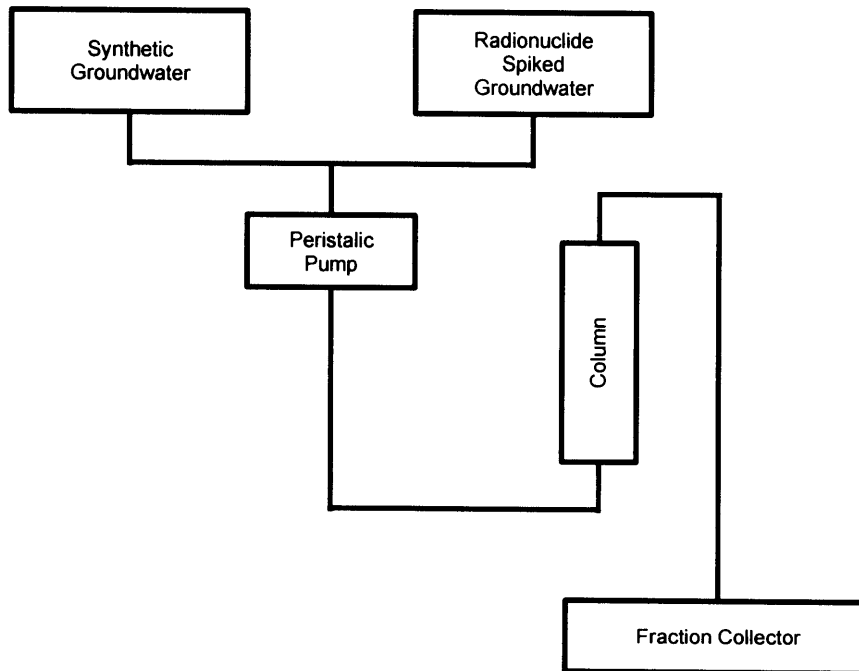


Figure 3.1. Experimental apparatus for column tests

of each end cap was drilled and tapped for 1/16 in. NPT tube fitting grooved to a depth of 0.5 cm to accept an O-ring and the column end. End caps were drilled on each corner to accept 3/16 in. allthread and the columns were clamped together using 3/16 in. wing nuts. The apparatus was interconnected with Masterflex® tubing (size 13) to allow a radionuclide spike (size 13) to allow a radionuclide spike to be introduced into the column and to allow the introduction of a water simulant to elute the radionuclide spike.

Procedures

Typical Studies

Interbed soil columns were dry-packed using the 0.25 mm fraction of the interbed composite. Each column was packed by adding approximately 1 cm of the soil to the assembled column apparatus and lightly tapping the column on a benchtop to compress the soil until the column was completely filled. Before each successive addition of soil to the column, the packed soil surface was agitated using a wooden dowel to avoid creating distinct layers of packed soil. When packed, each column had approximately 30 grams of soil corresponding to a dry bulk density of 1.7 to 1.9 g/mL and a pore volume of about 6 mL.

Column experiments were conducted using both unwashed and washed columns. In most of the experiments, the columns were unwashed, i.e. the first pore volume introduced into the dry column contained radioactivity. The rationale for this approach was that some vadose zone contamination scenarios involve contaminated water contacting dry soil and possibly mobilizing small particles as associated colloids. Washed columns were eluted for approximately 10 pore volumes with the water simulant before spiking with the radionuclide solution. After washing, a nominal one-pore volume spike of the appropriate radionuclide spiking solution was introduced into the column at a flow rate of 0.30 to 0.32 mL/min. Unwashed and washed columns were both eluted with the appropriate water simulant and effluent fractions were collected for ten to several thousand displaced pore volumes.

Redox Studies

Column experiments were also conducted to examine the effect of E_H on the mobility of An(IV) and (V). For the typical column studies outlined above E_H ranged between 50 and 100 mV. Attempts were made to raise the E_H to 400 to 500 mV by ozonating the water simulant for a period of six hours. During this period of time, the oxidized water

simulant was passed through the column in an attempt to oxidize surface functional groups on the interbed soil. The E_H of the water simulant was monitored at both the column influent and effluent. No attempt was made to measure the change in oxidation potential of the interbed soil before and after ozonolysis.

Colloid Studies

Batch and column filtration experiments were conducted to study the formation of true colloids and associated colloids and the attenuation of both types of colloids by the packed interbed columns. For each of these experiments, batch solutions and column eluants were filtered using either syringe filters (Anotop™ 25) to determine particulate fractions from 20 nm to 450 nm (20, 100, 200 and 450 nm) or centrifugal filters (Pall Filtron, Microsep™) to determine particulate fractions below 20 nm nominal (3 and 12 nm). The term 'nominal' refers to the manufacturer specification for ninety percent collection efficiency.

Formation of True Colloids: Experiments were conducted to determine if plutonium oxy-hydroxide colloids would form in a perched water simulant containing both EDTA and humic acid and to evaluate the effect of carbonate on the formation of these colloids. Quadruplicate samples for two sets of the perched water simulant were prepared containing a known activity of plutonium(IV). Samples were analyzed and filtered using an Anotop™ 25 (20 nm) syringe filter approximately one hour after preparation. The filtered sample was then allowed to stand for a period of seven days and filtered again. The seven day filtered samples were allowed to stand for seven additional days and were filtered and analyzed. Additional sets of two tubes were prepared in (1) MPWS without carbonate; (2) MPWS; (3) PWS without EDTA; and (4) PWS without humic acid. These replicate samples were also filtered and analyzed as noted above.

Attenuation of Colloids: To obtain an estimate of the degree to which a packed interbed column attenuates colloids, (both true colloids and associated colloids), a pair of columns were packed with interbed soil sieved to isolate the 106 to 250 μm size fraction. A freshly prepared PWS spiking solution containing plutonium(IV) was introduced onto the column and eluted for 200 DPV. These two columns were not washed prior to the spike and therefore likely contained colloids from the soil matrix. After 200 pore volumes of PWS was passed through the columns, an aged spiking solution that contained ap-

proximately 50% plutonium(IV) true colloids was introduced onto the columns and eluted for 200 DPV. This experiment represented a pair of washed columns. Finally, a suspension of soil colloids was prepared by suspending a mass of the <106 μm size fraction of the interbed soil in the PWS and filtering with syringe filters to isolate colloids <200 nm. Plutonium(IV) was added to the colloidal suspension and allowed to equilibrate for a period of 24 hours. These 'tagged' colloids were analyzed to determine the particulate fraction and spiked onto a pair of washed columns and eluted for 200 DPV. Recovery of plutonium(IV) and the fraction of particulate plutonium(IV) was determined. Details of these experiments are summarized in Appendix D.

Tritium Column Checks

Tritium was used as a conservative tracer to determine if the column packing procedure resulted in channeling or short-circuiting. For column studies that were designed to obtain breakthrough data for washed columns, the tritium tracer study was completed prior to spiking the radionuclide of interest onto the packed column. For studies designed to obtain breakthrough data for unwashed columns, the tracer study was performed after the target radionuclide had eluted from the column and the count rate was near background. In either case, tritium was introduced as a one-pore volume finite step spike onto the column and eluted from the column with five pore volumes of the water simulant.

Radionuclide Analysis

All radionuclide analyses were performed with an alpha/beta discriminating liquid scintillation counter (Model 1415, EG&G Wallac). Typically, a one mL aliquot was mixed with 10 mL of liquid scintillation cocktail (Wallac Hi-Safe II) and counted for ten minutes.

It was necessary to determine or verify aqueous phase oxidation states for some of the tests, especially those involving either plutonium(IV) or plutonium(V). Two methods were used, the HDEHP technique of Neu et al. (1994) and the DBM technique of Chopin et al. (1997). Details of the two techniques are given in Appendix E.

Data Analysis

The raw data from the column experiments consisted of radionuclide concentrations, C_i , in incremental effluent volumes, ΔV_i , collected at integrated volumes V_i . The concentrations were normalized by dividing by the concentration in the spike, C_0 , and the

integrated volume was converted to displaced pore volume (DPV) by dividing by the pore volume, V_p . Breakthrough curves were then plotted as normalized concentration as a function of time in DPV.

The breakthrough curves were characterized quantitatively by the retardation factor and corresponding fractional recovery. Retardation factors were calculated as the first moment of the travel time distribution,

$$R = \frac{\int C(V)V dV}{\int C(V)dV}$$

For unwashed columns, this becomes

$$R = \frac{\sum C_i V_i \Delta V}{\sum C_i \Delta V} - 0.5 \frac{V_s}{V_p} + 1$$

where V_s is volume of the spike. The second term in the expression occurs because the spike is introduced as a finite step and the third term occurs because the spike was the first pore volume introduced in the unwashed columns. For washed columns, the third term is deleted. Fractional recovery, f , was calculated from

$$f = \frac{\int_{V_1}^{V_2} C(V) dV}{C_0 \cdot V_s}$$

where V_1 and V_2 are the lower and upper bounds, respectively, of the portion of the breakthrough curve for which the recovery is calculated.

An estimate of the detection limit is shown on many of the breakthrough curves. This estimate is based on Currie's (Currie, 1968) equation,

$$LLD = 2.71 + 4.65\sqrt{B}$$

where LLD is the detection limit (net counts above background) and B is the number of background counts. Since this equation is strictly applicable to a single measurement, it is likely an overestimate when applied to breakthrough curves where trends are observed through a series of consecutive measurements.

4. COLUMN TEST VERIFICATION STUDIES

Tritium

Tritium tests were performed for five selected sets of column experiments to check for channeling. A total of 19 columns were tested. The breakthrough curves for 14 of these were normal in that the leading edge appeared at approximately one DPV, the trailing edge occurred at approximately two DPV, and the curves were symmetric. Presented in Figure 4.1 is one normal curve from each of the five selected sets of column experiments. The breakthrough curves for five of the columns were abnormal. For four of these, the leading edge appeared before one DPV and the curves were skewed to the right. These four curves are presented in Figure 4.2. The early appearance of the leading edge suggests channeling of water through a preferred flow path. Presented in Table 4.1 are fractional recoveries and retardation factors for the 19 tritium tests. It is interesting that the abnormal columns cannot be detected through retardation factor. The mean retardation factor for the normal columns (1.18 ± 0.04) was not significantly different from that for the abnormal columns (1.09 ± 0.16). This is because the early appearance of the breakthrough curve in the abnormal columns was offset by the tailing of the trailing edge. It is also interesting that the retardation factor for normal columns differed significantly from 1.0. The difference, which represents a volume of approximately 1 mL, seems too large to be the result of a systematic experimental bias. (The experimental data were corrected to account for the dead volume (0.5 to 1 mL) in tubing connecting the spike and the columns. No correction was made for the dead space between the tubing connector and the soil; however, this volume is less than 0.2 mL)

Strontium

In many of the actinide column tests, strontium was also included in the spiking solution. Although strontium is present in the SDA and its mobility in interbed is relevant in the site risk assessment, it was included in this study primarily as a form of quality control. The strontium breakthrough curves were used both as a basis for comparison with the actinide breakthrough curves and as a means for monitoring column-to-column variability, both hydraulic and geochemical. Presented in Figure 4.3 are four strontium breakthrough curves from four column

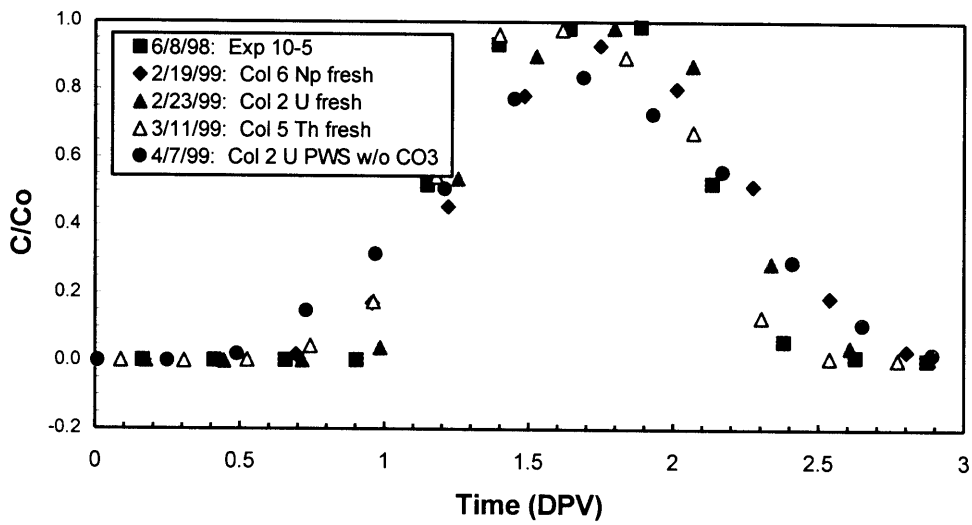


Figure 4.1. Tritium breakthrough curves

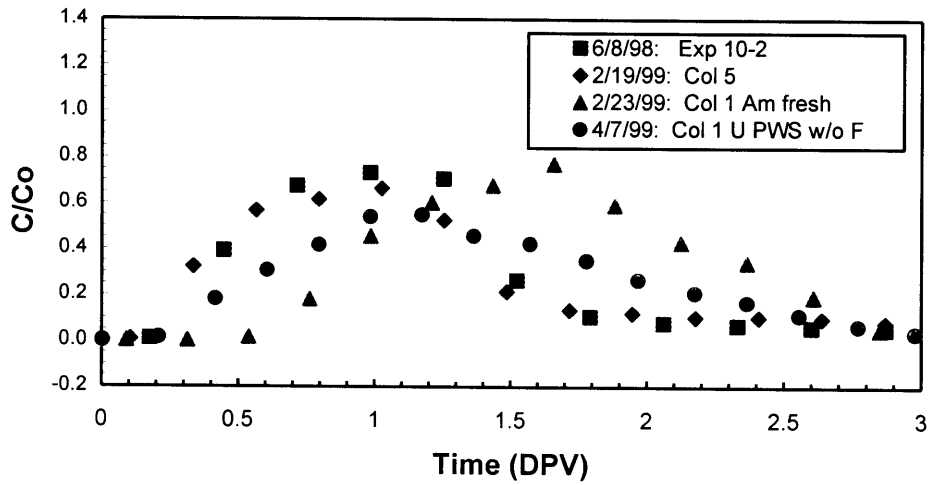


Figure 4.2. Tritium breakthrough curve exhibiting channeling

Table 4.1. Tritium Recoveries and Retardation Factors

Column	Recovery	Retardation Factor	Shape
6/18/98-Exp 10-1	0.79	1.12	Asymmetric peak
6/18/98-Exp 10-2	0.94	0.93	Early breakthrough & skewed right
6/18/98-Exp 10-3	0.99	1.20	OK
6/18/98-Exp 10-5	0.99	1.16	OK
2/19/99-Col 5	0.99	1.28	Early breakthrough & skewed right
2/19/99-Col 6-Np fresh	0.97	1.24	OK
2/19/99-Col 7-Np aged	0.99	1.18	OK
2/23/99-Col 1-Am fresh	0.98	1.16	Early breakthrough & skewed right
2/23/99-Col 2-U fresh	0.99	1.27	OK
2/23/99-Col 3-Am aged	1.01	1.23	OK
2/23/99-Col 4-U aged	0.98	1.21	OK
3/11/99-Col 5-Th fresh	0.96	1.12	OK
3/11/99-Col 6-Pu(IV) fresh	0.98	1.15	OK
3/11/99-Col 7-Th aged	1.00	1.15	OK
3/11/99-Col 8-Pu(IV) aged	0.97	1.18	OK
4/7/99-Col 1-U PWS w/o F	0.96	0.99	Early breakthrough & skewed right
4/7/99-Col 2-U PWS w/o CO ₃	1.01	1.17	OK
4/7/99-Col 3-U PWS w/o SO ₄	0.97	1.12	OK
4/7/99-Col 4-Np/Sr fast	0.98	1.14	OK

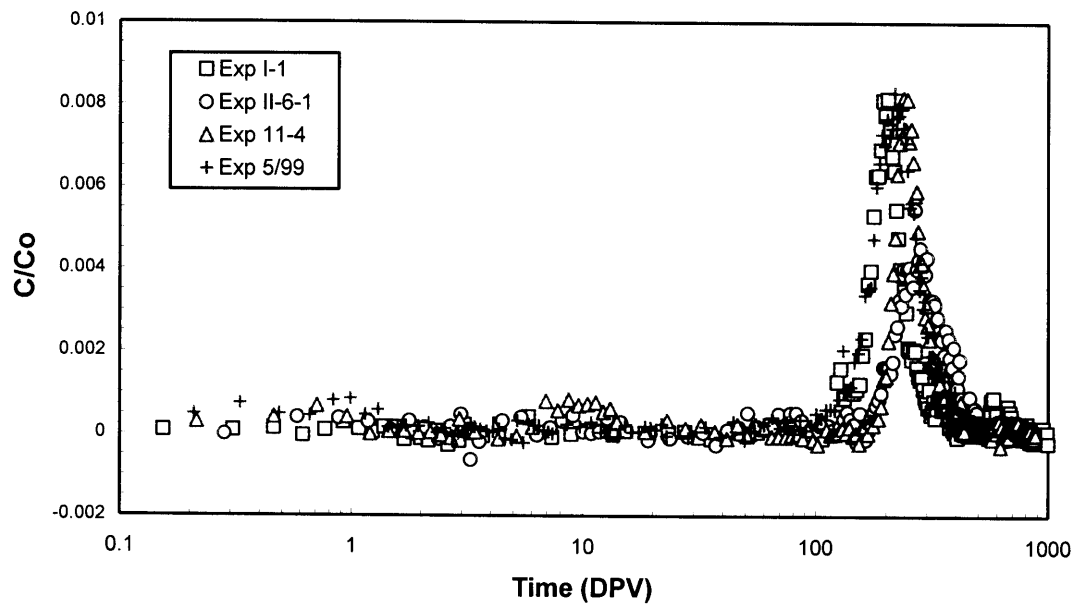


Figure 4.3. Strontium breakthrough curves

tests conducted at different times over the course of the study. Retardation factors and recoveries for these four tests along with those for the other strontium tests are given in Table 4.2. Strontium breakthrough was consistently characterized by a single peak in the 200–300 DPV range. Recoveries were generally within the limits of experimental uncertainty, which is estimated to be 10–15%. Retardation factors for the columns packed with the 106–250 μm size fraction were tightly grouped around 210 and were generally smaller than for the columns packed with the entire fraction smaller than 250 μm . This is likely due to the lower sorptive capacity per unit mass that would be expected for the larger sized particles. The recoveries, which ranged between 83 and 106%, and the retardation factors were not appreciably affected by either EDTA or washing of the column.

The consistency of the strontium behavior, regardless of the simulant, is not surprising from a chemical perspective. It merely reflects the fact that strontium is present as a divalent cation, which is stable with respect to EDTA, HA, carbonate, *etc.*, and that sorption is likely due to adsorption to negatively charged clay minerals. From an experimental quality control perspective, the consistency of the results is reassuring because it suggests some degree of uniformity over the course of the study of the physical/chemical characteristics of the interbed soil samples, the hydraulic properties of the columns, and the experimental procedure in general.

Mean Linear Velocity

Mean linear velocity for the C-D interbed is estimated to be on the order of 2 mm/d or 2×10^{-6} cm/s (Magnuson, 1998). In most of the column experiments, the mean linear velocity was approximately 8×10^{-3} cm/s. This is based on a volumetric flow rate of 0.3 cm^3/min , a pore volume of 6 cm^3 , and a column length of 8.0 cm. Thus, velocities in the column experiments were more than three orders of magnitude higher than the field estimates. This raised an obvious question regarding the effect of mean linear velocity on mobilities determined in column tests. Tests were conducted at both lower and higher velocities. The lowest velocity was 8×10^{-4} cm/s, which corresponds to the minimum flow rate possible with the peristaltic pumps. The results are presented in Figure 4.4, where retardation factor is given as a function of mean linear velocity for strontium, uranium, and neptunium. Although retardation factors increased when the mean linear velocity was reduced from 1×10^{-1} cm/s to 8×10^{-3} cm/s, there was very little change when it was further reduced to 8×10^{-4} cm/s. This flattening of the curve provides some

Table 4.2. Strontium Recoveries and Retardation Factors

Exp	Simulant	Recovery	Retardation Factor	Notes
I-1	PWS	1.05	250	Unwashed column
I-2	PWS	0.92	227	Washed column
I-3	PWS	1.06	280	Unwashed column
I-4	PWS	1.00	230	Washed column
II-6-1	PWS	0.92	294	Unwashed column
II-6-2	PWS	0.92	307	Unwashed column
II-7-1	PWS	0.89	204	Washed column; 106-250 μm
II-7-2	PWS	0.87	215	Washed column; 106-250 μm
II-7-3	PWS	0.89	209	Washed column; 106-250 μm
II-7-5	PWS	0.89	219	Washed column; 106-250 μm
II-11-2	PWS	0.94	315	Unwashed column
II-11-4	MPWS	0.84	289	Washed column
III-F-4	MPWS	0.83	240	Unwashed; 0.1 cm/s

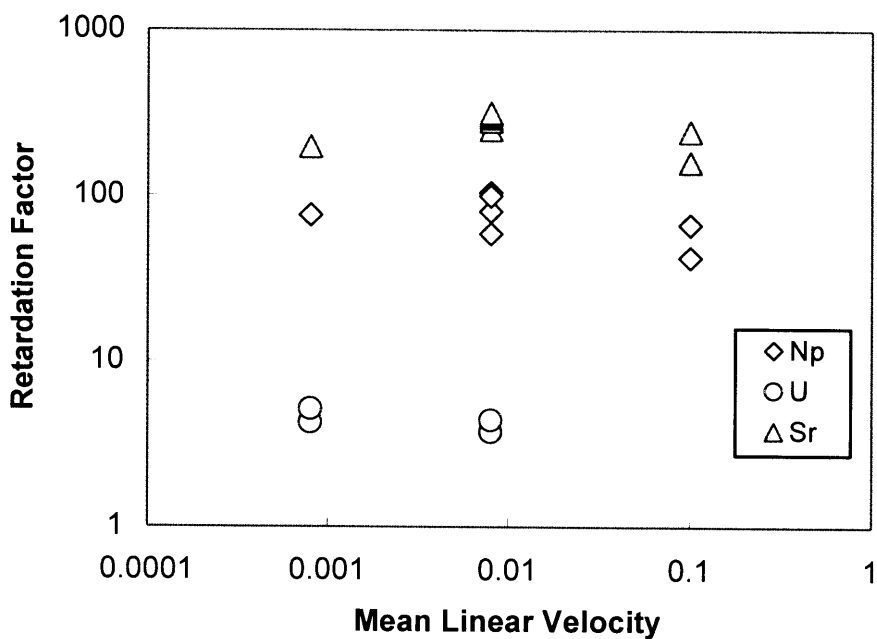


Figure 4.4. Retardation factor as a function of mean linear velocity for strontium, uranium, and neptunium

degree of confidence that mobilities obtained at the typical column test velocity of 8×10^{-3} cm/s are good predictors for lower velocities. However, this extrapolation is not without limitations. While the recoveries for strontium and uranium did not change (essentially 100%), there was a large reduction in recovery (from $\approx 65\%$ to $\approx 20\%$) for neptunium when the mean liner velocity was reduced from 8×10^{-3} to 8×10^{-4} cm/s. The reason for this, which is discussed later, is due to reduction of neptunium(V) to neptunium(IV) by the interbed. The kinetics of this reduction process is evidently much slower than that for the sorption process which governs strontium and uranium behavior.

Background Radiation

For the column tests, there are two sources of background radiation. One is the extrinsic radiation that is inherent in any radiological measurement and is independent of the experiment. The extrinsic background was determined by counting samples of the simulants used in the studies. The extrinsic background for the range of alpha energies relevant in this study was 7.5×10^{-4} (CPM/mL)/channel.

The other type of background, referred to here as intrinsic, is due to natural radioactivity in the sedimentary interbed which is leached from the column during the course of the experiment and is subsequently detected when the fractions are analyzed. Intrinsic background was determined by following the normal column test procedure but with the spike excluded. Presented in Figure 4.5 are data for the PWS (2 experiments) and the MPWS (1 experiment). The ordinate is net count rate (after subtraction of extrinsic background) normalized by the number of channels in the region of interest. Each data point is the mean of five measurements of each effluent fraction. Intrinsic background was elevated for the first three DPV, after which it did not differ significantly from zero. In addition, it was the same for both the PWS and the MPWS. The mean of intrinsic background for the first three DPV was 1.72×10^{-3} (CPM/mL)/channel.

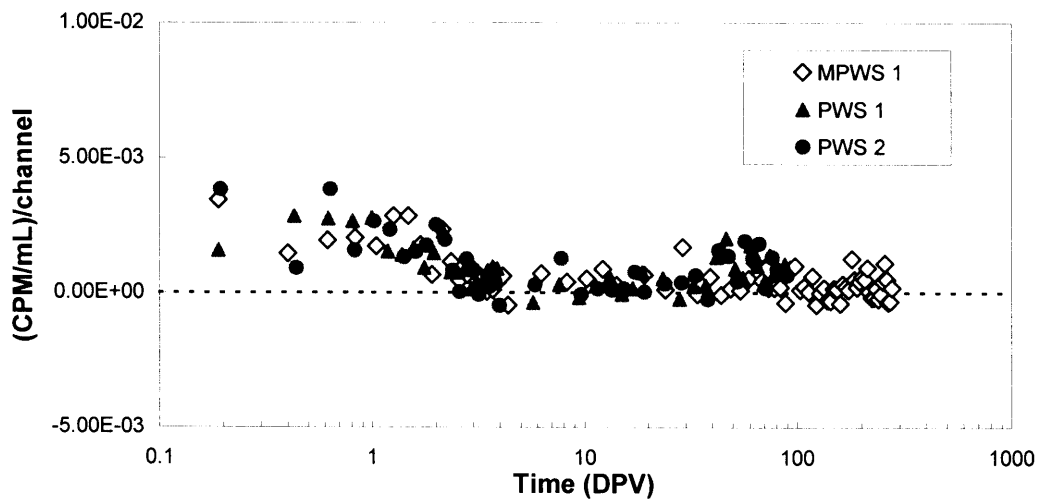


Figure 4.5. Intrinsic background

5. RADIONUCLIDE MOBILITIES

Americium

Breakthrough curves for americium under the influence of the PWS (*i.e.* with HA and EDTA) (solid circles) are given in Figure 5.1. The dashed line is the ratio of C/C_0 approximately corresponding to background (extrinsic and intrinsic). The breakthrough curves were substantially different from those presented in the previous section for strontium. Whereas the strontium breakthrough curves were characterized by a single peak containing essentially all of the activity in the spike, the americium curve was characterized by three fractions having distinctly different mobilities. There was a very small, high mobility component ($\ll 1\%$) that emerged from the column within the first few pore volumes, an intermediate mobility component ($\approx 50\%$) that emerged between 3 and 500 pore volumes, and a low mobility component ($\approx 50\%$) that did not emerge and was retained in the first 3 cm of the column. It is convenient to operationally define the fraction emerging in less than 3 DPV as high mobility, 3-500 DPV as intermediate mobility, and greater than 500 DPV as low mobility. Since similar behavior was observed for thorium, plutonium(IV), and neptunium, these definitions are also applied to their behavior, although the appropriate upper limit for the low mobility component varies somewhat.

Also shown in Figure 5.1 are breakthrough curves for americium under the influence of the modified perched water simulant (MPWS), *i.e.* with HA and EDTA removed. Two tests were conducted, one with a fresh spike and one with a spike aged for 24 hours. The breakthrough curves for the two spikes were essentially the same, and they were very similar to the PWS curve for the first few pore volumes. However, they differed dramatically from the PWS curve between 3 and 500 DPV, where the intermediate mobility component almost disappeared. The fractions and retardation factors for the intermediate mobility component are compared in Table 5.1.

The high mobility portion of the breakthrough curves is expanded in Figure 5.2, where data from a total of six experiments are presented. The additional data include two replicates of the fresh spike and an experiment in which the spike concentration was increased by approximately a factor of ten (denoted "high C_0 "). The breakthrough curves in the high mobility region and the recoveries for the high mobility component (Table 5.2) were surprisingly reproducible even though the concentrations in the effluent were a

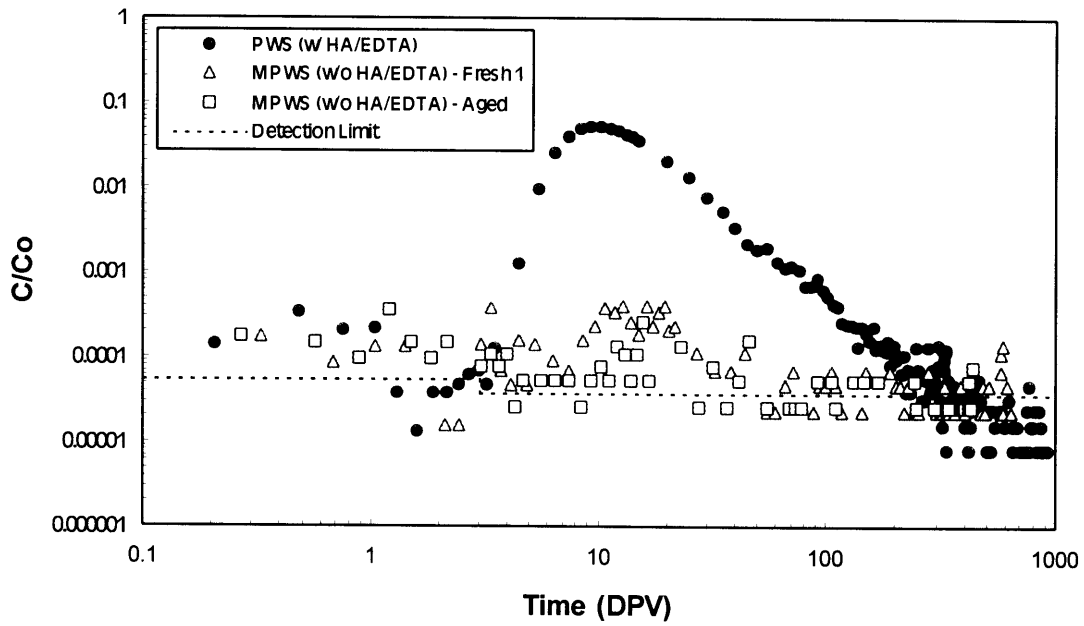


Figure 5.1. Americium breakthrough curves

Table 5.1. Recoveries and Retardation Factors for the Americium Intermediate Mobility Component

Simulant	Recovery (3–500 DPV)	Retardation Factor
PWS	0.5000	16
MPWS– Fresh Spike	0.0012	18
MPWS– Aged Spike	0.0003	18

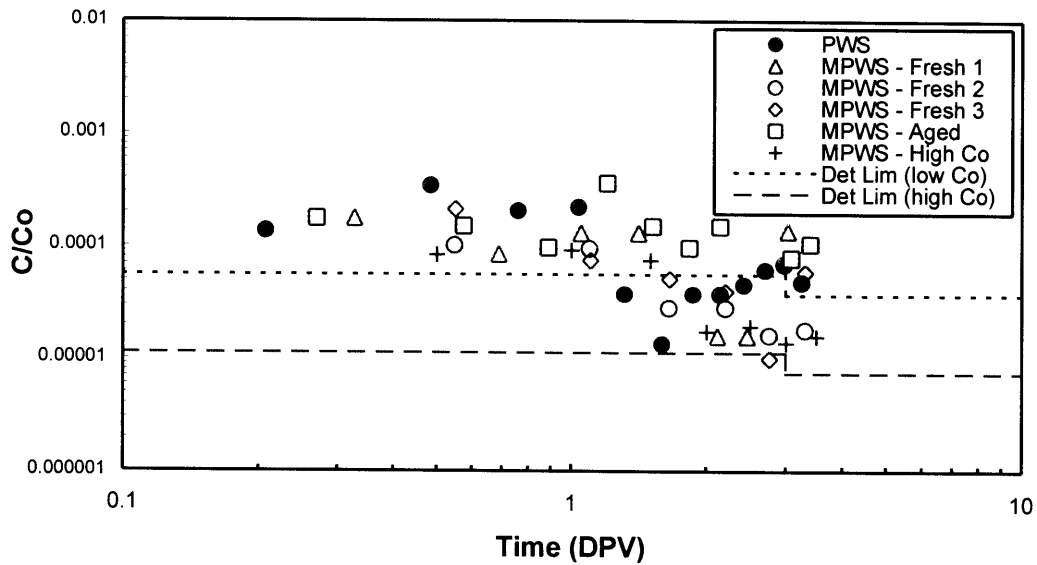


Figure 5.2. Expanded view of high mobility time period for americium

Table 5.2. Recoveries for the Americium High Mobility Component

Simulant	Recovery (<3 DPV)
PWS	0.00023
MPWS – Fresh Spike (1)	0.00031
MPWS – Aged Spike	0.00041
MPWS – Fresh Spike (2)	0.00013
MPWS – Fresh Spike (3)	0.00020
MPWS High C_0	0.00013

factor of 10,000 lower than those in the spike and there was considerable scatter in the data. Two detection limits are included in the graph, one for experiments conducted with the typical spike concentration (labeled “low C_0 ”) and one for the experiment conducted with an elevated spike concentration (labeled “high C_0 ”). Below 1 DPV, the concentrations in the “high C_0 ” experiment were almost an order of magnitude above the detection limit. The “high C_0 ” data resulted from an experiment to improve the precision of the high mobility portion of the breakthrough curve by increasing the americium concentration in the spike by an order of magnitude. The results are shown in Figure 5.3, where uncertainty estimates due to counting error (one standard deviation) are included. These data confirmed that the high mobility component was statistically different from background. Here, the C/C_0 corresponding to background was approximately 1×10^{-6} , and the effluent concentrations in the first 3 DPV were between one and two orders of magnitude higher. Also included in Figure 5.3 are analyses of selected effluent fractions filtered to 3 nm. The filtered and unfiltered concentrations were essentially the same, indicating that the high mobility component was either in a soluble or very small particulate (<3 nm) form.

From a predominance area diagram for the americium (III) hydroxide-carbonate system (E_H vs pH) (Appendix A), americium is predicted to exist as solid $Am_2(CO_3)_3$ species. Batch filtration experiments (Figure 5.4 and Appendix F) were qualitatively consistent with these predictions as the americium was quickly converted to a particulate form. Immediately following preparation of the spike, over 80% of the americium was in a particulate form larger than 3 nm, and after 24 hours, the fraction increased to almost 100%.

These data suggest the following conceptual model for americium. Americium transport in the columns is driven by its extremely low solubility and the formation of americium carbonate precipitates which are likely filtered mechanically¹. The high mobility component could be either soluble $Am_2(CO_3)_3$ or a particulate form which penetrates the soil matrix.

Thorium and Plutonium(IV)

The breakthrough curves for thorium under the influence of the PWS (solid circles in

¹ In a series of experiments described in Appendix D, it was observed that colloids, both “true” and “associated”, are attenuated by the soil matrix.

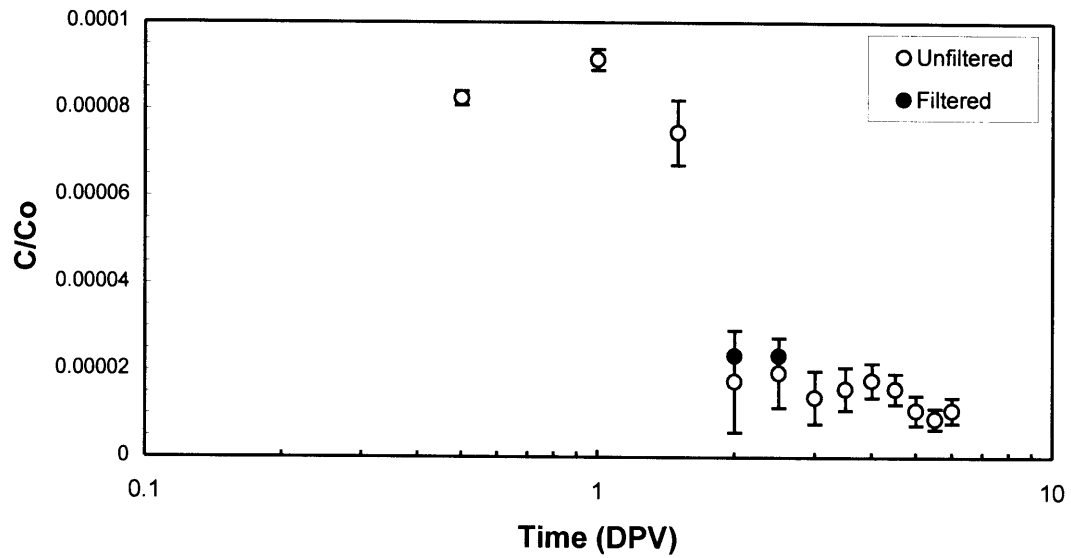


Figure 5.3. Americium high mobility component for an elevated C_0 – unfiltered and filtered (> 3 nm) analyses

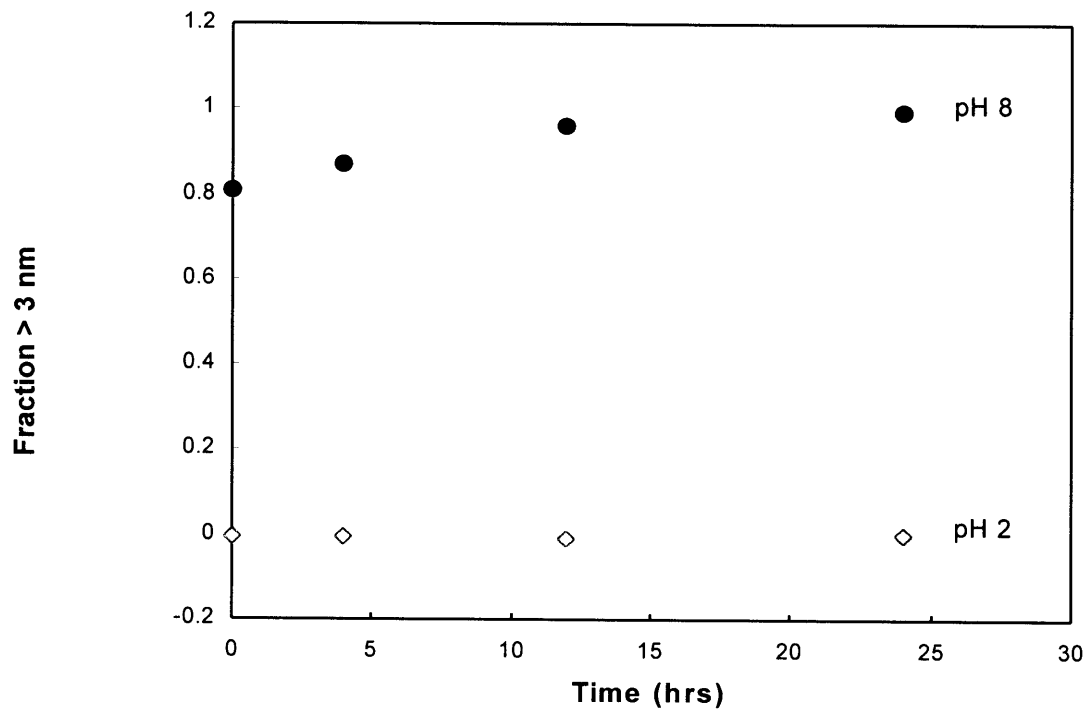


Figure 5.4. Particulate fraction as a function of aging time for americium

Figure 5.5) and MPWS (open symbols in Figure 5.5) were similar to americium. For the PWS, there was a very small, high mobility component ($\ll 1\%$) that emerged from the column within the first few pore volumes and a large intermediate mobility component that emerged between 3 and 500 pore volumes. The remainder of the thorium was retained in the column. For the MPWS, the intermediate mobility component almost disappeared, with the fractional recovery decreasing from almost 0.3 to less than 0.001 (Table 5.3). The high mobility component also declined, with the concentrations falling below the estimate of the detection limit. However, as noted previously, the detection limit is likely an over estimate. When the 0.1 to 10 DPV time period is expanded, and results of additional experiments focused on this region are added to the two experiments shown in Figure 5.5, the breakthrough curves are surprisingly reproducible (Figure 5.6). This reproducibility is also evident in the fractional recoveries (Table 5.4), which vary over less than an order of magnitude for the MPWS (with the normal silica concentration). If thorium from the spike was absent from the effluent, the fractional recoveries would vary about zero. More conclusive evidence regarding the existence of a high mobility component for thorium is found in the "high C_0 " experiment, where there was a well-defined peak extending from 1 to 6 DPV (Figures 5.6 and 5.7), and the recovery showed reasonable agreement with those for the other MPWS experiments (Table 5.4). These results suggest a high mobility component for thorium on the order of 10^{-5} , and the filtration analyses indicate that all of it was in a particulate form larger than 3 nm. This is consistent with the batch filtration results (Figure 5.8), which showed thorium to be entirely in a particulate form almost immediately after preparation of the spike. Since the PWS and MPWS were both oversaturated with respect to silica, it is possible that the particulate thorium was actually a thorium species sorbed to SiO_2 precipitates. Also included in Table 5.4 are results for experiments conducted with silica concentrations below saturation (denoted as "low Si"). The fractional recoveries for these tests were higher than for the tests with silica above saturation, suggesting that production of the thorium high mobility component may involve competition among more than one process.

The breakthrough curves for plutonium(IV) (Figure 5.9) under the influence of the PWS (solid symbols) and MPWS (open symbols) were similar to thorium and americium. There was a very small, high mobility component ($\ll 1\%$) that emerged from the column within the first few pore volumes and a large intermediate mobility component ($\approx 50\%$)

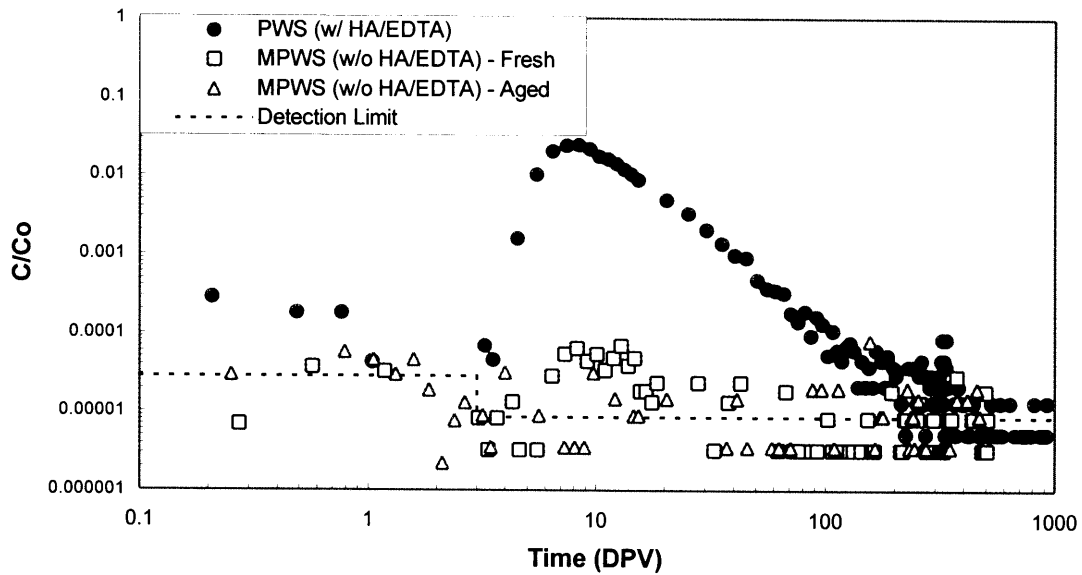


Figure 5.5. Thorium breakthrough curves

Table 5.3. Recoveries and Retardation Factors for the Thorium Intermediate Mobility Component

Simulant	Recovery (2.5 – 500 DPV)	Retardation Factor
PWS	0.27000	23
MPWS – Fresh Spike	0.00088	NA*
MPWS – Aged Spike	0.00070	NA*

*NA – not applicable

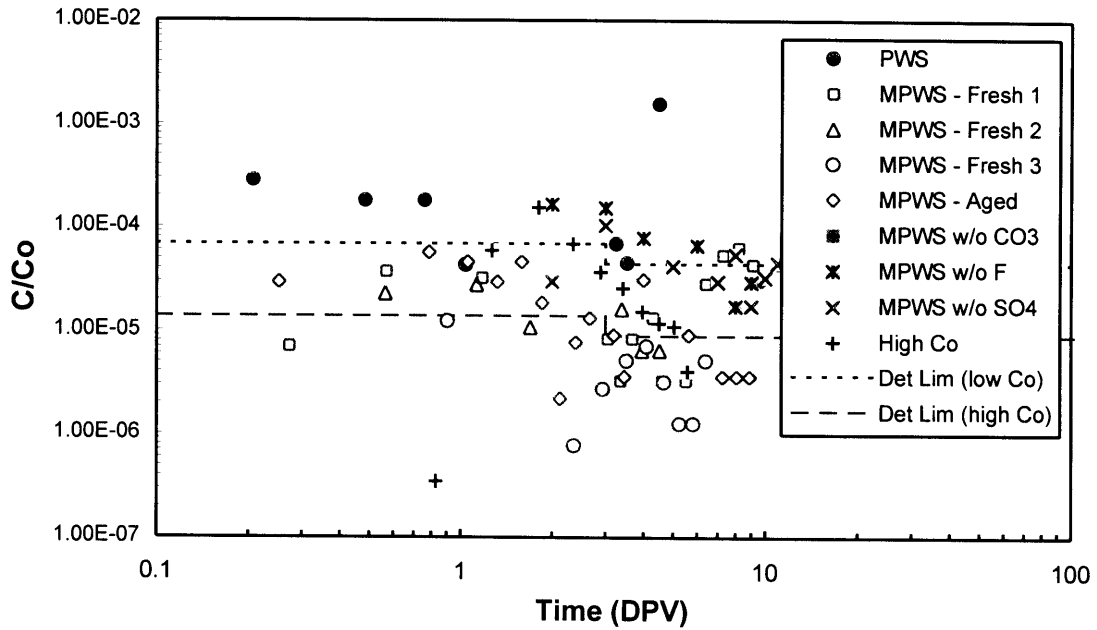


Figure 5.6 Expanded view of high mobility time period for thorium

Table 5.4. Recoveries for the Thorium High Mobility Component

Simulant	Recovery (<6 DPV)
PWS	0.000140
MPWS – Fresh Spike 1	0.000009
MPWS – Fresh Spike 2	0.000032
MPWS – Fresh Spike 3	0.000013
MPWS – Aged Spike	0.000063
MPWS – High C ₀	0.000014
MPWS w/o CO ₃ ²⁻ (low Si)	0.000100
MPWS w/o F ⁻ (low Si)	0.000250
MPWS w/o SO ₄ ²⁻ (low Si)	0.000180

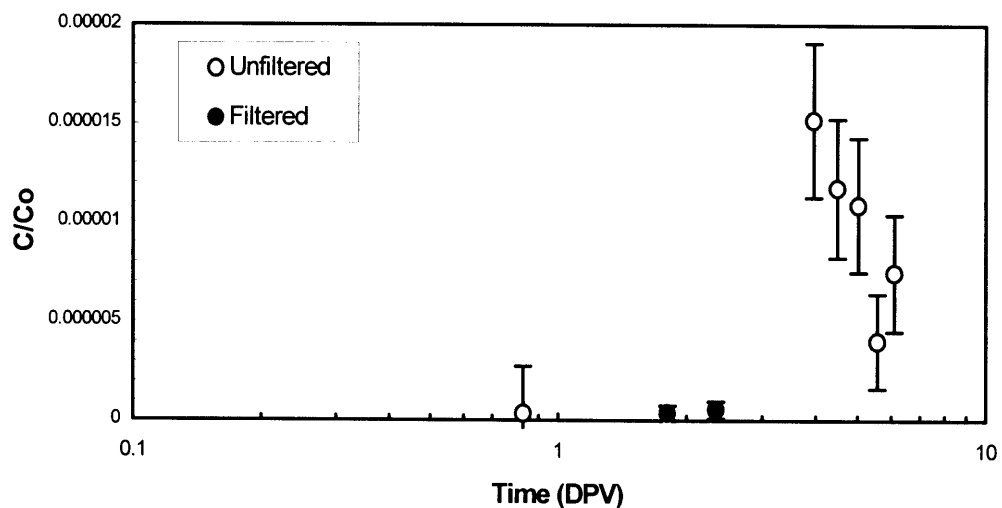


Figure 5.7. Thorium high mobility component for an elevated C_0 – unfiltered and filtered (> 3 nm) analyses

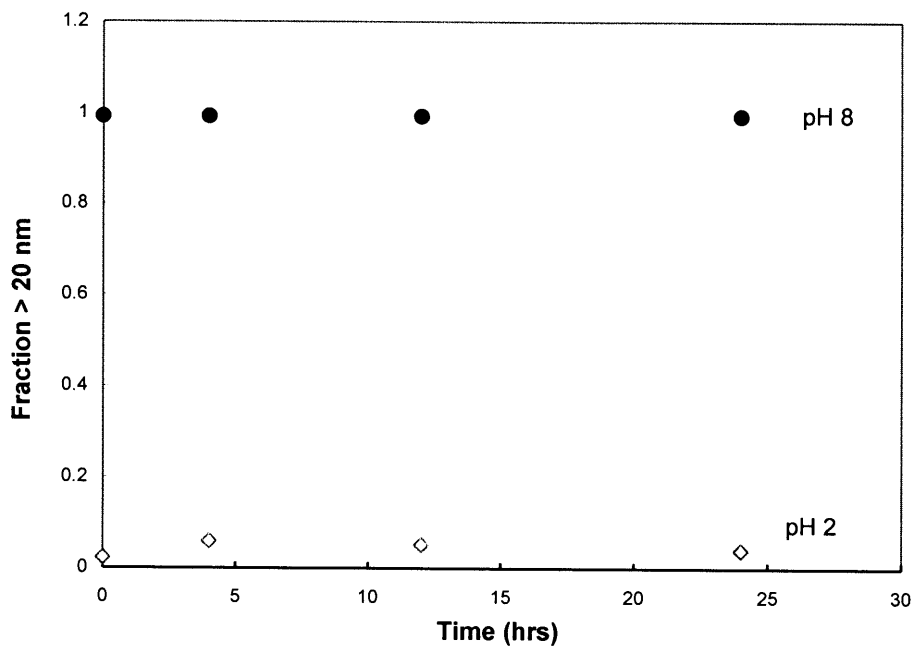


Figure 5.8. Particulate fraction as a function of aging time for thorium

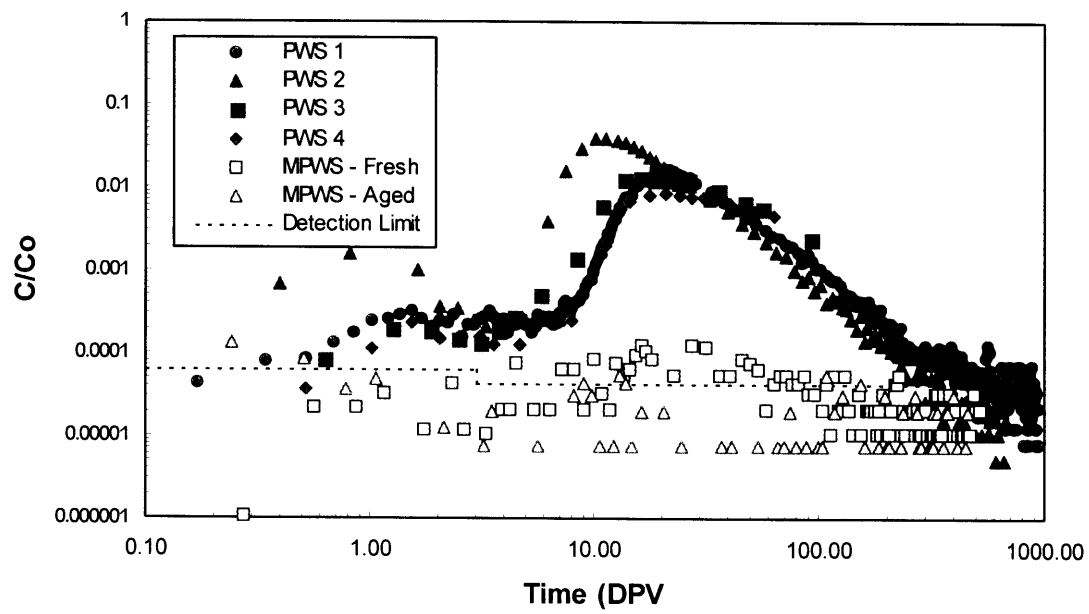


Figure 5.9. Plutonium(IV) breakthrough curves

that emerged between 3 and 500 pore volumes. The remainder of the plutonium(IV) did not emerge from the column within the first 1000 DPV. For the MPWS, distinct high and intermediate mobility components were not observed, although there appeared to be uniform, non-zero breakthrough throughout the experiment. Recoveries and retardation factors for the 3–1000 DPV time period are given in Table 5.5.

The 0.1 to 10 DPV time period is expanded in Figure 5.10 for the PWS and in Figure 5.11 for the MPWS. For the PWS experiments, the measurements during this time period were above the detection limit and were about an order of magnitude above background. The recoveries varied considerably, ranging from 10^{-3} to 10^{-5} (Table 5.6). For the MPWS experiments, the measurements were generally below the conservative estimate of the detection limit. However, in the “high C_0 ” experiment, there was a statistically significant peak beginning between 1 and 2 DPV (Figure 5.12), and the recovery was consistent with those from the other MPWS experiments, which were approximately an order of magnitude smaller than for the PWS. The recoveries were also consistent with those for thorium. However, unlike thorium, the plutonium(IV) high mobility form could not be definitively characterized as being particulate. In the batch filtration experiments (Figure 5.13 and Appendix F), approximately 60% was larger than 20 nm; and in the “high C_0 ” experiments, approximately 20–30% of the plutonium(IV) in the column effluent was larger than 12 nm. Speciation modeling of the spiked PWS (Meyers, 1999) within an E_H -pH envelop typical of natural waters predicted $\text{Pu}(\text{OH})_4$ to be the predominant solid phase. Modeling results are presented in Appendix G.

Neptunium and Plutonium(V)

Breakthrough curves for neptunium under the influence of the PWS (solid symbols in Figure 5.14) were similar to americium, thorium and plutonium(IV) in that they were characterized by a small component ($\ll 1\%$) with high mobility and a large component ($\approx 50\%$) with intermediate mobility. However, there were differences as well. One difference is that the tailing edge of neptunium’s intermediate mobility component did not decrease monotonically but instead had a small peak around 100 DPV. Also, neptunium’s high mobility component took the form of a well-defined peak, and the recovery was considerably larger than those for americium, thorium, or plutonium(IV). Even greater differences were observed for the MPWS. Whereas the intermediate mobility component for americium, thorium, and plutonium(IV) almost disappeared, it

Table 5.5. Recoveries and Retardation Factors for the Plutonium(IV) Intermediate Mobility Component

Simulant	Recovery (3 – 1000 DPV)	Retardation Factor
PWS 1	0.610	79
PWS 2	0.620	35
MPWS 1	0.012	N/A
MPWS 2	0.006	N/A

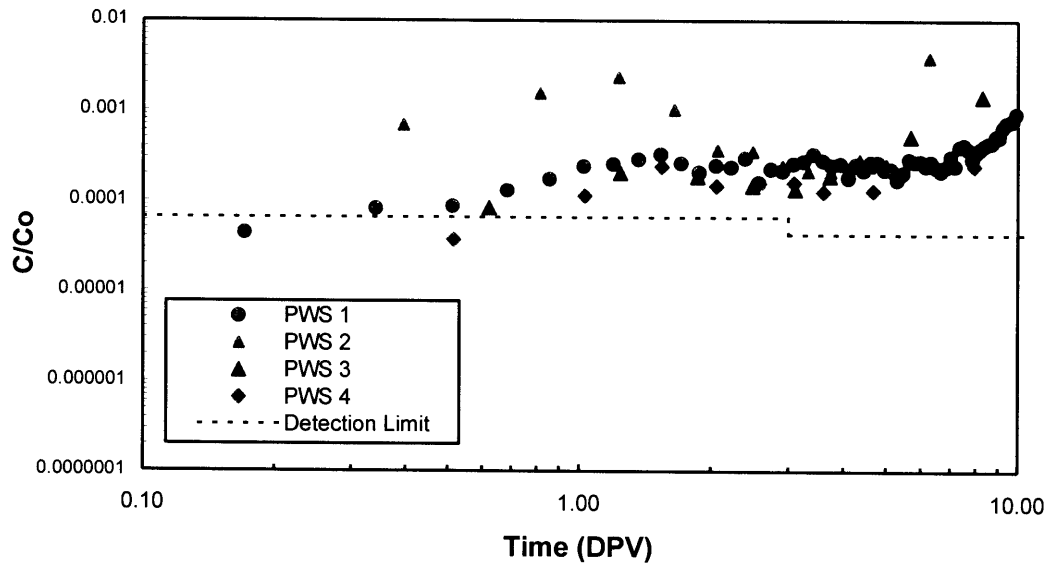


Figure 5.10. Expanded view of high mobility time period for plutonium(IV) for the PWS

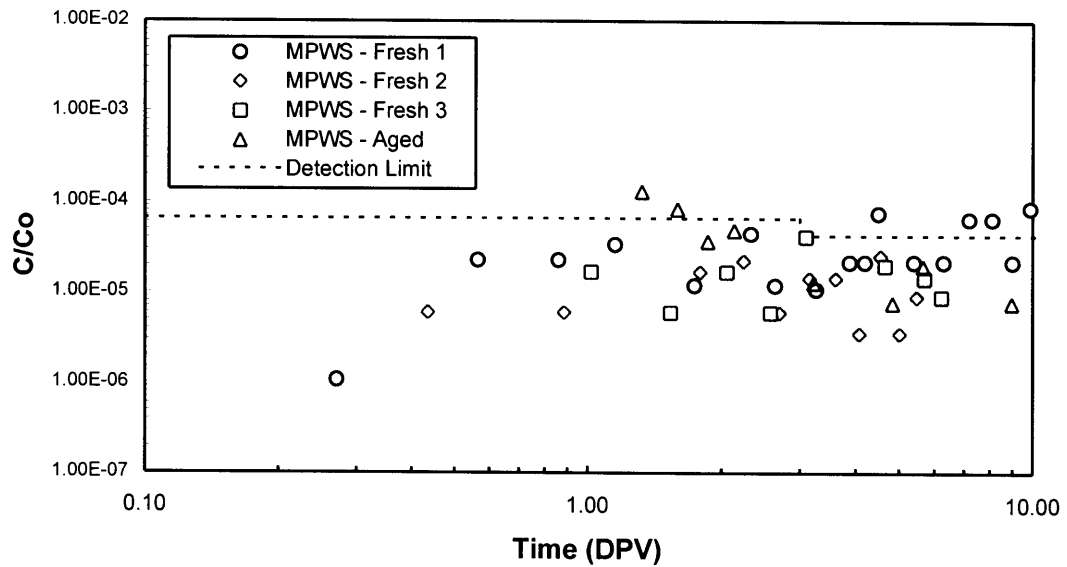


Figure 5.11. Expanded view of high mobility time period for plutonium(IV) for the MPWS

Table 5.6. Recoveries for the Plutonium(IV) High Mobility Component

Simulant	Recovery (< 5 DPV)
PWS 1	0.000700
PWS 2	0.002300
PWS 3	0.000340
PWS 4	0.000038
MPWS – Fresh 1	0.000030
MPWS – Fresh 2	0.000030
MPWS – Fresh 3	0.000017
MPWS – Aged	0.000050
MPWS – High C ₀	0.000028

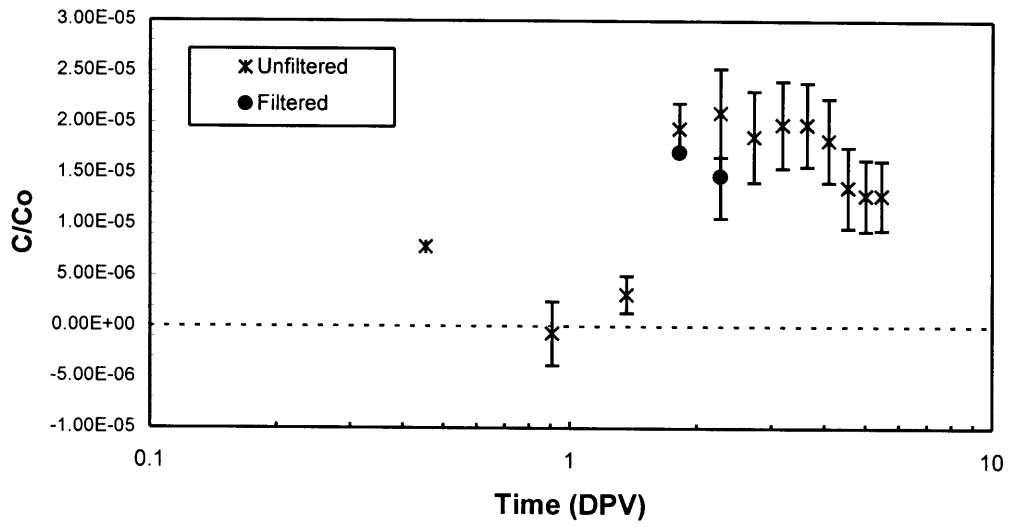


Figure 5.12. Plutonium(IV) high mobility component for an elevated C_0 – unfiltered and filtered (> 12 nm) analyses

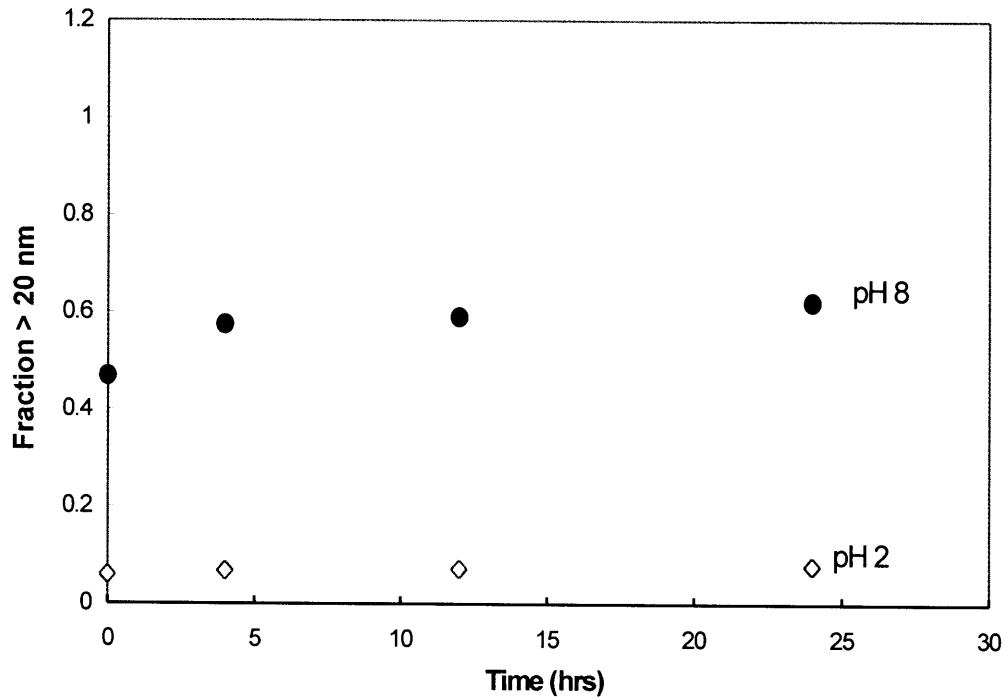


Figure 5.13. Particulate fraction as a function of aging time for plutonium(IV)

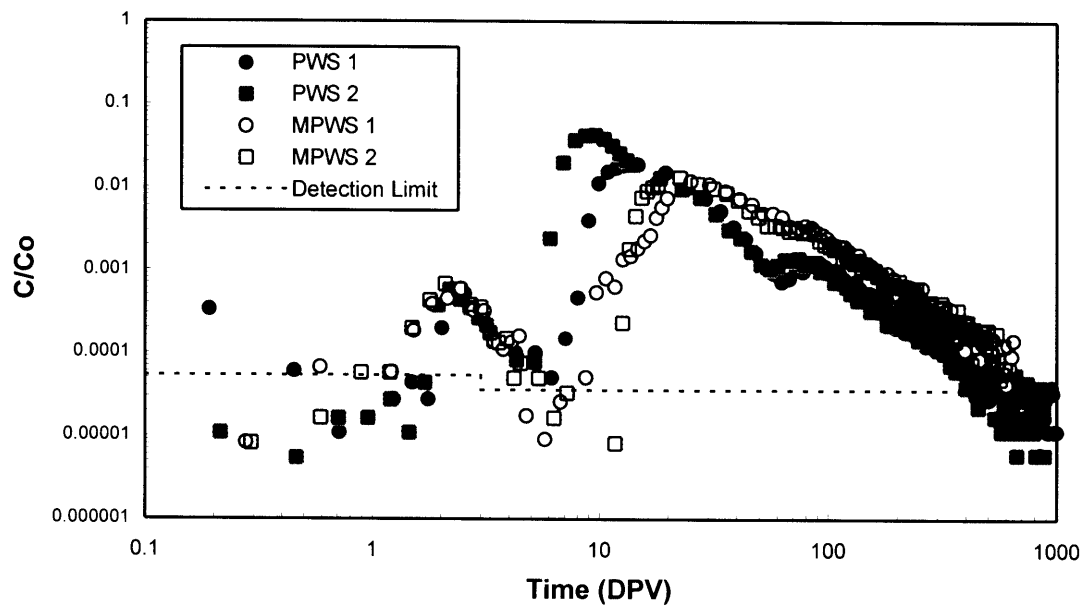


Figure 5.14. Neptunium breakthrough curves

showed little change for neptunium. Because of this, tests were conducted in which the ligands most likely to form complexes with neptunium were systematically removed from the PWS. Presented in Figure 5.15 are breakthrough curves for the PWS with CO_3^{2-} , F^- , and SO_4^{2-} removed independently. Qualitatively, there was very little change with the removal of F^- or SO_4^{2-} other than slight lateral shifts of the curves. However, removal of CO_3^{2-} resulted in striking changes. The high mobility component totally disappeared, and there was a significant change in the shape of the intermediate mobility component. Rather than peaking in the 10–30 DPV range, the intermediate mobility peaked near 100 DPV. In addition, the tailing edge decreased monotonically. These results suggested that CO_3^{2-} may play a role both in the high mobility component and in the 10–30 DPV peak in the intermediate mobility component.

To determine if either F^- or SO_4^{2-} plays a role in the 100 DPV peak, column experiments were conducted in which CO_3^{2-} was removed from the MPWS in combination with F^- and in combination with SO_4^{2-} . The breakthrough curves for these experiments are presented in Figure 5.16. The 100 DPV peak was still prominent, indicating that it is influenced by neither F^- nor SO_4^{2-} . Although these experiments were negative with respect to the 100 DPV peak, they may have revealed some more subtle influences. For the test with F^- and CO_3^{2-} removed, there was a peak during the 10–30 DPV time period (somewhat smaller than those in Figures 5.14 and 5.15). Yet, there was no peak when SO_4^{2-} was present along with F^- (and CO_3^{2-} removed) in Figure 5.15. This could occur if F^- is a stronger complexing agent than SO_4^{2-} with neptunium. The lack of sufficient thermodynamic data preclude modeling of the system. However, in the background section it is noted that the relative complexing strengths of common ligands with the actinides are ordered as $\text{OH}^- > \text{F}^- > \text{SO}_4^{2-}$. This suggests the possibility that the 100 DPV peak might be due to a neptunium hydroxide complex.

The expanded breakthrough curves are presented in Figure 5.17 and the “high C_0 ” curve is presented in Figure 5.18. In Figure 5.17, the circles and polygons represent experiments with CO_3^{2-} present and the various crossed symbols represent experiments with CO_3^{2-} removed. These data firmly establish a link between the high mobility component and CO_3^{2-} . The high mobility recovery was reproducible, ranging between

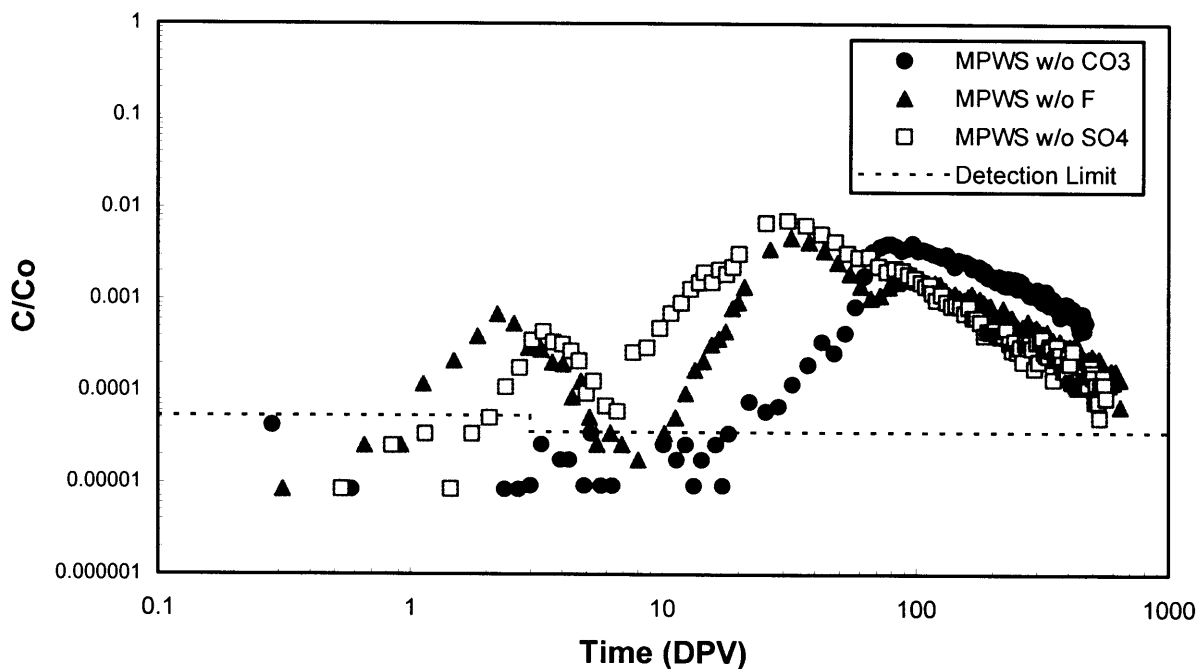


Figure 5.15. Effect of removing CO_3^{2-} , F^- , and SO_4^{2-} on neptunium breakthrough curves

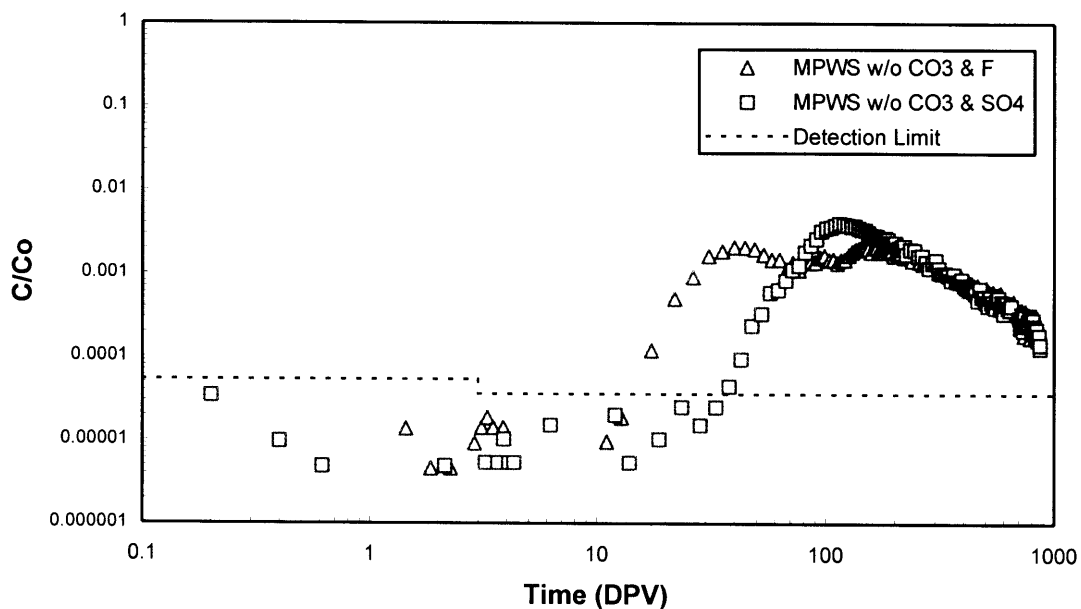


Figure 5.16. Effect of removing CO_3^{2-} , CO_3^{2-} & F^- , and CO_3^{2-} & SO_4^{2-} on neptunium breakthrough curves

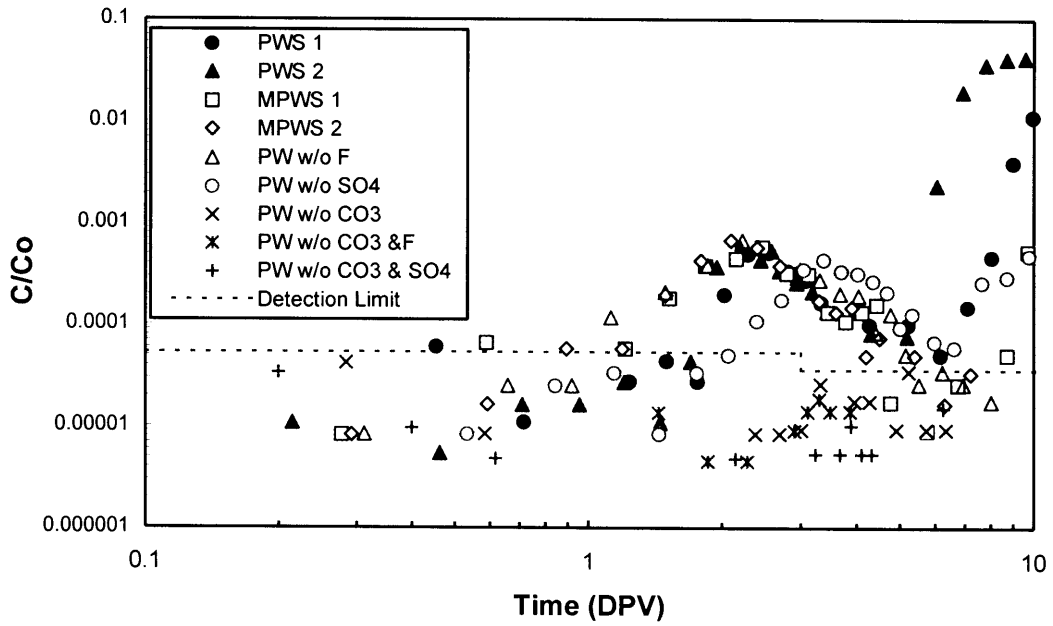


Figure 5.17. Expanded view of high mobility time period for neptunium

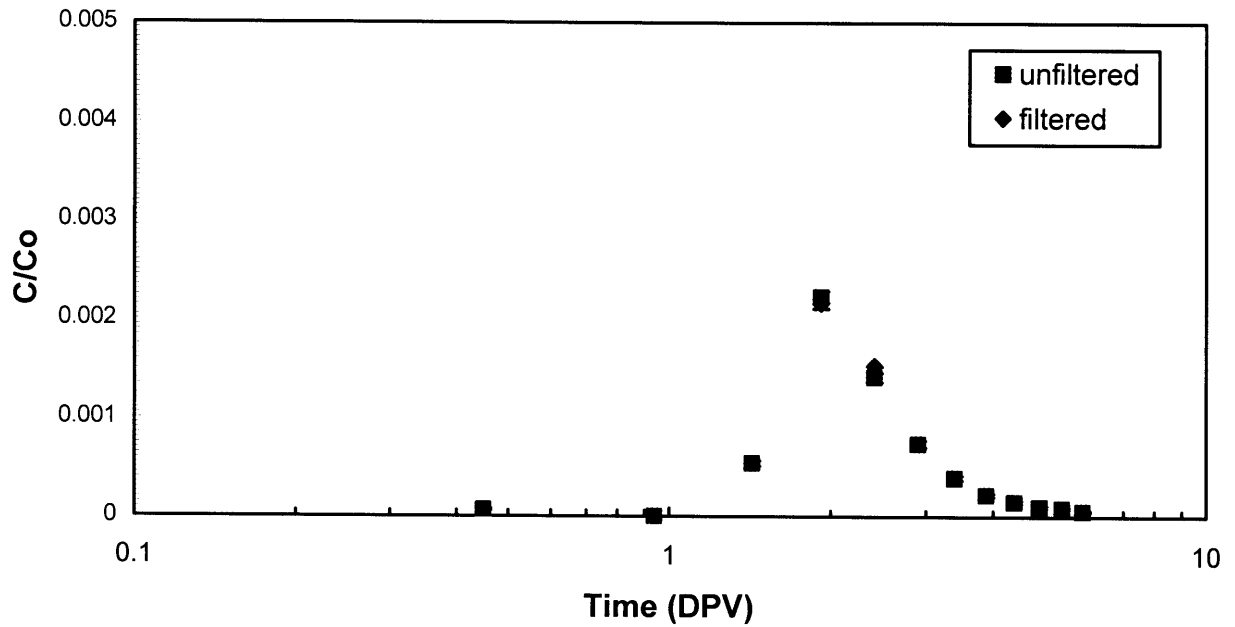


Figure 5.18. Neptunium high mobility component for an elevated C_0 – unfiltered and filtered (> 12 nm) analyses

0.00078 and 0.0010, and it was not affected by the removal of HA/EDTA, F⁻, or SO₄²⁻ (Table 5.7). Retardation factors for the high mobility component varied from 1.3 to 3.8. The “high C₀” data for neptunium (Figure 5.18), similar to americium, illustrate the significance of the high mobility component. Also similar to americium, the filtered and unfiltered concentrations were the same, indicating that the high mobility component is either soluble or very small particles (<12 nm).

Although the retardation factors for the intermediate mobility component were quite variable (Table 5.7), they are consistent with the qualitative observations above; *i.e.* they increased when CO₃²⁻ was removed. The recoveries for the intermediate mobility component were also quite variable, due both to variability in the eluent chemistries and to truncation of some experiments before the effluent concentrations returned to background levels. The latter is clearly evident in Figure 5.16, where the effluent concentrations were more than an order of magnitude above background (5 x 10⁻⁶) when the experiments were terminated. In experiments which were not terminated until background was reached the maximum recovery was 80%, and the typical recovery was around 60%. This implies recoveries for the low mobility component to be between 20 and 40%. One hypothesis for the low mobility component is reduction of some of the neptunium(V) to neptunium(IV) by reduced iron or manganese in the interbed material. Neptunium(IV) is highly insoluble and would have very low mobility (Brookins, 1988). To test this hypothesis, experiments were conducted under oxidizing conditions as described in the Materials and Methods section. The breakthrough curves for these tests are presented in Figure 5.19. These curves are similar to those in Figure 5.15 with the exception that, within the limits of experimental uncertainty, all of the neptunium in the spike was recovered (Table 5.8). This is supportive of the neptunium(V) to neptunium(IV) reduction hypothesis.

Presented in Figure 5.20 are column effluent data for plutonium(V) for the PWS and for the MPWS. Also included are background data obtained for an unspiked column. The ordinate is the gross count rate rather than the normalized concentration to facilitate comparisons with background. In contrast to neptunium(V), there was very little breakthrough of plutonium(V) - over 99.99% of the plutonium(V) was retained in the columns. This notwithstanding, there were sporadic releases of very small amounts of plutonium from the columns throughout the duration of the experiments. Since these releases were not characterized, we refrain from speculating about their physical/chemical form. However, this behavior is consistent with the sporadic

Table 5.7. Retardation Factors and Recoveries for Neptunium

Simulant	High Mobility			Intermediate Mobility	
	Range	R	Recovery	R	Recovery
PWS 1	< 7 DPV	2.5	0.00100	80	0.57
PWS 2	< 5 DPV	2.2	0.00078	58	0.67
MPWS 1	< 5 DPV	2.1	0.00093	104	0.68
MPWS 2	< 7 DPV	1.3	0.00100	99	0.64
MPWS w/o F ⁻	< 6 DPV	2.7	0.00100	156	0.40
MPWS w/o SO ₄ ²⁻	< 7 DPV	3.8	0.00078	97	0.41
MPWS w/o CO ₃ ²⁻	N/A	N/A	0.0	195	0.69
MPWS w/o CO ₃ ²⁻ & F ⁻	N/A	N/A	0.0	237	0.67
MPWS w/o CO ₃ ²⁻ & SO ₄ ²⁻	N/A	N/A	0.0	310	0.81

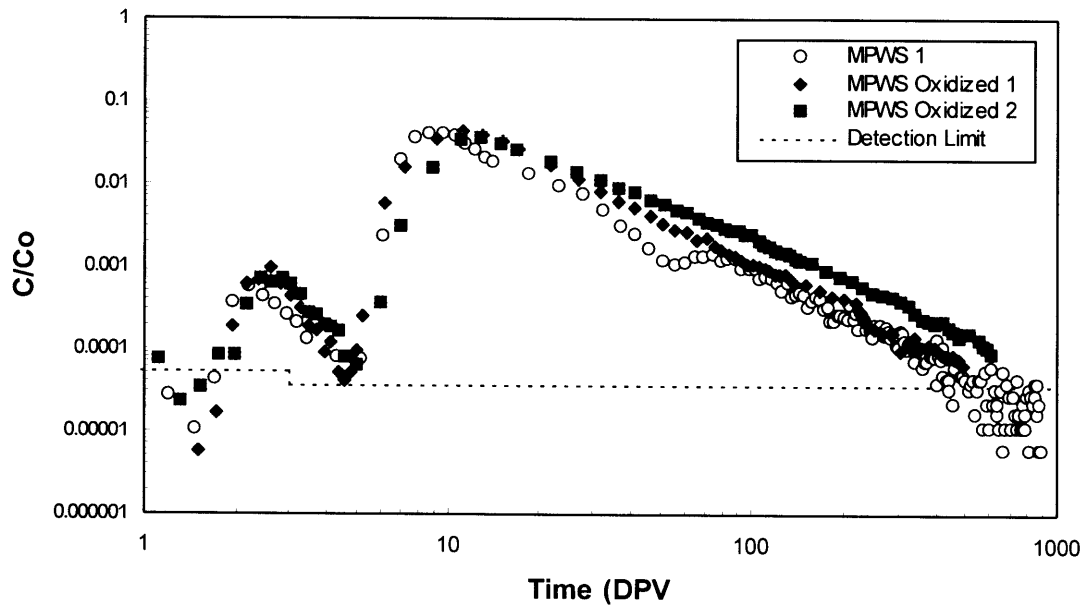


Figure 5.19. Neptunium breakthrough curves under oxidizing conditions

Table 5.8 Retardation Factors and Recoveries for Neptunium Under Oxidizing Conditions

Experiment	High Mobility Component		Intermediate Mobility Component	
	R	F	R	F
Oxidizing #1	1.6	0.0010	265	0.90
Oxidizing #2	1.5	0.0013	434	1.07

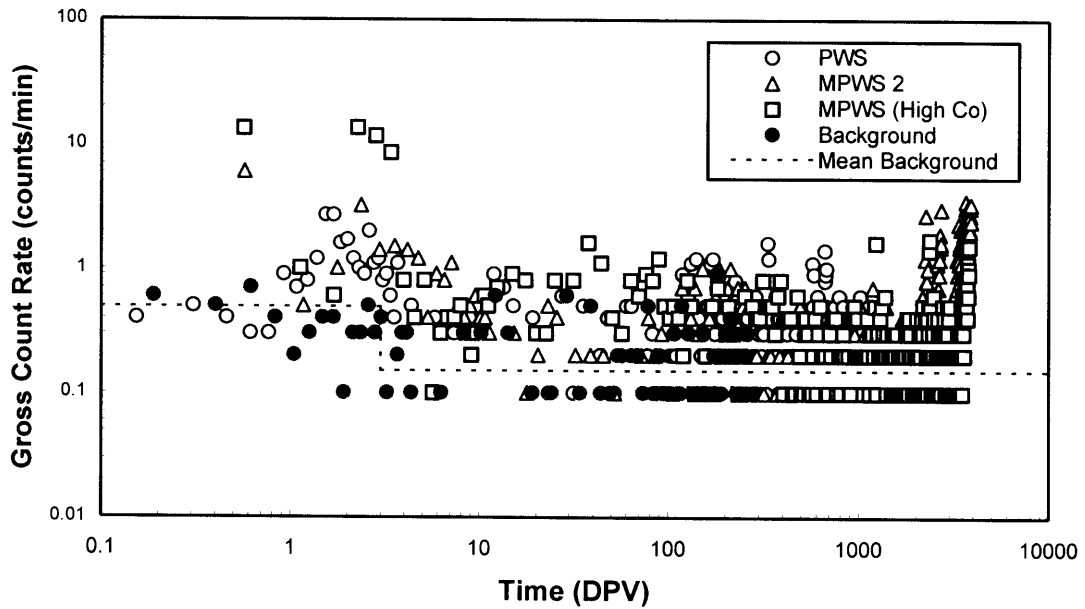


Figure 5.20. Plutonium(V) breakthrough curves

occurrence of americium and plutonium in monitoring data and with the stochastic nature of colloidal transport. There was a high mobility component, but it was smaller and less prominent than for neptunium. In two of these tests, changes in eluent chemistry were made between 2000 DPV and 3000 DPV. The first change was from pH8 to pH2 around 2300 DPV and the second was from pH2 to pH1 around 2700 DPV. These changes resulted in small increases in breakthrough, likely due to solubilization of plutonium hydroxide before the polymeric oxy-hydroxide formed.

The expanded breakthrough curves are presented in Figure 5.21. For the < 1 DPV time period, no breakthrough was apparent in two of the experiments and there was the possibility of breakthrough in the other two. For the 1–10 DPV period, there was a small amount of breakthrough in all of the experiments. Recoveries for discrete time periods are given in Table 5.9. For the 1–10 and 10–100 DPV time periods, the fractions were rather consistent, varying between 10^{-4} and 10^{-3} . The variability was larger, 10^{-5} to 10^{-3} , for the < 1 DPV period. They were not consistent for the other two time periods. The “high C_0 ” data are presented in Figure 5.22. Although there is definitely some breakthrough, it is very small. The filtered samples from the 1–2 DPV time period differed significantly from the unfiltered samples, indicating a mixture of species larger and smaller than 12 nm.

Based on the evidence presented above for reduction and subsequent immobilization of neptunium(V), the same mechanism was hypothesized for plutonium(V). Since plutonium(V) is more readily reduced than neptunium, it is possible that almost all of the plutonium is reduced rather than part of it as for neptunium. Presented in Figure 5.23 are breakthrough curves for experiments conducted under oxidizing conditions. Breakthrough did not increase under oxidizing conditions as it did for neptunium. This was not surprising given that plutonium(V) is more easily reduced than neptunium(V), and the reduction potential of the column effluent was below that required for plutonium(V) to be the predominant species.

Uranium

Breakthrough curves for uranium under the influence of the MPWS (experiments were not conducted for uranium with the PWS) are presented in Figure 5.24. These curves, in contrast to those for the other actinides, were characterized by a single peak containing all of the activity in the spike. Breakthrough began immediately, peaked

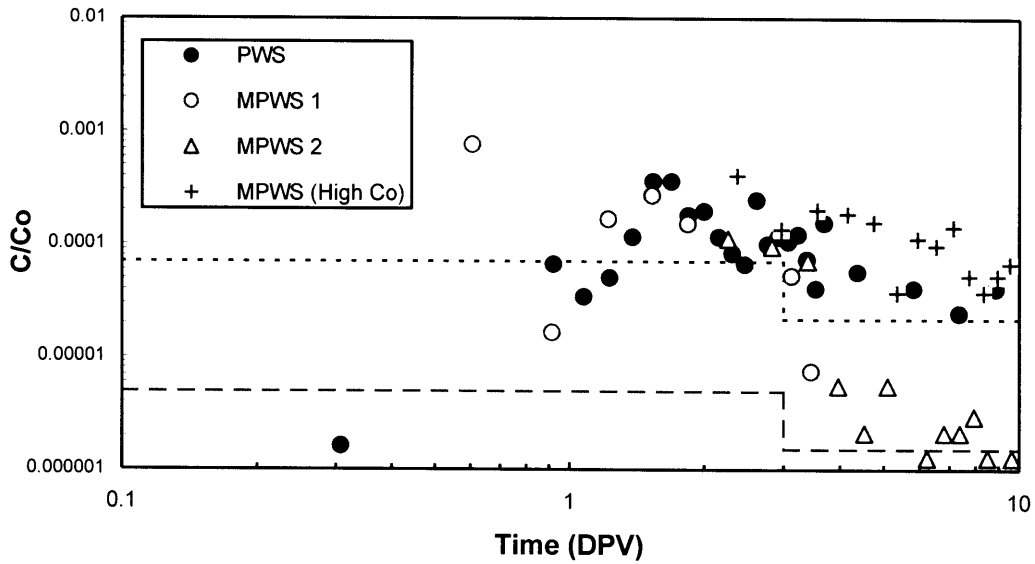


Figure 5.21. Expanded view of high mobility time period for plutonium(V)

Table 5.9. Plutonium(V) Recoveries for Discrete Time Periods

Experiment	Time Period (DPV)				
	< 1	1 – 10	10 – 100	100 – 1000	> 1000
PWS	2.7×10^{-5}	8.5×10^{-4}	6.9×10^{-4}	1.5×10^{-2}	N/A
MPWS 1	9.7×10^{-4}	1.8×10^{-4}	N/A	N/A	N/A
MPWS 2	3.6×10^{-4}	7.1×10^{-4}	5.1×10^{-4}	-2.5×10^{-5}	1.2×10^{-1}
MPWS (high C_0)	4.8×10^{-5}	1.3×10^{-4}	3.2×10^{-4}	3.1×10^{-4}	3.1×10^{-4}

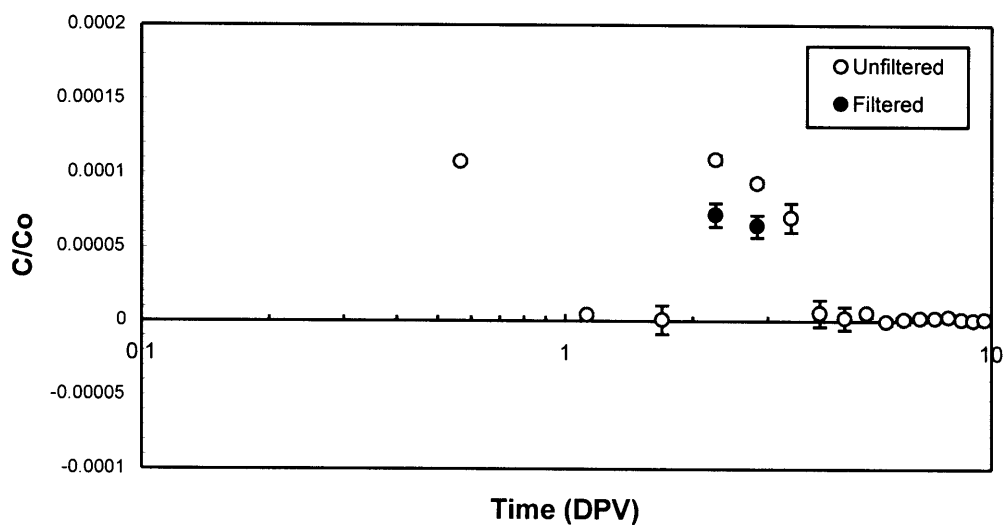


Figure 5.22. Plutonium(V) high mobility component for an elevated C_0 – unfiltered and filtered (>12 nm) analyses

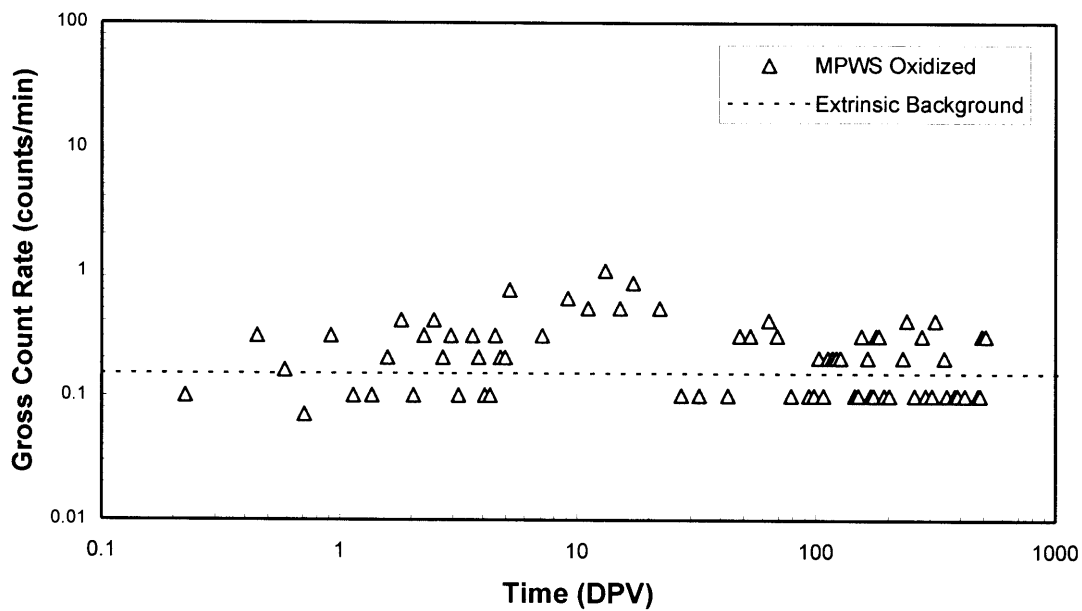


Figure 5.23. Plutonium(V) breakthrough curves under oxidizing conditions

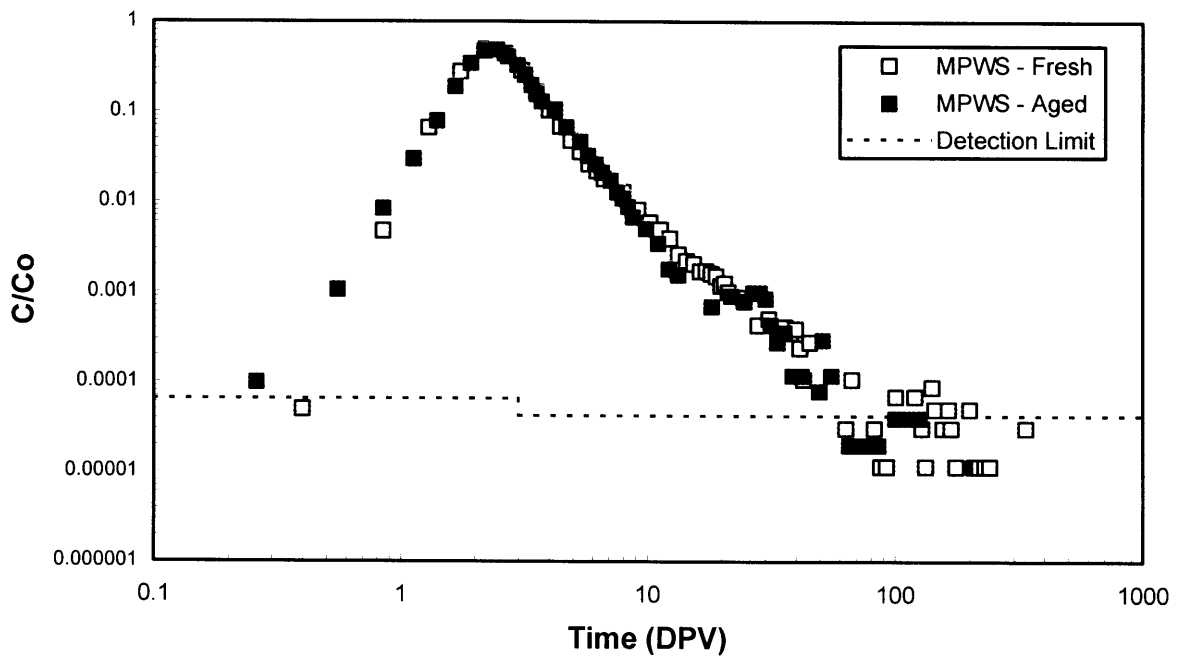


Figure 5.24. Uranium breakthrough curves

between 2 and 3 DPV, and was complete within 100 DPV. This behavior was not significantly affected by the removal of either F^- or SO_4^{2-} (Figure 5.25). However, it was greatly affected by the removal of CO_3^{2-} , which resulted in two distinct peaks, a small one at 10 DPV and a large one at 200 DPV. The peak at 10 DPV disappeared when CO_3^{2-} was removed in combination with F^- and when it was removed in combination with SO_4^{2-} (Figure 5.26). The leading edge of the peak at 200 DPV became sharper with the removal of F^- and sharper still with the removal of SO_4^{2-} , but the tailing edge did not change appreciably. Retardation factors and recoveries for the uranium experiments are presented in Table 5.10. For MPWS – fresh, MPWS – aged, MPWS w/o F^- , and MPWS w/o SO_4^{2-} , the experiments were not terminated until the concentrations reached background and the recoveries exceeded 90%. The other experiments were truncated before background was reached, and the recoveries varied from 73 to 77%. Although the missing uranium was probably contained in the truncated portion of the curve, the experiments would have to be extended to almost 10,000 DPV to verify this.

The breakthrough curves clearly indicate that a carbonate species is responsible for uranium transport under the influence of the MPWS. This is consistent with modeling results (Table 5.11), which predict $UO_2(CO_3)_3^{4-}$ and $UO_2(CO_3)_2^{2-}$ as the predominant species for the MPWS. When CO_3^{2-} is removed from the MPWS, the model predicts $UO_2(OH)_2$ and $UO_2(OH)_3^{1-}$ to dominate. Thus, the 200 DPV peak is likely due to the hydroxide species. Removal of F^- and SO_4^{2-} , in both the presence and absence of CO_3^{2-} , did not appreciably affect the speciation.

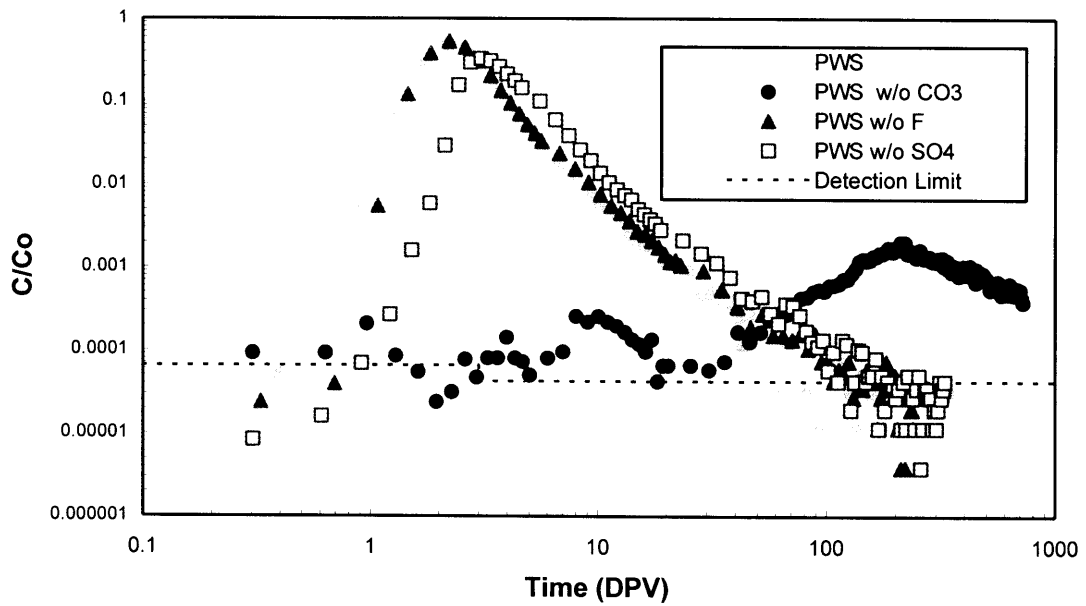


Figure 5.25. Effect of removing CO_3^{2-} , F^- , and SO_4^{2-} on uranium breakthrough curves

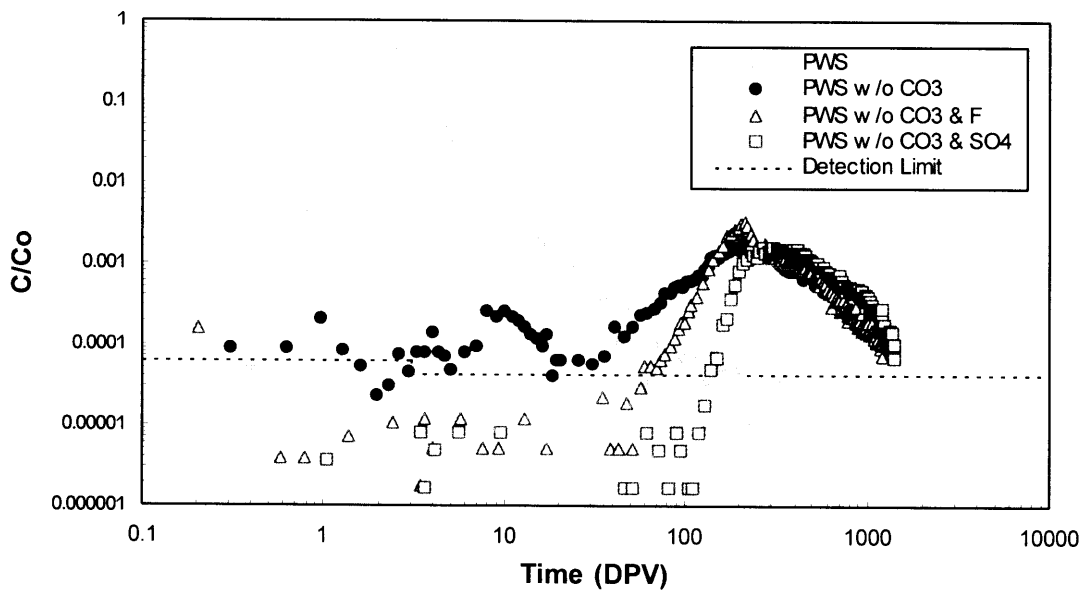


Figure 5.26. Effect of removing CO_3^{2-} , CO_3^{2-} & F^- , and CO_3^{2-} & SO_4^{2-} on uranium breakthrough curves

Table 5.10. Uranium Recoveries and Retardation Factors

Simulant	Time Period (DPV)	Recovery	R
MPWS – Fresh	0 – 100	0.91	3.2
MPWS – Aged	0 – 100	0.96	3.9
MPWS w/o F ⁻	0 – 240	0.93	5.1
MPWS w/o SO ₄ ²⁻	0 – 330	0.95	8.2
MPWS w/o CO ₃ ²⁻	5 – 20	0.002	12
	20 – 800	0.45	340
MPWS w/o CO ₃ ²⁻ and F ⁻	20 – 1220	0.77	690
MPWS w/o CO ₃ ²⁻ and SO ₄ ²⁻	20 – 1445	0.73	560

Table 5.11. Speciation Modeling Results for Uranium

RUN	% Distribution			
	UO ₂ (CO ₃) ₂ ⁻²	UO ₂ (CO ₃) ₃ ⁻⁴	UO ₂ (OH) ₂	UO ₂ (OH) ₃ ⁻¹
allow pptn	7.3	92.7	neg	neg
pptn excluded	7.0	93.0	neg	neg
<i>(all below pptn excluded, but no change if allowed)</i>				
+1.3 mg/l EDTA	7.0	93.0	neg	neg
<i>(note: U-EDTA species < ~10⁻³⁰ M; EDTA tied up with Ca and Mg)</i>				
no F ⁻	7.2	92.8	neg	neg
no CO ₃ ²⁻	neg	neg.	87.0	12.8
no SO ₄ ²⁻	7.6	92.4	neg	neg
no SO ₄ ²⁻ , CO ₃ ²⁻	neg	neg	87.1	12.7

6. CONCLUSIONS

This project was motivated by monitoring data suggesting that americium and plutonium may have migrated through one or more layers of sedimentary interbed below the SDA. Such behavior is inconsistent with traditional modeling approaches, which predict americium and plutonium mobilities in interbed to be very low and thus imply that interbed should be an effective barrier to migration. The original objective of the project was to determine if high mobility forms of plutonium could be observed in laboratory columns eluted with a perched water simulant. The simulant contained elevated, although not extreme, concentrations of potential chelating agents. As the project progressed, the scope expanded to include uranium and americium, which are important contaminants at the SDA, as well as thorium and americium, which are often cited as analogs for plutonium(IV) and plutonium(V), respectively. The objectives were also extended to attempt to provide mechanistic explanations for the observed behaviors.

Three major conclusions can be drawn regarding actinide transport under the influence of the perched water simulants used in these studies. These are as follows: (1) multiple physical/ chemical forms, each having distinctly different mobilities, are possible, (2) for time scales on the order of weeks and longer, actinide behavior is generally dominated by solid forms, and (3) high mobility forms, which differ among the actinides, are possible. The hypothesized physical/chemical forms of the contaminants are summarized in Table 6.1 and discussed below. As discussed below, these findings have important implications regarding the behavior of actinide contaminants below the SDA and the conceptual models used to predict their behavior.

Multiple physical/chemical forms, each having distinctly different mobilities, are possible: This phenomenon, which was not observed for strontium or uranium, was most pronounced for americium, thorium, and plutonium(IV) in the presence of EDTA and for neptunium in the presence and absence of EDTA. In these tests, the mobilities were characterized by a small (<1%) high mobility component with $R < 3$, a large ($\approx 50\%$) intermediate mobility component with $3 < R < 1000$, and a large ($\approx 50\%$) low mobility component with $R > 1000$. This finding has significant implications with respect to modeling because it suggests that the traditional approach of using batch distribution coefficients (K_D) to infer contaminant mobility may not be appropriate for some contaminants in some situations. The key, of course, is identifying those situations

Table 6.1. Summary of Hypothesized Physical/Chemical Forms (in the Absence of EDTA)

Radionuclide	High Mobility Component	Low Mobility Component
Americium(III)	Predominately particulate carbonate or hydroxy-carbonate species	Particulate carbonate or hydroxy-carbonate species
Thorium(IV)/Plutonium(IV)	Hydroxide species sorbed to silica precipitates and/or polymeric oxy-hydroxide precipitates	Hydroxide species sorbed to soil matrix and/or polymeric oxy- hydroxide precipitates filtered by the soil matrix
Neptunium(V)	Soluble carbonate species	Reduced to neptunium(IV) – same species as thorium(IV)/plutonium(IV)
Plutonium(V)	Predominately particulate forms, probably plutonium(IV) species. Soluble carbonates possible.	Reduced to plutonium(IV) – same species as thorium(IV)/plutonium(IV)
Uranium(VI)	Soluble carbonate species	In the long term, likely dominated by uranium mineralization

where an alternate approach is warranted. For example, the plutonium(IV) – EDTA complex which was responsible for the intermediate mobility component in the experiments is a transient species which would only be important at the SDA in an episodic infiltration event such as a flood.

The behavior of americium, thorium, and plutonium is dominated by solid species of low mobility: In the absence of EDTA, more than 99% of the americium, thorium, and plutonium(IV) had low mobilities ($R > 1000$) in the columns. This behavior is consistent with the thermodynamic phase diagrams which predict americium to be an insoluble carbonate or hydroxy-carbonate precipitate and thorium and plutonium(IV) to either be a hydroxide or an oxy-hydroxide polymer. The behavior is also consistent with sorption to silicate precipitates as speciation modeling predicts that the groundwater simulants are oversaturated with respect to silicates. Although not obvious, the behaviors of neptunium and plutonium(V) are also likely to be dominated by solid species. The neptunium data for “oxidized” columns and for normal columns at different flow rates both suggest reduction of neptunium(V) to neptunium(IV) by the interbed. Neptunium(IV) is hydrolyzed at pH 8 and likely forms the same immobile solid species as thorium and plutonium(IV). Plutonium(V) is more easily reduced than neptunium(V), and its low mobility component was greater than 99%, both in the presence and absence of EDTA. Thus, its behavior is likely governed by its reduction to the immobile plutonium(IV). The low mobility of plutonium(V) is contingent on its encountering redox active constituents in the path of migration. This seems likely below the SDA.

In the laboratory columns uranium had high mobility ($R \approx 3$) due to the soluble complexes that it forms with carbonate. While the carbonate species are likely to control transport in the short term and would be important in episodic transport scenarios, long term transport is affected by aging processes and is likely dominated by insoluble calcium and/or phosphate mineral species. Since the solubilities of these uranium mineral species are typically much lower than the uranyl carbonates, long-term uranium mobility below the SDA is likely to be much lower than suggested by the column experiments.

High mobility forms are possible: High mobility forms were observed for americium, thorium, plutonium(IV), neptunium, and plutonium(V). The physical/chemical nature of these forms differed. Effluent filtrations showed the americium and neptunium high mobility form to be smaller than 3 nm, thorium to be larger than 3 nm, and plutonium(IV) and plutonium(V) to have portions both smaller and larger than 3 nm. When combined

with batch filtration data and speciation modeling predictions, hypotheses are advanced regarding the nature of these high mobility forms as follows: americium – americium carbonate or hydroxy carbonate in either a soluble or small (<3 nm) precipitate form; thorium – thorium oxy-hydroxide polymer or hydrolyzed thorium sorbed to silicate precipitates (>3 nm); plutonium(IV) - plutonium oxy-hydroxide polymer or hydrolyzed plutonium sorbed to silicate precipitates; neptunium – soluble neptunium carbonate; plutonium(V) – plutonium carbonate complexes and the same species as above for plutonium(IV), due to reduction of plutonium(V) to plutonium(IV).

Collectively, these results provide a plausible explanation for the apparent disconnect between the transport model, which predicts interbed to be an effective barrier for plutonium and americium migration, and field data, which indicate penetration of that barrier. They are consistent with the transport model in that the column tests also show interbed to be an effective geochemical barrier ($R > 1000$). They differ from the transport model however, in that the interbed was experimentally found to be effective for most of the americium and plutonium rather than all of it as predicted. The results are, at the same time, consistent with the field data. The high mobility forms appear to be at least partly colloidal, and the transport of colloidal material through the subsurface is likely to be stochastic. In fact, some of the breakthrough curves, particularly those for plutonium(V), not only had a high mobility component early in the test but also exhibited sporadic release of very small amounts throughout the duration of the experiment. This is consistent with the sporadic occurrence of americium and plutonium in monitoring data.

Additional findings of potential interest are the effect of mean linear velocity and the ability of the interbed matrix to attenuate colloids. Decreasing the mean linear velocity an order of magnitude below the value used in most of the tests did not affect retardation factors for any of the contaminants that were tested (neptunium, uranium, and strontium). These results provide a measure of assurance that behavior predicted by the columns may be applicable at the much lower mean linear velocities that are typical below the SDA. However, this extrapolation needs to be applied with care because there can be kinetic effects which are significant. For example, fractional recovery for neptunium declined when the flow rate was reduced because the increase in residence time provided for a greater reduction from neptunium(V) to neptunium(IV) by the soil. Similarly, the intermediate mobility fractions that resulted from EDTA complexation with americium, thorium, and plutonium(IV) were short lived. The ability of the 106 to 250 μm

size fraction to attenuate colloids smaller than 20 nm was surprising and supports the findings that there is very little penetration of interbed by the colloidal forms.

7. REFERENCES

- Allard, B., Olofsson, U., Torstenfelt, B., Kipatsi, H. and Andersson, K., "Sorption of Actinides in Well-Defined Oxidation States in Geologic Media," Scientific Basis for Radioactive Waste Management – V, Lutze, W., editor, New York: Elsevier Publishing Company, 775-782, 1982.
- Bagnall, K.W., The Actinide Elements, New York: Elsevier Publishing Company, 18-32, 1972.
- Bidoglio, G., "Characterization of Am(III) Complexes with Bicarbonate and Carbonate Ions at Groundwater Concentration Levels," *Radiochemistry and Radioanalytical Letters*, **53**, 45-60, 1982.
- Brookins, D.G., Eh-pH Diagrams for Geochemistry, New York: Springer-Verlag, 1987.
- Brookins, D.G., "Aqueous Geochemistry of Rare Earth Elements," in Geochemistry and Mineralogy of Rare Earth Elements, Lipin, B.R. and McKay, G.A., editors, *Reviews in Mineralogy*, **21**, 1989.
- Buddemeir, R. W. and Hunt, J. R., "Transport of Colloidal Contaminants in Groundwater: Radionuclide Migration at the Nevada Test Site," *Appl. Geochem.*, **3**, 535-538, 1988.
- Choppin, G.R. and Stout, B.E., "Actinide Behavior in Natural Waters," *The Science of the Total Environment*, **83**, 203-216, 1989.
- Choppin, G.R., Liljenzin, J., and Rydberg, J., Radiochemistry and Nuclear Chemistry, New York: Elsevier Science Publishers, 639-670, 1994a.
- Choppin, G.R., Liljenzin, J., and Rydberg, J., Radiochemistry and Nuclear Chemistry, New York: Elsevier Science Publishers, 414-437, 1994b.
- Choppin, G.R., Bond, A.H. and Hromadka, P.M., "Redox Speciation of Plutonium," *J. Radioanalytical and Nucl. Chem.*, **219**(2), 203-210, 1997.
- Cleveland, J.M., The Chemistry of Plutonium, New York: Gordon and Breach Science Publishers, 1970.
- Currie, L.A., "Limits for Qualitative Detection and Quantitative Determination," *Anal. Chem.*, **40**(3), 586-593, 1968.
- Deutsch, W.J., Groundwater Chemistry: Fundamentals and Applications to Contamination, New York: Lewis Publishers, 47-61, 1997.
- Dozol, M. and Hagemann, R., "Radionuclide Migration in Groundwaters: Review of the Behaviour of Actinides," *Pure and Applied Chemistry*, **65**, 1081-1102, 1993.

- Fjeld, R. A., DeVol, T. A., Goff, R. W., Blevins, M. D., Brown, D. D., Ince, S. M., Elzerman, A.W. and Newman, M. E., "Characterization of Mobilities of Selected Actinides/Fission/Activation Products in Laboratory Columns Containing Subsurface Material from the Snake River Plain," submitted to *Nucl. Technol*, 2000.
- Fried, S., Friedman, A.M. and Weeber, R., "Studies of the Behavior of Plutonium and Americium in the Lithosphere," ANL-8096, 10-11, 1974.
- Hobart, D.E., "Actinides in the Environment," from Proceedings of *The Robert A. Welch Foundation Conference on Chemical Research, XXXIV, Fifty Years with Transuranium Elements*, Houston, TX, October 22-23, 1990.
- Jensen, B.S., "The Geochemistry of Radionuclides with Long Half-Lives: Their Expected Migration Behavior," Riso National Laboratory Report, Riso-R-430, Roskilde, Denmark, 1980.
- Kaplan, D. I., Bertsch, P. M., Adriano, D. C. and Orlandini, K. A., "Actinide Association with Groundwater Colloids in a Coastal Plain Aquifer," *Radichimica Acta* **66/67**, 181-187, 1994.
- Kaplan, D.I., Gervais, T.L. and Krupka, K.M., "Uranium(VI) Sorption to Sediments Under High pH and Ionic Strength Conditions," *Radiochimica Acta*, **80**, 201-211, 1998.
- Keller, C., The Chemistry of the Transuranium Elements, Weinheim/Bergstr., Germany: Verlag Chemie, GmbH, 117-130, 1971.
- Kersting, E. B., Efurud, D. W., Finnegan, D.L., Rokop, D. J., Smith, D.K. and Thompson, J.L., "Migration of Plutonium in Ground Water at the Nevada Test Site," *Nature*, **397**(7), 56-59, 1999.
- Kim, J.I., "Chemical Behaviour of Transuranic Elements in Natural Aquatic Systems," Handbook on the Physics and Chemistry of the Actinides, Freeman, A.J. and Keller, C., editors, New York: Elsevier Science Publishers, 413-455, 1986.
- Kim, J.I., "Actinide Colloid Generation in Groundwater," *Radiochimica Acta*, **52/53**, 71-81, 1991.
- Kohler, M., Curtis, G.P., Kent, D.B., and Davis, J.A., "Experimental Investigation and Modeling of Uranium(VI) Transport under Variable Transport Conditions," *Water Resources Research*, **32**(12), 3539-3551, 1996.
- Langmuir, D., Aqueous Environmental Geochemistry, Upper Saddle River, NJ: Prentice Hall, Inc., 486-543, 1997.
- Lieser, K.H., and Hill, R., "Hydrolysis and Colloid Formation of Thorium in Water and Consequences for its Migration Behaviour – Comparison with Uranium," *Radiochimica Acta*, **56**, 37-45, 1992.
- Livens, F.R., Morris, K., Parkman, R., and Moyes, L., "Actinide Chemistry in the Far Field," *Nuclear Energy*, **35**(5), 331-337, 1996.

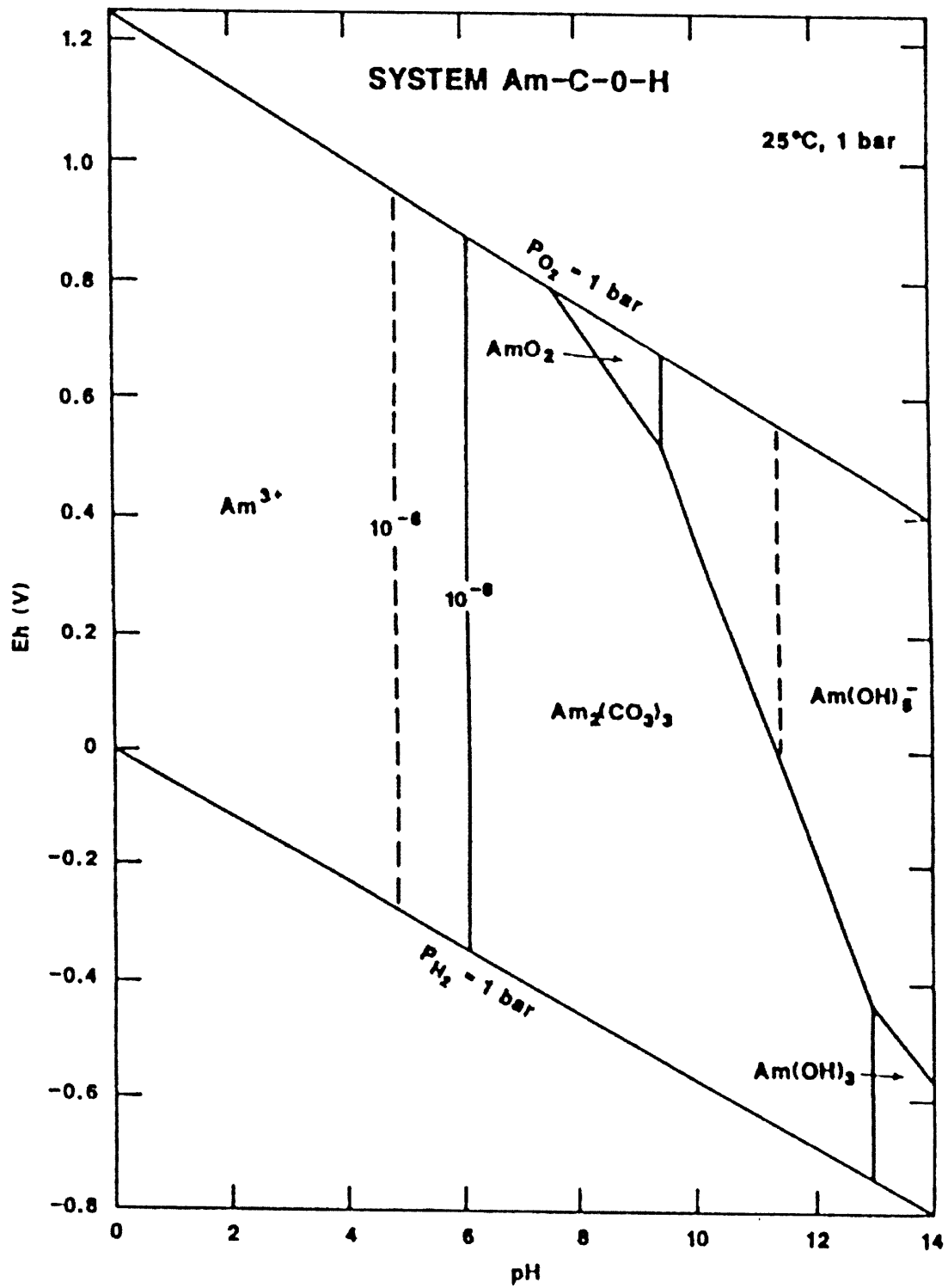
- Looney, B. B., Grant, M. W. and King, C. M., "Estimation of Geochemical Parameters for Assessing Subsurface Transport at the Savannah River Site," DPST-85-904, E. I. Du Pont de Nemours and Company, Savannah River Laboratory, Aiken, SC., 1987.
- Marty, R. C., Bennett, D. and Thullen, P., "Mechanism of Plutonium Transport in a Shallow Aquifer in Mortandad Canyon, Los Alamos National Laboratory, New Mexico," *Environ. Sci. Technol.* **31**, 2020-2027, 1997.
- McCarthy, J. F., Sanford, W. E. and Stafford, P.L., "Lanthanide Field Tracers Demonstrate Enhanced Transport of Transuranic Radionuclides by Natural Organic Matter," *Environ. Sci. Technol.*, **32**, 3901-3906, 1998.
- McCubbin, D. and Leonard, K.S., "Influence of Some Seawater Components on the Sorption Behaviour of Neptunium(V)," *Radiochimica Acta*, **69**, 97-102, 1995.
- Morse, J.W. and Choppin, G.R., "The Chemistry of Transuranic Elements in Natural Waters," *Reviews in Aquatic Sciences*, **4**(1), 1-22, 1991.
- Nagasaki, S., Tanaka, S. and Suzuki, A., "Interfacial Behavior of Actinides with Colloids in the Geosphere," *Journal of Nuclear Materials*, **248**, 323-327, 1997.
- Nagasaki, S., Tanaka, S. and Suzuki, A., "Geochemical Behavior of Actinides in High-Level Radioactive Waste Disposal," *Progress in Nuclear Energy*, **32**, 141-161, 1998.
- Nakayama, S., Arimoto, H., Yamada, N., Moriyama, H. and Higashi, K., "Column Experiments on Migration Behaviour of Neptunium(V)," *Radiochimica Acta*, **44/45**, 79-182, 1988.
- Nash, K.L., Cleveland, J.M., and Rees, T.F., "Speciation Patterns of Actinides in Natural Waters: a Laboratory Investigation," *Journal of Environmental Radioactivity*, **7**, 131-157, 1988.
- Neck, V., Fanghanel, Th. and Kim, J.I., "Mixed Hydroxo-Carbonate Complexes of Neptunium(V)," *Radiochimica Acta*, **77**, 167-175, 1997.
- Neu, M.P., Hoffman, D.C., Roberts, K.E., Nitsche, H. and Silva, R.S., "Comparison of Chemical Extractions and Laser Spectroscopy for the Determination of Plutonium Species in Near Neutral Carbonate Solutions." *Radiochimica Acta*, **66**, 265-272, 1994.
- Newton, T.W. and Sullivan, J.C., "Actinide Carbonate Complexes in Aqueous Solution," Handbook on the Physics and Chemistry of the Actinides, Freeman, A.J. and Keller, C., editors, New York: Elsevier Science Publishers, 387-406, 1985.
- Nitsche, H., "Solubility Studies of Transuranium Elements for Nuclear Waste Disposal: Principles and Overview," *Radiochimica Acta*, **52/53**, 3-8, 1991.
- Nitsche, H. and Edelstein, N.M., "Solubilities and Speciation of Selected Transuranium Ions: A Comparison of a Non-Complexing Solution with a Groundwater from the Nevada Tuff Site," *Radiochimica Acta*, **39**, 23-33, 1985.
- Nitsche, H. and Silva, R.J., "Investigation of the Carbonate Complexation of Pu(IV) in Aqueous Solution," *Radiochimica Acta*, **72**, 65-72, 1996.

- Penrose, W.R., Polzer, W. L., Essington, E.H., Nelson, D.M. and Orlandini, K.A., "Mobility of Plutonium and Americium Through a Shallow Aquifer in a Semiarid Region," *Environ. Sci. Technol.*, **24**, 228-234, 1990.
- Rai, D. and Ryan, J.L., "Crystallinity and Solubility of Pu(IV) Oxide and Hydrated Oxide in Aged Aqueous Suspensions," *Radiochimica Acta*, **30**, 213-216, 1982.
- Ramsay, J.D.F., "The Role of Colloids in the Release of Radionuclides from Nuclear Waste," *Radiochimica Acta*, **44/45**, 165-170, 1988.
- Silva, R.J., Bidoglio, G., Rand, M.H., Robouch, P.B., Wanner, H. and Puigdomenech, I., Chemical Thermodynamics of Americium, New York: Elsevier Scientific Publishing, 1995.
- Silva, R.J., "The Behavior of Americium in Aqueous Carbonate Systems," *Materials Research Society Symposia Proceedings*, Pittsburgh, PA: Materials Research Society, **26**, 875-881, 1984.
- Silva, R.J., "Mechanisms for the Retardation of Uranium(VI) Migration," *Materials Research Society Symposia Proceedings*, Pittsburgh, PA: Materials Research Society, **257**, 323-330, 1992.
- Silva, R.J. and Nitsche, H., "Actinide Environmental Chemistry," *Radiochimica Acta*, **70/71**, 377-396, 1995.
- Snoeyink, V.L. and Jenkins, D., Water Chemistry, New York: John Wiley & Sons, 197-242, 1980.
- Stumm, W. and Morgan, J. J., Aquatic Chemistry: Chemical Equilibria and Rates in Natural Waters, New York: John Wiley & Sons, 1996.
- Thompson, J. L., "Actinide Behavior on Crushed Rock Columns", *J. Radioanal. Nucl. Chem.* **30**, 353-364, 1989.
- USGS, 1999. U.S. Geological Survey with Idaho Operations Office, Dept. of Energy, under Interagency Agreement DE-A107-97ID13556, Review of the Transport of Selected Radionuclides in the Interim Risk Assessment for the Radioactive Waste Management complex, Waste Area Group 7 Operable Unit 7-13/14, Idaho National Engineering and Environmental Laboratory, Idaho, Volume 1, 1999.
- van Gunten, H.R. and Benes, P., "Speciation of Radionuclides in the Environment," *Radiochimica Acta*, **69**, 1-29, 1995.
- Watters, R.L., "Aquatic Chemistry of Plutonium," Plutonium Chemistry, American Chemical Society, Symposium Series No.216, Carnall, W.T. and Choppin, G.R., editors, 297-315, 1983.
- Wood, W.W. and Low, W.H., "Aqueous Geochemistry and Diagenesis in the Snake River Plain Aquifer System, Idaho," *Geological Society of America Bulletin*, **97**, 1456-1466, 1986.
- Yamaguchi, T., Sakamoto, Y. and Ohnuki, T., "Effect of the Complexation on Solubility of Pu(IV) in Aqueous Carbonate System," *Radiochimica Acta*, **66/67**, 9-14, 1994.

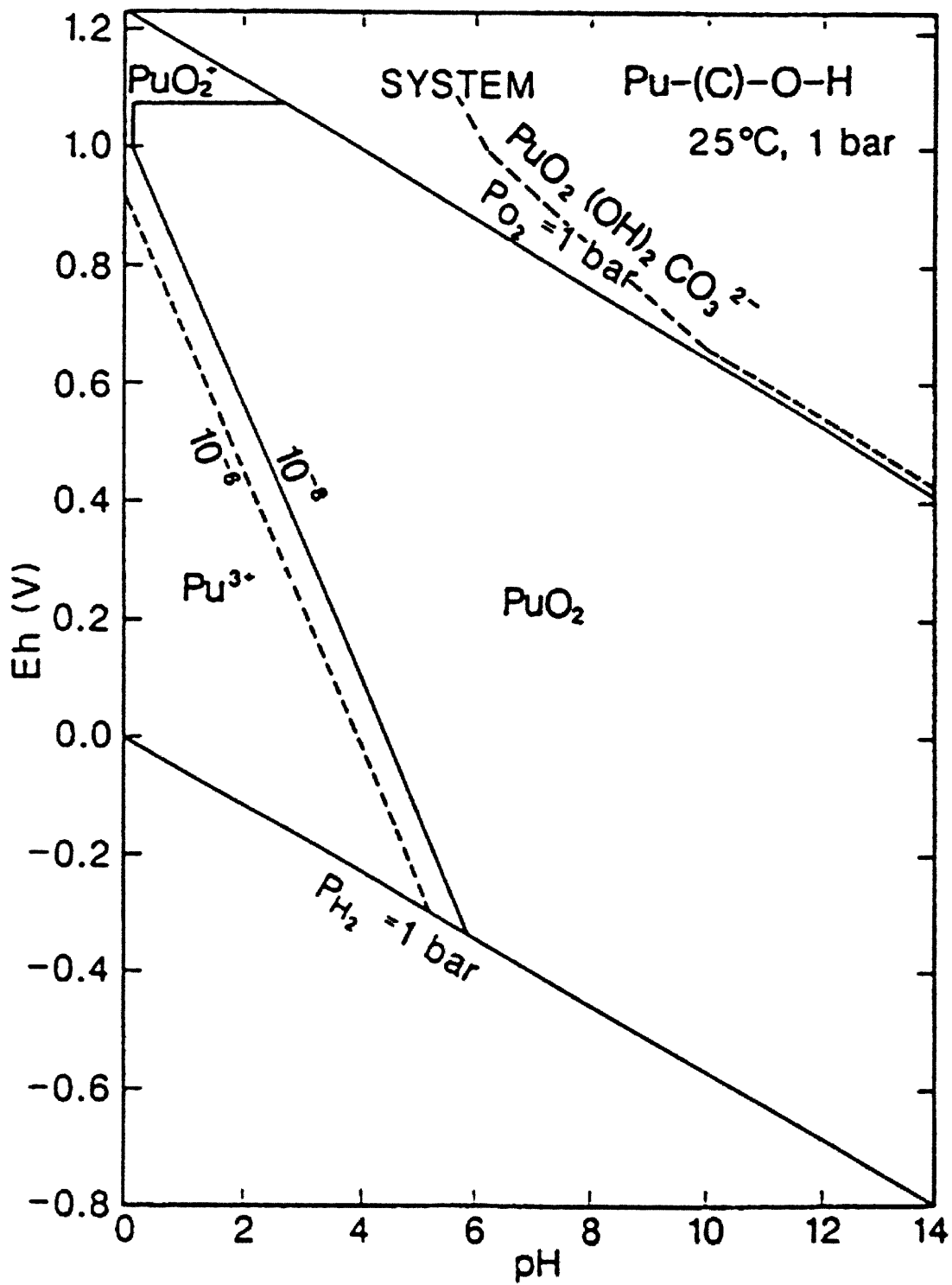
APPENDICES

APPENDIX A

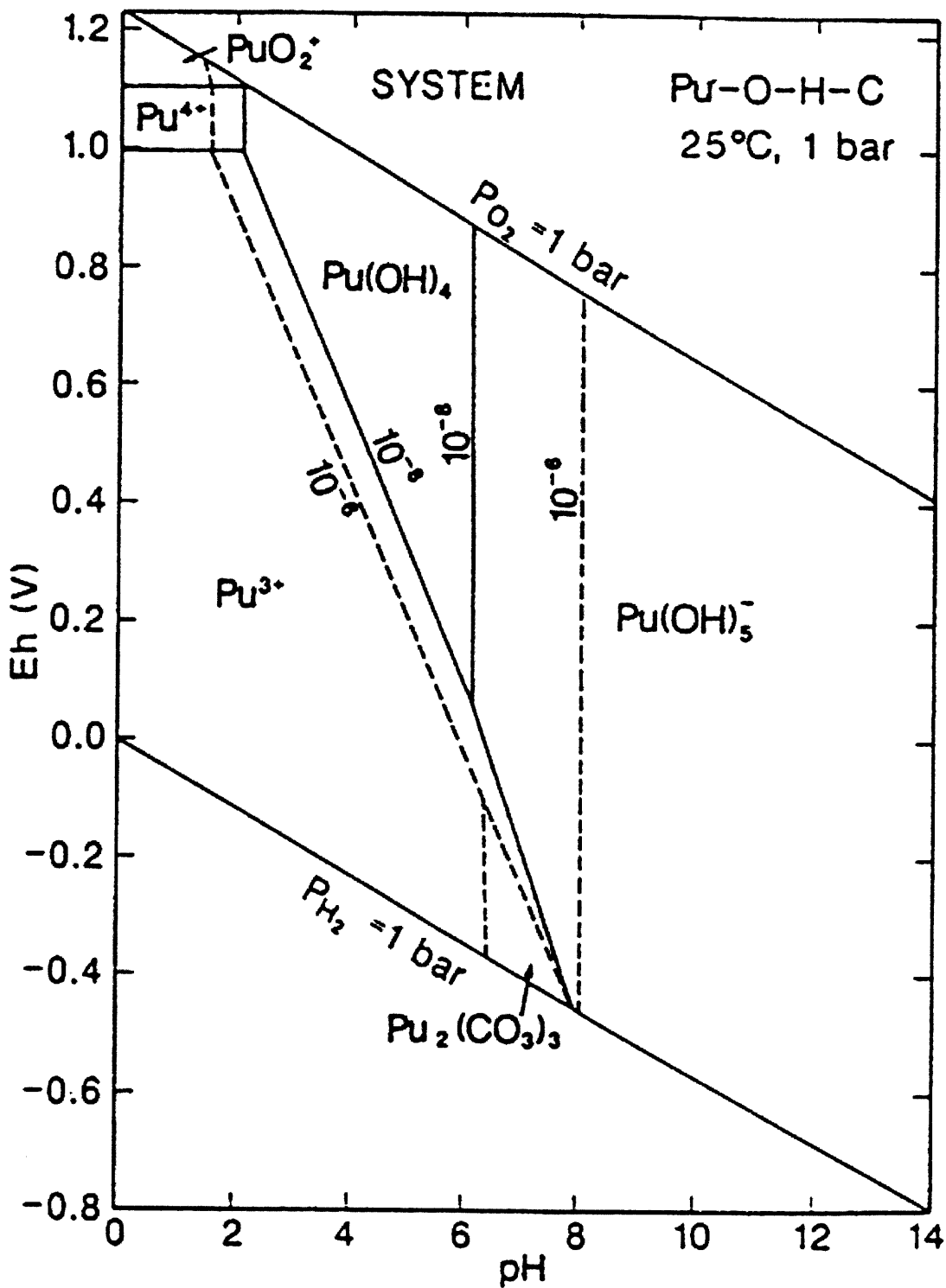
E_H-pH Diagrams



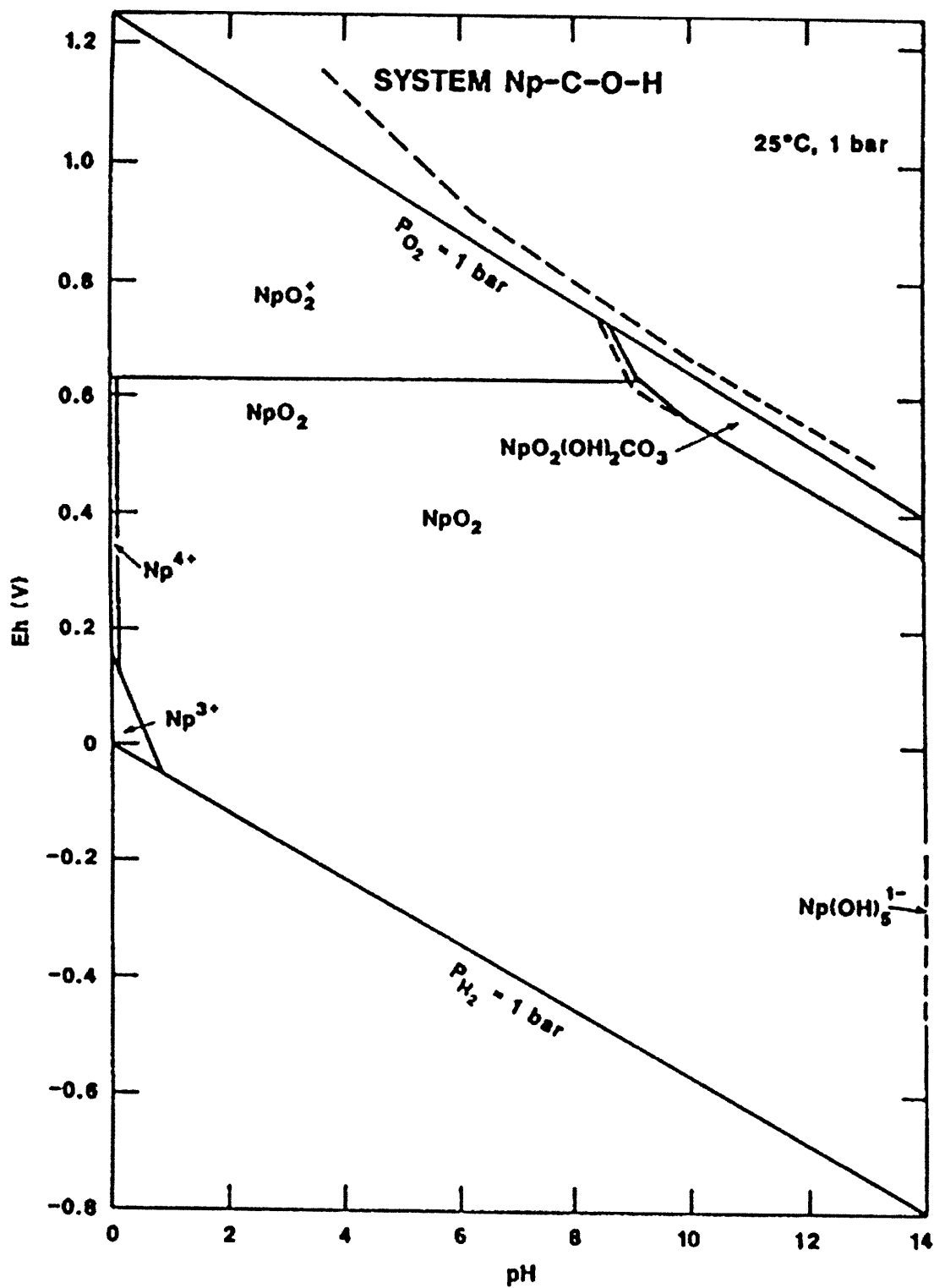
A-1 Am-C-O-H System



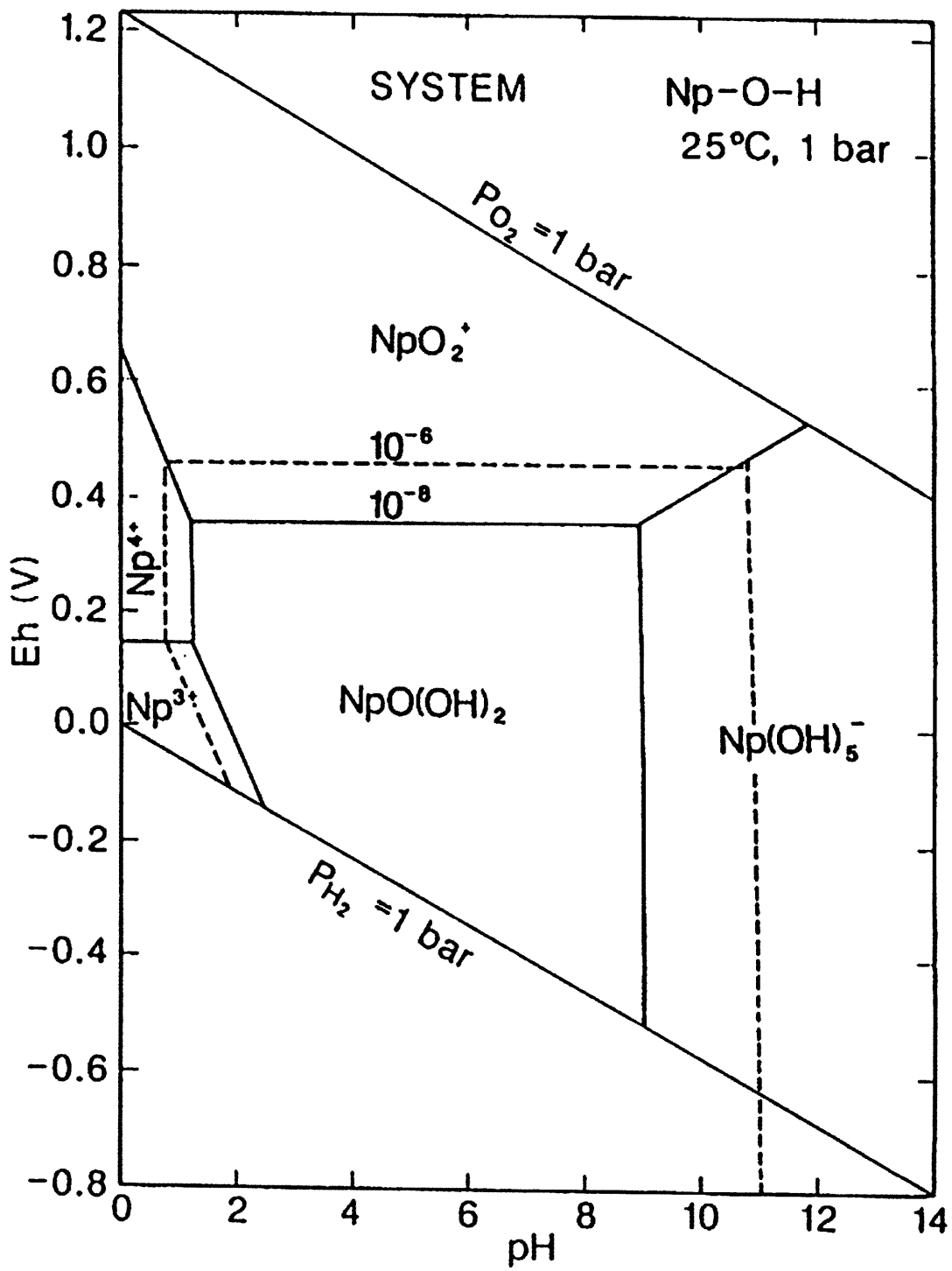
A-2 Pu-(C)-O-H System



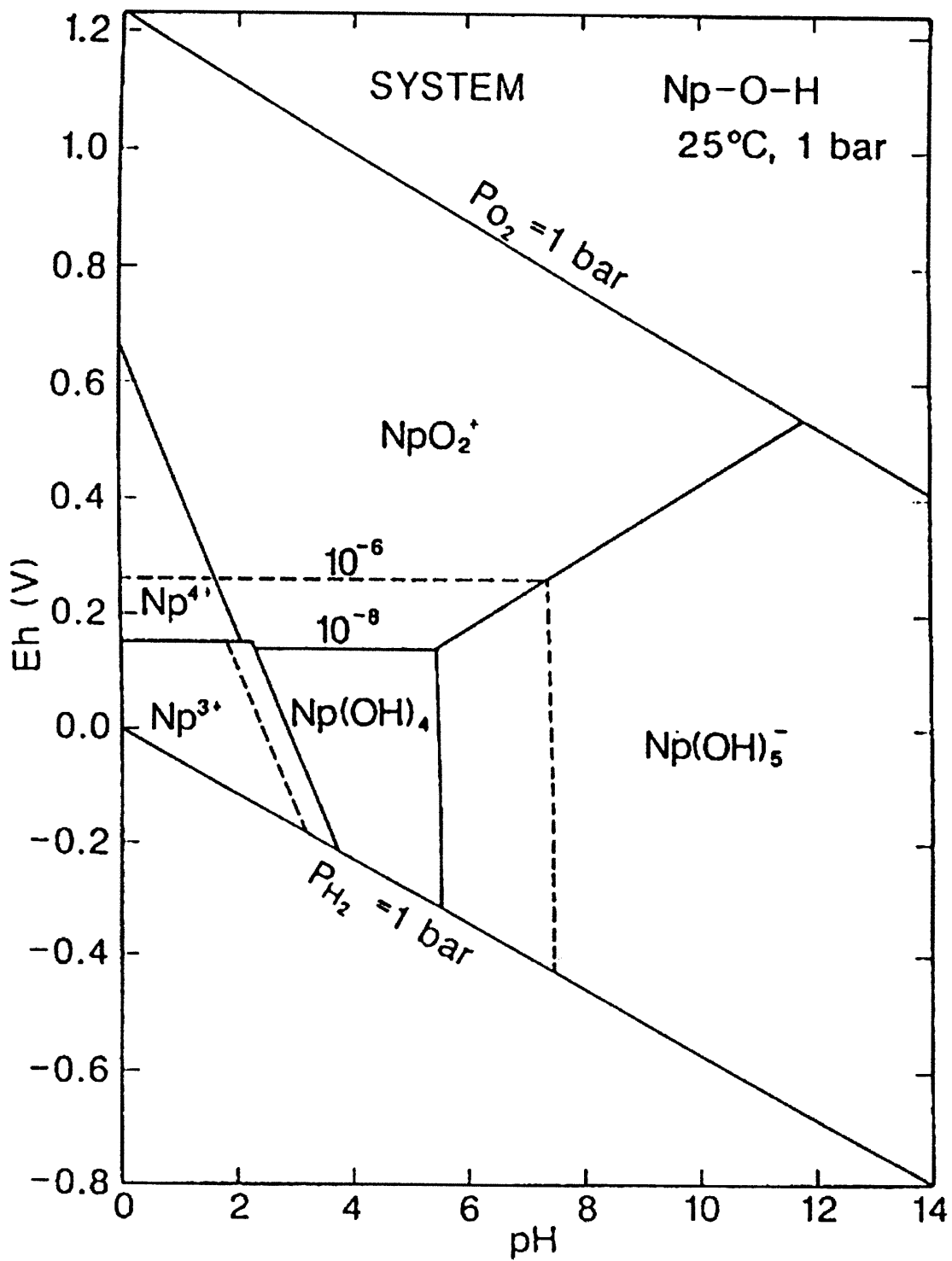
A-3 Pu-O-H-C System



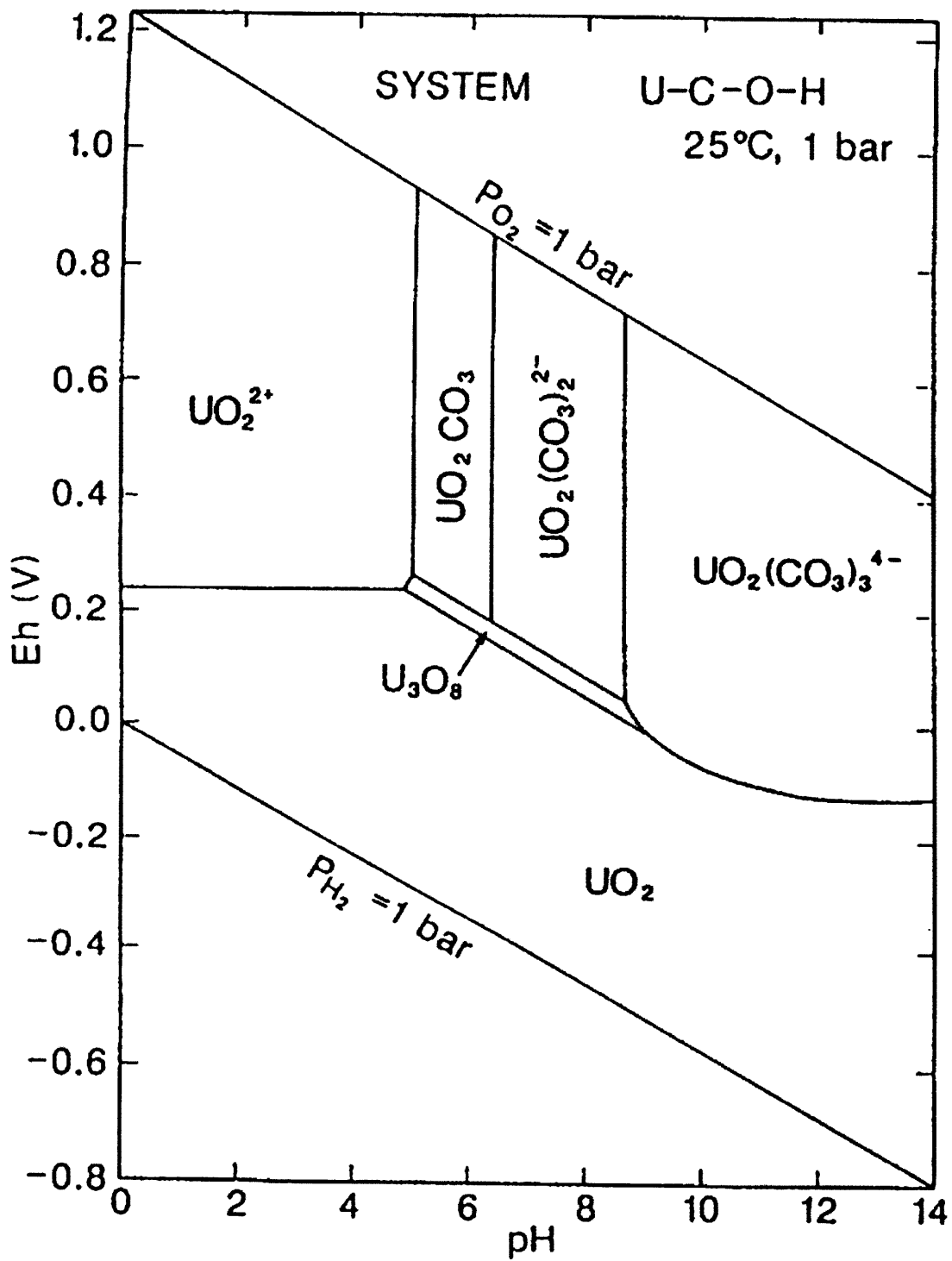
A-4 Np-C-O-H System



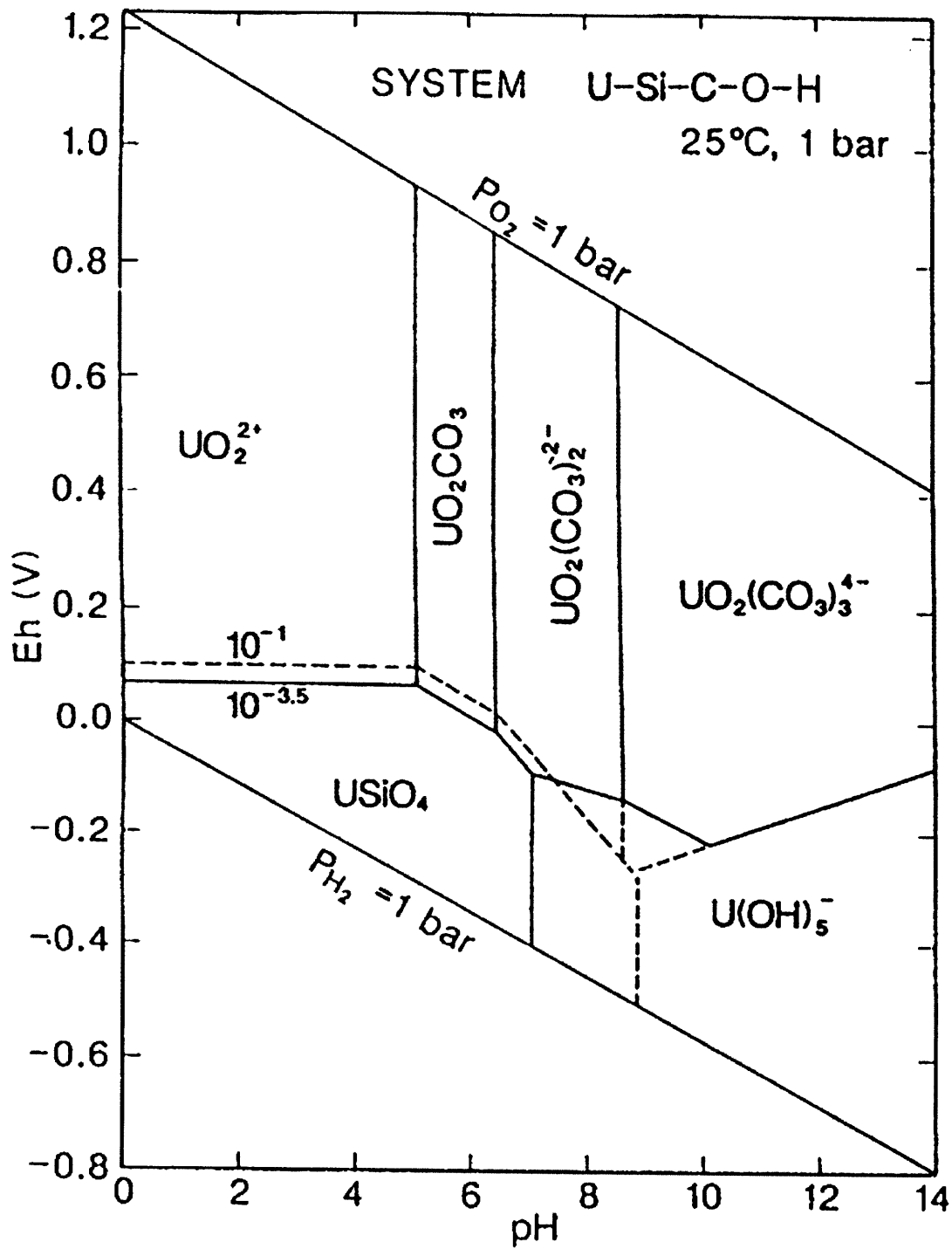
A-5 Np-O-H System



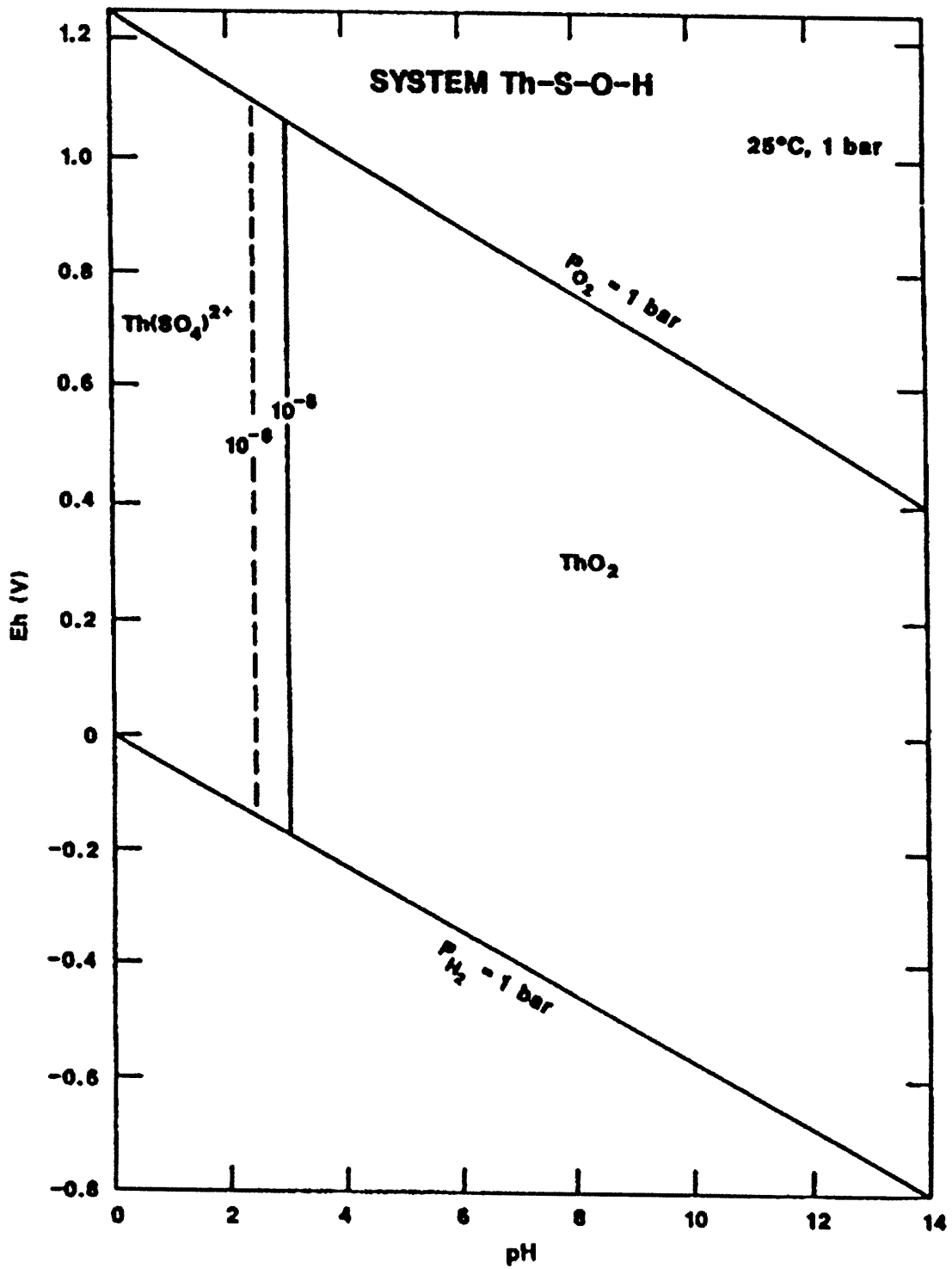
A-6 Np-O-H System



A-7 U-C-O-H System



A-8 U-Si-C-O-H System



A-9 Th-S-O-H System

APPENDIX B

Detailed Physical and Chemical Description of the Sedimentary Interbed

Table B-2. Extractable Mn and Free Fe Oxides for Interbed Samples

Sample	Depth	Extractable Mn (ppm)	DCB ^a Extractable Fe (as % of Fe ₂ O ₃)
M6S	166-176	0.7	1.09
M6S	386	0.7	1.37
M6S	322-338	3.0	1.37
M7S	213-214	0.2	1.14
M7S	329-330	0.3	2.86 ^b
Interbed	Composite	1.9	1.77

^a DCB=Dithionite-Citrate Buffer Extractable Iron

^b sample was still reddish in color after the DCB treatment, which indicates that free iron oxide removal may have been incomplete.

Table B-3. Chemical Analyses for the M6S and M7S Borehole and Composite Interbed Samples Used in Experiments*
 The Interbed is Compositied from M6S and M7S Boreholes.

Location	Depth ft.	Extractable Bases						CEC Sum Cations	CEC NH ₄ OAc PH 7.0	ECEC Bases + Al meq/100g	pH
		Ca meq/100g	Mg meq/100g	K meq/100g	Na meq/100g						
M6S	166-177	11.15	1.66	0.68	1.85		15.34	4.1	15.34	8.4	
M6S	386	4	1.33	0.57	1.2		7.1	3.3	7.1	9.3	
M6S	322-338	17.7	6.06	1.4	1.42		26.58	20.3	26.58	7.1	
M7S	213-214	1.5	0.42	0.57	0.73		3.22	5.7	3.22	9	
M7S	329-330	10.5	2.82	1.14	0.82		15.28	12.5	15.28	7.7	
Interbed	Composite	14.1	1.66	0.73	0.9		17.39	4.6	17.39	8.7	

Location	Extractable acidity	Base sat		Extractable Al saturation meq/100g
		Sum Cations	%	
M6S	0	100	0	0
M6S	0	100	0	0
M6S	0	100	0	0
M7S	0	100	0	0
M7S	0	100	0	0
Interbed	0	100	0	0

* Samples collected on 5/24/93.

APPENDIX C

Activity and Molar Concentration of Actinides Used in this Investigation

Table C-1. Activity and Molar Concentrations of Actinides Used in this Investigation

Radionuclide	Date	Water	Half-Life (yrs)	Decay constant	Co (CPM/ml)	Molar Conc. (mol/L)
Thorium-230	11.16.98	SPW base	7.540E+04	2.91506E-13	7802	7.40618E-07
		SPW w/o F	7.540E+04	2.91506E-13	8258	7.83905E-07
		SPW w/o CO3	7.540E+04	2.91506E-13	6010	5.70509E-07
		SPW w/o SO4	7.540E+04	2.91506E-13	8182	7.7669E-07
	3.1.99	SPW 0 hr.	7.54E+04	2.91506E-13	20179	1.91553E-06
		SPW 24 hr.	7.54E+04	2.91506E-13	18553.3	1.7612E-06
	8.99	SPW base	7.54E+04	2.91506E-13	41636.9	3.95245E-06
		SPW base	7.54E+04	2.91506E-13	52478	4.98156E-06
		SPW base	7.54E+04	2.91506E-13	1162283	1.10332E-04
	Neptunium-237	2.8.99	SPW w/ HA & EDTA	2.140E+06	1.02708E-14	12220
SPW 0 hr.			2.140E+06	1.02708E-14	12153	3.27427E-05
SPW 24 hr.			2.140E+06	1.02708E-14	12286	3.3101E-05
4.12.99		SPW w/o F	2.140E+06	1.02708E-14	11966.9	3.22413E-05
		SPW w/o CO3	2.140E+06	1.02708E-14	11935.5	3.21567E-05
		SPW w/o SO4	2.140E+06	1.02708E-14	11987.2	3.2296E-05
6.99		Exp 11 w/o HA & EDTA	2.140E+06	1.02708E-14	18566	5.00206E-05
		Exp 11 w/ HA & EDTA	2.140E+06	1.02708E-14	18242	4.91477E-05
7.21.99		SPW w/o CO3 & F	2.140E+06	1.02708E-14	22298.4	6.00765E-05
		SPW w/o CO3 & SO4	2.140E+06	1.02708E-14	20814.5	5.60786E-05
8.99		SPW base	2.140E+06	1.02708E-14	20729.4	5.58493E-05
		SPW base	2.140E+06	1.02708E-14	20655.6	5.56504E-05
		SPW base	2.140E+06	1.02708E-14	64387.3	1.73473E-04
Americium-241	1.25.99	SPW 0 hr.	4.327E+02	5.07963E-11	4398	2.39585E-09
		SPW 24 hr.	4.327E+02	5.07963E-11	3847	2.09569E-09
	6.99	Exp 11 w/o HA & EDTA	4.327E+02	5.07963E-11	16193	8.82127E-09
Uranium-233	1.25.99	SPW 0 hr.	1.592E+05	1.38063E-13	5322	1.06668E-06
		SPW 24 hr.	1.592E+05	1.38063E-13	5128	1.0278E-06
	3.25.99	SPW w/o F	1.592E+05	1.38063E-13	13143.6	2.63436E-06
		SPW w/o CO3	1.592E+05	1.38063E-13	13242.6	2.6542E-06
		SPW w/o SO4	1.592E+05	1.38063E-13	13826.5	2.77123E-06
		SPW w/o CO3,SO4	1.592E+05	1.38063E-13	30742.9	6.16176E-06
		SPW w/o CO3,F	1.592E+05	1.38063E-13	29066.7	5.8258E-06
		DDI pH 7.6-8.5 (column 1)	1.592E+05	1.38063E-13	14588	2.92386E-06
		DDI pH 7.6-8.5 (column 3)	1.592E+05	1.38063E-13	14588	2.92386E-06
		Plutonium-239	3.1.99	SPW 0 hr - Pu(IV)	2.410E+04	9.12015E-13
SPW 24 hr - Pu(IV)	2.410E+04	9.12015E-13		8565.9	2.599E-07	

APPENDIX D

Colloid Attenuation by Interbed Columns

Colloid Attenuation by Interbed Columns

A series of column experiments was conducted to determine (1) the efficacy of washing columns to remove colloidal fines from the column packing material and (2) to determine if either associated or true colloids were attenuated in the columns by the interbed composite soil. To conduct these experiments, the composite interbed soil was sieved to isolate the 106-250 μm particle fraction. Replicate columns were packed with this particle size fraction using the packing techniques discussed in Chapter 3.

The first experiment was designed to determine if colloids were washed from the column during the first few pore volumes of eluant. A spiking solution containing approximately 0.18 μCi of ^{238}Pu was added to 15.7 ml of the PWS followed by pH adjustment to ≈ 9.2 . Approximately one pore volume of the spiking solution was introduced into each of the replicate columns and eluted for approximately 200 pore volumes. The particulate fraction in the column effluent was determined by filtering selected eluant fractions using 0.02- μm x 25-mm syringe filters.

A second experiment was conducted using the replicate columns from the first experiment and represented packed columns that had been washed for 200 pore volumes. A Pu spiking solution was prepared similar to the above preparation and spiked onto the columns as noted above. Again, eluant fractions were filtered to determine the particulate fraction.

A third experiment using the same packed columns, representing packed columns washed with 400 pore volumes of the PWS, was conducted to determine the degree to which associated colloids were attenuated by the column packing. A suspension of interbed colloids $<0.2 \mu\text{m}$ was prepared by mixing interbed particles $<106 \mu\text{m}$ in the PWS by shaking for 24 hours, and filtering at 0.45 μm and then at 0.2 μm . Approximately 0.18 μCi of ^{238}Pu was added to the colloidal suspension and shaken for 24 hours to tag the interbed colloids. A one-pore volume spike of the colloidal suspension was introduced into the pair of columns and eluted for 200 pore volumes with the PWS. As noted above, eluant fractions were filtered at 0.2 μm to determine the particulate fraction in the column effluents.

Results of these experiments are summarized in Table D-1. Results from the first set of experiments show breakthrough from columns 1 and 2 to be 29 and 27 % respectively and the particulate fraction between 83 and 90 %. Filtration of the original spiking solution after 24 hours indicated that 40 to 47 % was in particulate form, likely plutonium oxy-hydroxide colloids. The remainder of the particulate fraction (83-90 % less 40-47 %) may have been colloidal "fines" from the unwashed column. If this was true, results from the second set of experiments should indicate a particulate fraction near 50 % if in fact colloidal "fines" were efficiently washed from the columns during the 200-pore volume eluant. Results from the second pair of columns show breakthrough of 34 % with a particulate fraction between 54 and 72 %, consistent with expectations. In the third set of columns, colloids ($<0.2 \mu\text{m}$) were introduced into the washed columns and one would expect a significant portion of the

colloidal mass to be retained in the column. In experiment 3, breakthrough was in fact reduced from approximately 30 % to 12 and 17% respectively, and the particulate fraction was reduced. This suggests that the columns effectively attenuated colloids from the spiking solution.

In summary, the data from experiments 1 and 2 suggest that the column matrix can attenuate true colloids and the data from experiment 3 that the column matrix also attenuates associated colloids (from experiment 3). Recalling that the columns were packed with interbed particles within a range of 106 to 250 μm , columns packed with interbed soil < 250 μm to include particles <106 μm should more effectively attenuate both true and associated colloids.

Table D-1. Results of Colloid Attenuation Experiments

Experiment-Column	Breakthrough -%	Particulate Pu-%
Expt 1, Col 1	29	85-90
Expt 1, Col 2	27	83-90
Expt 2, Col 1	34	65-72
Expt 2, Col 2	34	54-72
Expt 3, Col 1	12	11-23
Expt 3, Col 2	17	10-17

APPENDIX E

Plutonium Oxidation State Analysis Procedure

Plutonium Oxidation State Analysis

The Bis(2-ethylhexyl) hydrogen phosphate (HDEHP) extraction was used to determine the oxidation state of plutonium in the absence of a holding oxidant. It was also performed on americium, neptunium, and uranium samples to verify the procedure.

HDEHP Extraction (Neu, *et al.*, 1994)

This process involves four separate extractions, which when combined yielded an oxidation state distribution for an aqueous sample of plutonium solution. The four extractions are as follows:

1. Extraction of Pu (IV) into organic phase
2. Extraction of Pu (III) and Pu (IV) into organic phase
3. Extraction of Pu (IV) and Pu (VI) into organic phase
4. Extraction of Pu (III), Pu (IV), Pu (V), and Pu (VI) into organic phase. The Pu remaining in the aqueous phase is termed "unextractable" and is assumed to be in the Pu (IV) polymeric form or in an unextractable complex.

Required Chemicals

- I. 2.25 mL of plutonium solution
- II. 99% thenoyltrifluoroacetone (TTA)
- III. 99% toluene
- IV. 1.0 M HCl
- V. 5.0 M HCl
- VI. 99% HDEHP
- VII. 99% $K_2Cr_2O_7$
- VIII. Wallac/LKB 'HiSafe'2 liquid scintillation cocktail

Required Equipment

- 2 Calibrated adjustable 100-1000 μL Eppendorf pipettor and tips (at 0.25 and 0.50 mL)
- twelve 2-dram vials
- Centrifuge for the 2-dram vials
- Timer
- 20 mL plastic liquid scintillation vials with poly-seal caps (9 per analysis)
- Wallac liquid scintillation detector

Initial Steps

1. Dissolve 2.22 g of the 99% TTA in 20 mL of toluene in a glass scintillation vial that has been covered in aluminum foil to prevent exposure of the solution to light. This will yield a solution that is 0.5 M TTA. This solution will photo-decompose, turning from pale yellow to copper, so it should be stored in a drawer away from light and made just prior to use to minimize the effects of this decomposition.
2. Transfer 3.225 g (3.3 mL) of HDEHP solution into 20 mL of toluene to yield a solution that is 0.5 M in HDEHP.
3. Add 0.02354 g of $\text{K}_2\text{Cr}_2\text{O}_7$ to 20 mL of 1.0 M HCl solution to yield a solution that is 1.0 M in HCl and 4.0 mM in $\text{K}_2\text{Cr}_2\text{O}_7$ [8.0 mM in Cr (VI)].
4. Prepare nine 20 mL plastic liquid scintillation vials by filling each with 10 mL of 'HiSafe'2. These should be placed in two separate protocols due to the difference in quench for the solutions. One protocol should be used for the two TTA/organic samples and another for the aqueous and HDEHP/organic samples.

Extraction Procedure

1. Transfer a 0.25 mL aliquot of the plutonium solution to one of the scintillation vials filled with 'HiSafe'2 to determine the Pu concentration in the original sample.

Extraction 1 - determination of Pu (IV)

2. Transfer 0.5 mL of the TTA/toluene solution to one of the 2-dram vials.
3. Add 0.5 mL of 1.0 M HCl solution to this 2-dram vial.
4. To a second 2-dram vial, add 0.10 mL of 5.0 M HCl solution.
5. Add 0.5 mL of the plutonium solution to the vial containing the 5.0 M HCl and gently swirl to ensure complete mixing.

6. Pour the contents of the vial containing the TTA solution into the vial containing the Pu solution. Be sure to completely empty both the aqueous and organic phases from the vial.
Cap the vial and shake gently for 2m 30s to ensure complete extraction.
7. Centrifuge the vial to facilitate phase separation. Be sure to carefully counterbalance the centrifuge.
8. Place 0.25 mL of the organic phase [Pu (IV)] into one of the scintillation vials filled with 'HiSafe'2.
9. Transfer 0.5 mL of the aqueous phase into a clean 2-dram vial. Depress the pipettor as the tip travels through the organic phase, using the air stream to prevent the introduction of any organic phase into the sample. Now transfer 0.25 mL of this aqueous solution [Pu (III), Pu (V), Pu (VI), and Pu (P)] into one of the scintillation vials filled with 'HiSafe'2, again taking caution to avoid drawing any of the thin film of organic phase from the top of the sample.

Extraction 2 - determination of Pu (III + IV)

Note that extraction 2 is identical to extraction 1, with the exception substituting a 1.0 M HCL/4.0 mM $K_2Cr_2O_7$ solution for the 1.0 M HCl solution from step 2 in step 11. This serves to oxidize any Pu (III) to Pu (IV), which will subsequently be extracted into the TTA/organic phase.

10. Transfer 0.5 mL of the TTA/toluene solution to one of the 2-dram vials.
11. Add 0.5 mL of 1.0 M HC/4mM $K_2Cr_2O_7$ solution to this 2-dram vial.
12. To a second 2-dram vial, add 0. 10 mL of 5.0 M HCl solution.
13. Add 0.5 mL of the plutonium solution to the vial containing the 5.0 M HCl and gently swirl to ensure complete mixing.
14. Pour the contents of the vial containing the TTA solution into the vial containing the Pu solution. Be sure to completely empty both the aqueous and organic phases from the vial.
Cap the vial and shake gently for 2m 30s to ensure complete extraction.

15. Centrifuge the vial to facilitate phase separation. Be sure to carefully counterbalance the centrifuge.
16. Place 0.25 mL of the organic phase [Pu (III), Pu (IV)] into one of the scintillation vials filled with 'HiSafe'2.
17. Transfer 0.5 mL of the aqueous phase into a clean 2-dram vial. Depress the pipettor as the tip travels through the organic phase, using the air stream to prevent the introduction of any organic phase into the sample. Now transfer 0.25 mL of this aqueous solution [Pu (V), Pu (VI), and Pu (P)] into one of the scintillation vials filled with 'HiSafe'2, again taking caution to avoid drawing any of the thin film of organic phase from the top of the sample.

Extraction 3 - determination of Pu (IV + VI)

Note that extraction 3 is identical to extraction 1 except for the substitution of a 0.5 M HDEHP/toluene solution for the TTA/toluene solution from step 1 in step 18. The HDEHP will extract both Pu (IV) and Pu (VI) from the aqueous solution.

18. Transfer 0.5 mL of the HDEHP/toluene solution to one of the 2-dram vials.
19. Add 0.5 mL of 1.0 M HCl solution to this 2-dram vial.
20. To a second 2-dram vial, add 0.10 mL of 5.0 M HCl solution.
21. Add 0.5 mL of the plutonium solution to the vial containing the 5.0 M HCl and gently swirl to ensure complete mixing.
22. Pour the contents of the vial containing the HDEHP solution into the vial containing the Pu solution. Be sure to completely empty both the aqueous and organic phases from the vial.
Cap the vial and shake gently for 2m 30s to ensure complete extraction.
23. Centrifuge the vial to facilitate phase separation. Be sure to carefully counterbalance the centrifuge.
24. Place 0.25 mL of the organic phase [Pu (IV), Pu (VI)] into one of the scintillation vials filled with 'HiSafe'2.
25. Transfer 0.5 mL of the aqueous phase into a clean 2-dram vial. Depress the pipettor as the tip travels through the organic phase, using the air stream to prevent the

introduction of any organic phase into the sample. Now transfer 0.25 mL of this aqueous solution [Pu (III), Pu (V), Pu (P)] into one of the scintillation vials filled with 'HiSafe'2, again taking caution to avoid drawing any of the thin film of organic phase from the top of the sample.

Extraction 4 - determination of Pu (III + IV + V + VI)

Note the extraction 4 is identical to extraction 2 except for the substitution of HDEHP/toluene solution for the TTA/toluene solution from step 10 in step 26. In this extraction, the dichromate solution oxidizes the Pu (III) to Pu (IV) and the Pu (V) to Pu (VI), both of which are subsequently extracted by the HDEHP.

26. Transfer 0.5 mL of the HDEHP/toluene solution to one of the 2-dram vials..
27. Add 0.5 mL of 1.0 M HCl/4.0 mM $K_2Cr_2O_7$ solution to this 2-dram vial.
28. To a second 2-dram vial, add 0.10 mL of 5.0 M HCl solution.
29. Add 0.5 mL of the plutonium solution to the vial containing, the 5.0 M HCl and gently swirl to ensure complete mixing.
30. Pour the contents of the vial containing the HDEHP solution into the vial containing the Pu solution. Be sure to completely empty both the aqueous and organic phases from the vial.
Cap the vial and shake gently for 2m 30s to ensure complete extraction.
31. Centrifuge the vial to facilitate phase separation. Be sure to carefully counterbalance the centrifuge.
32. Place 0.25 mL of the organic phase [Pu (III), Pu (IV), Pu (V), Pu (VI)] into one of the scintillation vials filled with 'HiSafe'2.
33. Transfer 0.5 mL of the aqueous phase into a clean 2-dram vial. Depress the pipettor as the tip travels through the organic phase, using the air stream to prevent the introduction of any organic phase into the sample. Now transfer 0.25 mL of this aqueous solution [Pu (P)] into one of the scintillation vials filled with 'HiSafe'2, again taking caution to avoid drawing any of the thin film of organic phase from the top of the sample.

34. Count each sample for 10 minutes using the Wallac liquid scintillation detector.

Determination of the oxidation state distribution may be obtained via a mass balance on plutonium during each extraction step of the process.

The mass balance algorithm shown in Table E-1 was used to determine the plutonium fraction in each oxidation state for the extraction.

Table E-1. Oxidation state determination algorithm for the HDEHP extraction procedure

Oxidation States	Phase	Counts, DPM 0.25 mL	Volume per Extraction (mL)	Fraction in Oxidation State	Fraction Recovered
ALL	Original Sample	C_0	0.5	-	
IV	TTA Organic	C_1	0.5	$\frac{0.5 C_1}{0.5C_1+1.1C_2}$	$0.5C_1+1.1C_2$
					$0.5C_0$
III, V, VI, P	TTA Aqueous	C_2	1.1	$\frac{1.1C_2}{0.5C_1+1.1C_2}$	$0.5C_1+1.1C_2$
					$0.5C_0$
III, IV	TTA/Cr Organic	C_3	0.5	$\frac{0.5 C_3}{0.5C_3+1.1C_4}$	$0.5C_3+1.1C_4$
					$0.5C_0$
V, VI, P	TTA/Cr Aqueous	C_4	1.1	$\frac{1.1C_4}{0.5C_3+1.1C_4}$	$0.5C_3+1.1C_4$
					$0.5C_0$
IV, VI	HDEHP Organic	C_5	0.5	$\frac{0.5 C_5}{0.5C_5+1.1C_6}$	$0.5C_5+1.1C_6$
					$0.5C_0$
III, V, P	HDEHP Aqueous	C_6	1.1	$\frac{1.1C_6}{0.5C_5+1.1C_6}$	$0.5C_5+1.1C_6$
					$0.5C_0$
III, IV, V, VI	HDEHP/Cr Organic	C_7	0.5	$\frac{0.5 C_7}{0.5C_7+1.1C_8}$	$0.5C_7+1.1C_8$
					$0.5C_0$
P	HDEHP/Cr Aqueous	C_8	1.1	$\frac{1.1C_8}{0.5C_7+1.1C_8}$	$0.5C_7+1.1C_8$
					$0.5 C_0$

APPENDIX F

Aging Filtration Experimental Data

Table F-1. Summary of aging filtration experiments

	Time	Unfiltered 1 (cpm)	Unfiltered 2 (cpm)	Average (cpm)	Filtered 1 (cpm)	Filtered 2 (cpm)	Average (cpm)	Soluble fraction	RPD
Americium	0	4597	4490	4543	4584	4575	4580	100.8	0.023
	4	4539	4518	4528	4558	4550	4554	100.6	0.005
	12	4640	4613	4627	4673	4675	4674	101.0	0.006
	24	4675	4717	4696	4690	4704	4697	100.0	0.009
PH 8	0	3771	3728	3749	739	723	731	19.5	0.011
	4	2938	2866	2902	500	498	499	13.3	0.025
	12	2731	2720	2726	146	148	147	3.9	0.004
	24	2694	2564	2629	33	22	28	0.7	0.049
Uranium	0	5325	5204	5264	5271	5253	5262	100.0	0.023
	4	5286	5264	5275	5265	5264	5265	99.8	0.004
	12	5257	5298	5277	5276	5305	5290	100.2	0.008
	24	5345	5299	5322	5348	5352	5350	100.5	0.009
PH 8	0	5250	5211	5230	5140	5102	5121	97.9	0.007
	4	5216	5210	5213	5168	5081	5124	98.3	0.001
	12	5203	5204	5204	5230	5124	5177	99.5	0.000
	24	5340	5309	5324	5191	5157	5174	97.2	0.006

Table F- 1 (continued). Summary of aging filtration experiments

	Time	Unfiltered 1 (cpm)	Unfiltered 2 (cpm)	Average (cpm)	Filtered 1 (cpm)	Filtered 2 (cpm)	Average (cpm)	Soluble fraction	RPD
Neptuniurn	0	3773	3763	3768	3812	3767	3789	100.6	0.003
	4	3840	3790	3815	3811	3828	3820	100.1	0.013
	12	3826	3832	3829	3856	3815	3836	100.2	0.002
	24	3867	3903	3885	3877	3893	3885	100.0	0.009
	0	4186	4110	4148	4120	4039	4079	98.4	0.018
	4	4118	4120	4119	3948	3959	3953	96.0	0.000
	12	4158	4193	4175	4002	3920	3961	94.9	0.009
	24	4256	4230	4243	3989	3945	3967	93.5	0.006
Thorium	0	1518	1478	1498	1472	1460	1466	97.9	0.026
	4	1522	1525	1524	1426	1445	1436	94.2	0.002
	12	1521	1516	1519	1451	1434	1443	95.0	0.004
	24	1560	1554	1557	1517	1476	1496	96.1	0.004
	0	8128	7964	8046	66	68	67	0.8	0.020
	4	6968	6945	6957	61	69	65	0.8	0.003
	12	6745	6528	6636	66	61	63	0.8	0.033
	24	5468	6048	5758	59	59	59	0.7	0.101

Table F- 1 (continued). Summary of aging filtration experiments

	Time	Unfiltered 1 (cpm)	Unfiltered 2 (cpm)	Average (cpm)	Filtered 1 (cpm)	Filtered 2 (cpm)	Average (Ccpm)	Soluble fraction	RPD	
Plutonium(IV)	pH 2	0	3886	3884	3885	3673	3638	3655	94.1	0.000
		4	3923	3959	3941	3653	3698	3675	93.3	0.009
		12	3953	4004	3978	3737	3651	3694	92.9	0.013
		24	4035	4026	4031	1722	3710	3716	92.2	0.002
pH 8	pH 8	0	3755	3742	3749	2199	1784	1991	53.1	0.003
		4	3830	3829	3830	1414	1840	1627	42.5	0.000
		12	3873	3857	3865	1597	1566	1581	40.9	0.004

THE CONTENTS OF THIS SECTION ARE
THE HIGHEST QUALITY AVAILABLE

INITIAL MO DATE 9/27/01

APPENDIX G

Plutonium and Uranium Modeling Data

ACTINIDE MOBILITY AT THE SOIL CONSOLIDATION UNIT

Jonathan Myers, International Technology Corporation, Albuquerque, New Mexico, **James D. Navratil**, Lockheed Martin Idaho Technologies Company, Idaho Falls, Idaho

7/17/98 Draft

The migration behavior of actinides (such as plutonium and uranium) in the subsurface at the Idaho Nuclear Technology and Engineering Center (INTEC), formally the Idaho Chemical Processing Plant (ICPP), is not well understood. This information deficiency prevents the accurate prediction of potential impacts of actinides in the planned Soil Consolidation Unit (SCU) at the INTEC. More rigorous estimates of distribution coefficient (K_d) values for soil/solution pairings in the sedimentary interbed and potential SCU liner materials, as well as contaminated soils at the INTEC, are needed to support accurate cleanup decisions and to develop a realistic Waste Acceptance Criteria for the SCU.

The potential for plutonium to leach from the Tank Farm Soils (TFS) must also be evaluated. If the leachable concentration of plutonium is lower than the maximum concentration limit (MCL) allowed for plutonium, then the K_d is of much less importance since the MCL would not be exceeded in the aquifer in any case. However, the current TFS inventory represents over 90% of the plutonium source for potential transport through the vadose zone. The current groundwater modeling approach assumes a K_d for plutonium of 22 in interbed sediments between the TFS (source) and the aquifer. The resulting calculated risk values are above 1 in 10,000 excess cancer risk for exposure to plutonium when the peak modeled concentration occurs (Rodriguez, et al., 1997).

This brief summary and interpretation report is based on existing data and will present the current state of knowledge of plutonium and uranium mobility issues for the TFS. The data review includes a description of waste processes generating the actinides in the TFS, summary of available soil characterization data, evaluation of the ability of the TFS to sorb actinides for the applicable range of solution chemistries, and the effect of co-releases on the mobility and chemical forms of actinides released from the TFS.

Actinide Generating Waste Processes

The INTEC has been in operation since 1954 and has historically been a uranium reprocessing facility for defense projects and for research and storage of spent nuclear fuel. After fuel dissolution and extraction, several types of high-level radioactive liquid wastes have been produced. In the past inadvertent releases of radioactivity have contaminated some of the subsurface at the INTEC.

The INTEC fuel dissolution processes produced a solution of uranyl nitrate for several cycles of solvent extraction processing. The purposes of the solvent extraction processes were to separate the uranium from the residual fission products and transuranic elements, recover most of the uranium as product, and after reducing its volume, transfer the waste material to storage. The first-cycle solvent extraction process preferentially separated uranium from fission products using tributyl phosphate (TBP) in a hydrocarbon diluent, whereas subsequent extraction cycles separated the transuranics. The second- and third-cycle extraction processes used methyl isobutyl ketone to purify the uranium product from the first-cycle extraction.

Following reprocessing, the wastes were directed to the high-level liquid waste (HLLW) Tank Farm or process equipment waste (PEW) Evaporator Facility. Table 1 summarizes the estimates

of volume, duration, and quantity of radioactivity released at each of the three tank farm sites as well as the other two known or estimated release sites. Chemical components in the first two releases will be highlighted below since they account for the majority of the activity released.

The majority of liquid waste stored in the Tank Farm was generated during the first-, second, and third-cycle extraction processes. These raffinates include high-level wastes that are composed of first- and second-cycle raffinates and intermediate-level wastes that are composed of third-cycle raffinates blended with concentrated bottoms from the PEW Evaporator. Additional wastes stored in the Tank Farm include fluoride and cadmium bearing wastes from the fluorinel process, decontamination wastes containing fluoride from waste calcining and other process salvage streams (Rodriguez, et al., 1997).

The release identified with CPP-28 and CPP-79 is assumed to be first cycle waste; therefore, radionuclide estimates relied exclusively on data from the analysis of first cycle waste (Rodriguez, et al., 1997). The data of Rhodes (1972) provides the results of non-radioactive chemical analyses of first cycle waste samples obtained from the tank farm in September 1971. These data are shown in Table 2. Table 3 provides average non-radioactive chemical composition of tank farm waste for estimating constituents in CPP-31 (Donovan, 1989). Rodriguez, et al., (1997) provides the maximum, minimum, and average value of the total mass release estimates for nonradioactive constituents from CPP-28, CPP-79 and CPP-31. These data were used to formulate the information in the last two sections of this report.

Available Soil Characterization Data

There has been some sampling of the TFS, but the analysis performed was mainly for radiological content of the soils. No actinide speciation data are available. The available information on chemical contamination in the soils is shown in Table 4. Additional descriptive information on CPP-28, -79 and -31 follows.

In 1974, soil with radioactive contamination up to 40 R/hr was encountered at a depth of about 1.8-m (6 ft) below ground surface (bgs) at CPP-28. The leak was later determined to be from a hole inadvertently drilled through one side of a pipe during original construction in 1955. HLLW consisting of first-cycle raffinate most likely leaked through secondary containment to the surrounding soil and may have occurred as early as 1955 (Rodriguez, et al., 1997).

Six soil borings were drilled on October 10, 1994, and one soil sample was collected from the bottom of a borehole. The depth of sample collection for the beta-gamma radiation measurements ranged from 2.0 to 3.0 m (6.5 to 10 ft) bgs. Only one soil sample indicated radiological contamination at a level of 40 R/hr beta-gamma on contact. Isotopic analyses were not performed on any of the soil samples. It is now believed that most of these boreholes were not drilled deep enough to intercept soil contamination.

No sampling data are available to accurately delineate the extent of contaminated soil in the vicinity of site CPP-28. Contaminants have likely migrated further to the south than to the north due to the presence of a tank immediately north of site CPP-28. It is also possible, if not likely, that preferential migration pathways may be present in the form of sandy backfill commonly

placed in pipeline excavations. Considering the high radiation levels on the 9.1-m (30-ft) sample, it is also likely that contamination extends downward to the soil/basalt interface at a depth of about 12.8 (42 ft).

CPP-79 was originally defined as soil contaminated by the releases of waste solutions in July and August of 1986 due to an obstruction in a transfer line. A second, deeper zone of contamination at this site is believed to be related to the release of HLLW at site CPP-28. During a CPP-79 investigation, one soil boring was drilled in the alluvium near the release to determine the type and concentration of the residual contamination and to characterize the deeper soils in the Tank Farm area. A total of 15 split-spoon samples were collected from the borehole. The split-spoon samples were screened in the field for gross beta-gamma radiation and a total of seven samples were selected from the zones having the highest radiation for further analysis. Samples were analyzed for VOCs, mercury, cadmium, nitrate/nitrite, pH, and radionuclides. These results are summarized on Table 4.

An investigation of the source of contamination at site CPP-31 revealed that in November 1972 HLLW was released to the surrounding soil during a transfer between two tanks. The release was caused by a failure of a waste transfer line where it was speculated that the highly acidic BLLW corroded the transfer line, located about 2 ft bgs. Soil sample data are not available to delineate the extent of chemical contamination.

Chemical Forms and Mobility of Actinides Released from TFS

The solubility and speciation of plutonium and uranium in INEEL groundwater was calculated using version 7.2b of the EQ3NR code (Wolery, 1992) along with version 8 release 6 of the "composite" thermodynamic database compiled by Lawrence Livermore National Laboratory. This version of the database contains a total of 80 elements, 1768 aqueous species, 93 gases, and 1130 solid phases. The 31 aqueous plutonium species and 11 solid plutonium-bearing phases that are part of the database are listed in Table 5. Table 6 shows the 79 aqueous uranium species considered in the model.

Two groundwater compositions were used in the model. A high fluoride composition is based on a synthetic INEEL perched groundwater formulation provided in Fjeld et al., 1998; and a low fluoride composition is based on analyses of perched groundwater samples collected near the Chemical Processing Plant (Rodriguez, et al., 1997). The compositions of these two formulations are provided in Table 7. The effects of pH were assessed by using a pH of 8, which is the undisturbed groundwater value, and a pH of 6, which may represent groundwater impacted by tank farm waste. Modeling results indicate that both groundwaters are in equilibrium with calcite (CaCO_3) at a pH of 8, and are undersaturated with respect to calcite at an assumed pH of 6. The high fluoride groundwater is in equilibrium with fluorite (CaF_2) at both pH values. The redox state of the groundwater is a key parameter affecting plutonium solubility and speciation but is poorly characterized. The redox was varied in the calculations over a range of redox potentials to assess the effects of this parameter in both the high-fluoride and low-fluoride groundwaters. The concentrations of plutonium and uranium were controlled by assuming equilibrium with an appropriate stable solid phase.

The effect of other ligands originally present in the waste solutions, such as TBP and its hydrolysis products, and naturally occurring organics, such as humic acids, were not considered in the calculations. These ligands are assumed to play a lesser role in transport as compared to hydrolysis reactions and colloid formation.

Plutonium-Solubility and Speciation The predicted solubility of plutonium for three cases (low F^- at pH 8, high F^- at pH 8, and high F^- at pH 6) is shown as a function of redox potential (+200 to +700 mV) in Table 8 and Figure 1. $Pu(OH)_4$ was the predicted stable phase at pH 6 over the 200 to 700 mV redox range considered. At pH 8, $Pu(OH)_4$ was the predicted stable phase below a redox potential 630 mV and $PuO_2(OH)_2$ was predicted above a redox potential of 630 mV. Results for all three cases show a marked increase in solubility above a redox potential of 500 mV, corresponding to the oxidation of Pu IV species to the more soluble Pu V and Pu VI species. The low fluoride composition shows lower solubilities than the other groundwater compositions under oxidizing conditions because of the absence of fluoride species. The solubility under oxidizing conditions is limited above a redox potential of 630 mV by the precipitation of $PuO_2(OH)_2$, which controls the solubility at 2×10^{-7} M.

In the high fluoride groundwater at a pH of 8, the solubility above 630 mV is also limited by the precipitation of $PuO_2(OH)_2$. A pH of 6 is too low for the precipitation of $PuO_2(OH)_2$ so the solubility continues to rise above 630 mV under the control of $Pu(OH)_4$. At redox potentials below 300 mV, the solubility at pH 8 remains quite low ($\sim 2 \times 10^{-9}$ M). However, at pH 6, Pu III species (Pu^{+3} , $PuSO_4^+$, and $Pu(SO_4)_2^-$) become stable and contribute to increasing solubility.

The speciation of plutonium in the low fluoride pH 8 composition is shown in Table 9 and Figure 2; the high fluoride pH 8 composition is shown in Table 10 and Figure 3; and the high fluoride pH 6 composition is shown in Table 11 and Figure 4. The species shown contribute >99 percent of the total solubility. The complexity of plutonium speciation is evident in these results. At redox potentials above 500 mV, which is a likely condition in the vadose zone, between three and five different species are present at significant percentages of the total dissolved plutonium.

These species have a variety of different charges, including -2, -1, 0, and +1. Under oxidizing conditions, anionic fluoride species [$PuO_2F_4^{-2}$ and $PuO_2F_3^-$] dominate in the high fluoride compositions, and the anionic carbonate form [$PuO_2(CO_3)_2^{-2}$] dominates in the low fluoride composition. Under reducing conditions, the neutral $Pu(OH)_4$ form dominates, but at pH 6, the Pu III species become increasingly significant as the redox potential drops below 300 mV.

Uranium Solubility and Speciation The predicted solubility of uranium in two groundwaters (low F^- at pH 8 and low F^- at pH 6) is shown as a function of redox potential (-300 to +650 mV at pH 8, and -200 to +800 mV at pH 6) in Table 12 and Figure 5. At a pH of 8, calcium uranate ($CaUO_4$) is the stable phase above +50 mV and uraninite (UO_2) is the stable phase below +50 mV. At a pH of 6, uranyl carbonate (UO_2CO_3) is the stable phase above +150 mV and uraninite is the stable phase below +150 mV.

Results for both cases (low F^- at pH 8 and low F^- at pH 6) show low solubilities in the range of 5×10^{-10} M below a redox potential of ~ 0 mV, with a marked increase to 1×10^{-4} M above -150 mV. This increase in solubility of almost six orders of magnitude corresponds to the oxidation of U (IV) species to the more soluble U (VI) species as well as a shift in the controlling phase from

the tetravalent uraninite to the hexavalent CaUO_4 (pH 6) or UO_2CO_3 (pH 8) as the redox potential increases.

The speciation of uranium in the low F^- groundwater at a pH of 8 is shown in Table 13 and Figure 6, and the speciation in the low F^- groundwater at a pH of 6 is shown in Table 14 and Figure 7. The species shown contribute to >99 percent of the total solubility. Under reducing conditions (below -100 mV at pH 8, and below +100 mV at pH 6), the speciation is dominated by the neutral tetravalent $\text{U}(\text{OH})_4$ form. Under oxidizing conditions, a mixture of hexavalent uranyl carbonate, hydroxy, and mixed carbonate-hydroxy species are dominant. At pH 8 above -100 mV, the speciation is dominated by $\text{UO}_2(\text{CO}_3)_3^{4-}$, $\text{UO}_2(\text{CO}_3)_2^{2-}$, and $(\text{UO}_2)_2\text{CO}_3(\text{OH})_3^-$ in that order. At pH 6 above +100 mV, the speciation is dominated by $\text{UO}_2(\text{CO}_3)_2^{2-}$, $(\text{UO}_2)_2\text{CO}_3(\text{OH})_3^-$, $\text{UO}_2\text{CO}_3(\text{aq})$, $\text{UO}_2(\text{OH})_2(\text{aq})$, UO_2OH^+ , and $\text{UO}_2(\text{CO}_3)_3^{4-}$ in that order. The difference in uranium speciation at pH 8 versus pH 6 is indirectly caused by carbonate speciation. At pH 6, most of the total dissolved carbon is in the form of HCO_3^- which is a form that is unavailable for uranium complexation. At higher pH condition, a greater proportion of total dissolved carbon is in the form of CO_3^{2-} , which is a strong uranium complexing ligand.

Ability of TFS to Sorb Actinides

Adsorption of dissolved groundwater constituents along flow paths is a complex process that can be subject to a large number of site-specific variables. There are however, a few generalizations that can be drawn from the speciation results. At neutral pH clay minerals have a net negative surface charge, and iron- and manganese-oxides have a net positive surface charge. Because of these surface charges, cationic (positively charged) species tend to adsorb on clay minerals; anionic (negatively charged) species tend to adsorb on iron- and manganese-oxide minerals; and neutral species tend to display little or no adsorption (Drever, 1982). The higher the charge on the species, the stronger the attraction on mineral surfaces with opposite charge, and the stronger the repulsion on mineral surfaces with the same charge.

The soils in the vicinity of the tank farm are dominantly composed of silt (13 to 88%) and sand (S to 85%), with lesser amounts of clay (2 to 15%) (INEL, 1994). This type of soil is predicted to provide fairly good adsorption of cationic species, but poor adsorption of anionic or neutral species. The percentage of plutonium existing as cationic species is at a maximum of 30 to 70 percent (depending on the composition) at a redox potential of -550 mV, but the percentage of cationic species is much less at both higher and lower redox potentials. For instance, the speciation of plutonium at 700 mV and a pH of 8 in the high fluoride groundwater is $\text{PuO}_2\text{F}_4^{2-}$ (46%), PuO_2F_3^- (45%), and $\text{PuO}_2(\text{CO}_3)_2^{2-}$ (9%). The uranium speciation is likewise dominated by anionic species under oxidizing conditions, and neutral species under reducing conditions. These dominant plutonium and uranium species would not be expected to adsorb very strongly on silty tank farm soils.

Modeling the transport of uranium or plutonium when they are present as several different species with different charges presents a problem. The use of a single K_d is an oversimplification because each of the species will migrate at different velocities. The situation is compounded by the fact that in a system at equilibrium, the ratios between all of the species of a given element are fixed. The selective adsorption of one or more species will create disequilibrium in the aqueous phase as

it migrates along the flow path. The system will respond by re-apportioning the remaining dissolved

element between the stable species in an attempt to re-establish the equilibrium ratios. The rate at which the transformations between species occur varies. Transformations involving changes in the plutonium or uranium valence state occur more slowly than simple transformations such as $\text{PuO}[\text{F}_3]^- + \text{F}^- \rightleftharpoons \text{PuO}_2\text{F}_4^{-2}$, or $\text{UO}_2\text{CO}_3(\text{aq}) + \text{CO}_3^{-2} \rightleftharpoons \text{UO}_2(\text{CO}_3)_2^{-2}$. Adsorption and desorption processes simultaneously occur at different rates, and the groundwater moves at some rate. The relative differences between rates of species transformation, adsorption, desorption, and groundwater flow, control the extent to which chemical equilibrium is maintained in the water-sediment system.

The use of a weighted average K_d may accurately describe the transport of the central portion of the plume, but it may seriously underestimate the velocity of the leading edge of the plume. The use of a conservative (low) K_d based on the most mobile form may accurately describe the leading edge of the plume, but the concentrations at the leading edge may be insignificant. An alternative approach is to apportion the total dissolved plutonium among the major species and assigning a different K_d to each one. These species can then be treated as separate constituents in a transport model, and then summed to predict concentration (or dose) versus time at a receptor site. Transformations between the species would be difficult to account for in such a model, and may introduce large uncertainties in the results.

The use of empirical break-through curves from column sorption experiments on native soils can provide insight into actinide mobility and can validate speciation modeling results. Differences in the transport properties of each of the major species that are present will show up as inflections in the cumulative break-through curve. The experiments can be scaled so that the water velocities are in the same range as the actual conditions, or alternatively, can be performed at several higher velocities and the results extrapolated to the actual conditions. These experiments, coupled with solubility-speciation modeling, provide the best approach to estimating actinide mobility.

References

Donovan, R. I., 1989, Tank Farm Inventory, Westinghouse Idaho Nuclear Company, Inc., Letter and Attachment to A. P. Hoskins: RID-08-89, August 14, 1989.

Drever, J. I., 1982, The Geochemistry of Natural Waters, Prentice-Hall Inc.

Fjeld, R. A., 1998, J. T. Coats; W. W. Elzerman and J.D. Navratil, "Column Studies of Plutonium Transport in Sedimentary Interbed From the Snake River Plain," Proceedings of WM'98, 38-08.

INEL, 1994, "Technical Memorandum on the Hydrogeology at the Idaho Chemical Processing Plant", Lockheed Idaho Technologies Company, Idaho National Engineering Laboratory, Idaho Falls, Idaho.

Rhodes, D. W., 1972, Composition of First- and Second-Cycle Wastes, Allied Chemical Corp. Interoffice Correspondence: Rhod-4-72, August 7, 1972.

Rodriguez, et al., 1997, Comprehensive RI/FS for the ICCP OU 3-13 at the INEEL-Part A, RI/BRA Report, DOE/ID-10534, November 1997.

Wolery, T. J., 1992, EQ3NR, "A Computer Program for Geochemical Aqueous Speciation-Solubility Calculations: Theoretical Manual, Users Guide, and Related Documentation (Version 7. 0)", Lawrence Livermore National Laboratory, UCRL-MA- 110662 PT III.

Table 1 Release estimate summary for liquid release sites in the vadose zone.

Release Name	Release ^a Volume	Release ^b Duration	Begin ^b Date	End ^b Date	Estimate of Total Activity Released
	(1)	(days)			(Ci)
CPP-28/79	13,736	6,84	1/1/56	10/1/74	32,661
CPP-31	52,990	2	11/1/72	11/30/72	28,000
1986	9,508	2	7/7/86	8/2/86	43
CPP-02	181,074,400	4,74	1/1/54	12/31/66	493
CPP-80	399,318	2,55	1/1/83	12/31/89	550

^aRelease volume for CPP-28/79 is determined by bounding calculations on the maximum throughput of a 1/8" diameter hole in a transfer line assuming a total volume of 1.234×10^{-7} L (3.26×10^6 gal) passed through the line under a pressure of 1.83 m(6ft) see Appendix; the release volume for CPP-31 is provided in Allied Chemical Corp.(1975); the release volume for the 1986 is provided in WINCO (1986); the release volume for CPP-02 is provided in USGS (1974); the release volume for CPP-80 is provided in WINCO (1993).

^b The release duration and dates for CPP-28/79 are estimated by assuming the release occurred from the time of construction (approximately 1/1/56) until time of Discovery of the release (10/1/74); release duration and dates for CPP-31 are provided in Allied Chemical Corp. (1975); the release duration and dates for the 1986 are provided in WINCO (1986); the release duration and dates for CPP-02 are provided in USGS (1974); the release duration and dates for CPP-80 are provided in WINCO (1993).

^cThe total activity release estimate for CPP-28/79 is determined using a release volume of 13,736 L (3,629 gal) with an activity concentration of 2.38 Ci/L (9 Ci/gal); activity release estimate for CPP-31 is provided in Allied Chemical Corp. (1975); the total activity release estimate for the 1986 is determined using a maximum process equipment waste (PEW) activity concentration of 1×10^7 d/min/ml (0.017Ci/gal) and a release volume of 9508 L(2512 gal); the total activity release estimate for CPP-02 is provided in USGS (1974); the total activity release estimate for CPP-80 is provided in WINCO (1993).

Table 2 Non-radioactive chemical constituents of first cycle waste -From Rhodes (1972)

Non-radionuclide	WM-185	WM-187	WM-198	Units
H+	1.5	1.62	1.72	M
Al+3	0.6	0.64	0.69	M
Zr+4	0.4	0.44	0.48	M
F-	3.1	3	3.52	M
B	2.1	2.08	2.34	g/L
N03-	2.3	2.32	2.4	M
Fe+3	0.25	0.225	0.298	g/L
Cl-		12	37	mg/L
Na	2	60	74	mg/L
H+	1.522E-0	1.633E-03	1.734E-03	kg/L
Al+3	1.835E-0	1.727E-02	1.862E-02	kg/L
Zr+4	4.014E-0	4.014E-02	4.379E-02	kg/L
F-	5.928E-0	5.700E-02	6.687E-02	kg/L
B	2.160E-0	2.080E-03	2.340E-03	kg/L
N03-	1.463E-0	1.439E-01	1.488E-01	kg/L
Fe+3	2.570E-0	2.250E-04	2.980E-04	kg/L
Cl-	9.000E-0	1.200E-05	3.700E-05	kg/L
Na	2.900E-0	6.000E-0	7.400E-05	kg/L

Table 3 Non-radioactive chemical constituents of tank- farm waste from Donovan (1989).

Nonradionuclide	WM-180	WM-181	WM-182	WM-183	WM-184	WM-185	WM-186	WM-187	WM-188	WM-189	Units
H+	1.92	1.51	0.83	1.71	0.43	1.71	1.4	1.51	1.79	1.8	Normal
NO ₃	5.79	3.24	4.11	4.5	4.63	5.05	2.93	1.39	1.78	2.28	M
Al	0.55	0.21	1.19	0.5	0.81	0.71	0.35	0.43	0.29	0.18	M
Na	1.78	0.83	0.02	0.7	1.98	1.38	0.96	0.02	0.03	0.05	M
K	0.23	0.12		0.1	0.13	0.18	0.16		0.01	0.04	M
F	0.05	0.08	0.07	0.0	0.04	0.15	0.04	2.32	1.74	0.28	M
Zr		0.01	0.01			0.01		0.31	0.26	0.03	M
B	0.26	0.17	0.13	0.1	0.08	0.29	0.22	1.62	1.81	0.26	g/L
Cd	0.17	0.49	0.20	0.1	0.02	0.10	0.19	5.82	11.59	1.22	g/L
Ca		1.78		1.5	0.44	2.55	2.52			4.35	g/L
Cl	0.74	0.27	0.05	0.2	1.54	1.08	0.7	0.05	0.05	0.12	g/L
Cr		0.13		0.6	0.11	0.28				0.09	g/L
Fe	1.41	0.66	1.14	3.0	1.11	1.22	1.01	0.3	0.37	0.25	g/L
Pb		0.21		0.2	0.20	0.17					g/L
Hg		0.10		0.5	0.31	0.86					g/L
Mo		0.05		0.0	0.05	0.05				0.05	g/L
Mn		0.71		0.7	0.46	1.05.16					g/L
Ni		0.07		0.3	0.07	0.10				0.05	g/L
P		0.19		0.1	0.73	0.08					g/L
SO ₄	2.97	3.85	4.18	0.81	6.66	3.73	3.2	3.49	6.59	0.86	g/L

Table 4 Available Data on Chemical Contaminants in Soil Samples

Table 5 Plutonium-bearing aqueous species and solid phases considered in model

Aqueous Species

Bare cation	Pu^{+4}	
Oxy	PuO_2^+	PuO_2^{+2}
Hydroxy	$\text{Pu}(\text{OH})_2^{++}$ $\text{Pu}(\text{OH})_4(\text{aq})$ $\text{PuO}_2\text{OH}(\text{aq})$ PuOH^{+2}	$\text{Pu}(\text{OH})_3^+$ PuOH^{+3} PuO_2H^+
Phosphates	$\text{Pu}(\text{HPO}_4)_2(\text{aq})$ $\text{Pu}(\text{HPO}_4)_4^{-4}$ PuHPO_4	$\text{Pu}(\text{HPO}_4)_3^{-2}$ $\text{PuH}_2\text{PO}_4^{+2}$ $\text{PuO}_2\text{H}_2\text{PO}_4^+$
Sulfates	$\text{Pu}(\text{SO}_4)_2(\text{aq})$ PuSO_4 $\text{PuO}_2\text{SO}_4(\text{aq})$	$\text{Pu}(\text{SO}_4)_2^-$ PuSO_4
Fluorides	PuF^{+3} PuF^{+3} PuO_2F^+ PuO_2F_3^-	PuF_2^{+2} $\text{PuF}_4(\text{aq})$ $\text{PuO}_2\text{F}_2(\text{aq})$ $\text{PuO}_2\text{F}_4^{-2}$
Carbonates	$\text{PuO}_2(\text{CO}_3)_2^{-2}$	
Chlorides	PuO_2Cl^+	
<u>Solid Phases</u>	Plutonium $\text{Pu}(\text{HPO}_4)_2$ $\text{Pu}(\text{OH})_4$ PuF_3 PuO_2 PuO_2HPO_4	$\text{Pu}(\text{OH})_3$ Pu_2O_3 PuF_4 $\text{PuO}_2(\text{OH})_2$ $\text{PuO}_2\text{OH}(\text{am})$

Table 6 Uranium-bearing aqueous species considered in the model

Bare cation	U^{+3}	U^{+4}		
Oxy	UO_{2+}	UO_{2++}		
Oxy/Hydroxy	UOH^{+3} $UO_2(OH)_3^-$ $(UO_2)_3(OH)_7$	$U(OH)_4(aq)$ $UO_2(OH)_4^{-2}$ $(UO_2)_3(OH)_4+2$	UOH_2OH^+ $(UO_2)_2OH^{+3}$ $(UO_2)_3(OH)_5^+$	$UO_2(OH)_2(aq)$ $(UO_2)_2(OH)_2^{+2}$ $(UO_2)_4(OH)_7^+$
Carbonate	$U(CO_3)_4^{-4}$ $UO_2(CO_3)_3^{-4}$	$U(CO_3)_5^{-5}$ $UO_2(CO_3)_3^{-5}$	$UO_2CO_3(aq)$ $(UO_2)_3(CO_3)_6^{-6}$	$UO_2(CO_3)_2^{-2}$
Hydroxycarbonate	$(UO_2)_2CO_3(OH)_3$	$(UO_2)_3(OH)_5CO_2+$	$(UO_2)_3O(OH)_2(HCO_3)+$	$(UO_2)_{11}(CO_3)_6(OH)_{12}^{-2}$
Nitrate/Azide	UNO_3^{+3} $UO_2(N_3)_2(aq)$	$U(NO_3)_2^{+2}$ $UO_2(N_3)_3^-$	$UO_2NO_3^+$ $UO_2(N_3)_4^{-2}$	$UO_2N_3^+$
Sulfate	USO_4^{+2}	$UO_2SO_4(aq)$	$UO_2(SO_4)_2^{-2}$	$U(OH)_2SO_4$
Sulfite/Thio	$UO_2SO_3(aq)$	$UO_2(SO_3)_2^{-2}$	$UO_2S_2O_3(aq)$	
Phosphate	$UO_2PO_4^-$ $UO_2(H_2PO_4)_2(aq)$	$UO_2H_2PO_4^+$ $UO_2(H_2PO_4)(H_3PO_4)^+$	$UO_2H_3PO_4^{+2}$	$UO_2HPO_4(aq)$
Fluoride	UF^{+3} UF_5^-	UF_2^{+2} UF_6^{-2}	UF^{3+}	$UF_4(aq)$
Oxyfluoride	UO_2F^+	$UO_2F_2(aq)$	$UO_2F_3^-$	$UO_2F_4^{-2}$
Chloride	UCl^{+3}			
Oxychloride	UO_2Cl^+	$UO_2Cl_2(aq)$	$UO_2ClO_3^+$	
Iodide/Iodate	UI^{+3}	$UO_2IO_3^+$	$UO_2(IO_3)_2(aq)$	
Bromide/Bromate	UBr^{+3}	UO_2Br^+	$UO_2BrO_3^+$	
SCN	$USCN^{+3}$ $UO_2(SCN)_2(aq)$	$U(SCN)_2^{+2}$	UO_2SCN^+	$UO_2(SCN)_3^-$
Organics	$U(\text{Butanoate})^{+2}$ $U(\text{Formate})_2^+$	$U(\text{Butanoate})_2^+$ $U(\text{Propanoate})^{+2}$	$U(\text{Pentanoate})^{+2}$ $U(\text{Propanoate})_2^+$	$U(\text{Formate})^{+2}$

Table 7 Groundwater compositions used in solubility speciation model

Constituent	Concentration (mg/l)	
	High Fluoride ¹	Low Fluoride ²
Na ⁺	570	285
K ⁺	10	10
Ca ⁺²	10	10
Mg ⁺²	17	17
Fe ⁺²	1.61	
	0.01	
Al ⁺³	0.7	0.001
Zr(OH) ₂ ⁺²	0.023	0.001
SiO ₂ (aq)	21	0.001
Cl ⁻	220	125
NO ₃ ⁻	7.8	300
HCO ₃	763	294
SO ₄ ⁻²	350	61.4
F ⁻	20	0.36
TDS	1960	1103
pH	6.0,8.0	6.0,8.0
Eh	+200 to +700 mV	-300 to +700 mV

¹From Fjeld, et al., 1998

²From Rodriguez, et a 1.,1997

Table 8 Plutonium solubility and controlling solid phase in three INEEL perched groundwater compositions

Redox (mV)	Low Fluoride, pH 8 Solubility	Phase	High Fluoride, pH 8 Solubility (M)	Phase	High Fluoride, pH 6 Solubility	Phase
700	1.9E-07	PuO ₂ (OH) ₂	5.7E-06	PuO ₂ (OH) ₂	4.9E-04	Pu(OH) ₄
650	2.6E-07	PuO ₂ (OH) ₂	5.8E-06	PuO ₂ (OH) ₂	1.0E-05	Pu(OH) ₄
630	1.6E-07	Pu(OH) ₄	2.5E-06	Pu(OH) ₄	2.2E-06	Pu(OH) ₄
600	3.4E-08	Pu(OH) ₄	2.7E-07	Pu(OH) ₄	2.3E-07	Pu(OH) ₄
550	5.5E-09	Pu(OH) ₄	1.0E-08	Pu(OH) ₄	9.6E-09	Pu(OH) ₄
525	3.1E-09	Pu(OH) ₄	3.9E-09	Pu(OH) ₄	3.8E-09	Pu(OH) ₄
500	2.3E-09	Pu(OH) ₄	2.4E-09	Pu(OH) ₄	2.4E-09	Pu(OH) ₄
450	1.8E-09	Pu(OH) ₄	1.8E-09	Pu(OH) ₄	1.9E-09	Pu(OH) ₄
400	1.8E-09	Pu(OH) ₄	1.8E-09	Pu(OH) ₄	1.8E-09	Pu(OH) ₄
300	1.7E-09	Pu(OH) ₄	1.7E-09	Pu(OH) ₄	1.9E-09	Pu(OH) ₄
250	1.7E-09	Pu(OH) ₄	1.7E-09	Pu(OH) ₄	2.4E-09	Pu(OH) ₄
200	1.7E-09	Pu(OH) ₄	1.7E-09	Pu(OH) ₄	5.9E-09	Pu(OH) ₄

Table 9 Plutonium speciation in low fluoride pH 8 groundwater

Eh (mV)	Stable Solid	Solubility (M)	$\text{PuO}_2(\text{CO}_3)_2^-$ (%)	PuO_2^+ (%)	$\text{Pu}(\text{OH})_4(\text{aq})$ (%)	$\text{PuO}_2\text{OH}(\text{aq})$ (%)
700	$\text{PuO}_2(\text{OH})_2$	1.9E-07	93.43	6.46		
650	$\text{PuO}_2(\text{OH})_2$	2.6E-07	66.69	32.33		
630	$\text{Pu}(\text{OH})_4$	1.6E-07	47.63	50.29	1.10	
600	$\text{Pu}(\text{OH})_4$	3.4E-08	21.29	72.26	5.07	1.36
550	$\text{Pu}(\text{OH})_4$	5.5E-09	2.71	64.40	31.67	1.21
525	$\text{Pu}(\text{OH})_4$	3.1E-09		42.80	55.70	0.80
500	$\text{Pu}(\text{OH})_4$	2.3E-09		22.38	77.05	
450	$\text{Pu}(\text{OH})_4$	1.7E-09		3.98	95.92	
400	$\text{Pu}(\text{OH})_4$	1.7E-09			99.38	
350	$\text{Pu}(\text{OH})_4$	1.7E-09			99.90	
300	$\text{Pu}(\text{OH})_4$	1.7E-09			99.97	
250	$\text{Pu}(\text{OH})_4$	1.7E-09			99.98	
200	$\text{Pu}(\text{OH})_4$	1.7E-09			99.98	

Table 10 Plutonium speciation in high fluoride pH 8 groundwater

Eh (mV)	Stable Solid	Solubility (M)	PuO ₂ F ₄ ²⁻ (%)	PuO ₂ F ₃ ⁻ (%)	PuO ₂ (CO ₃) ₂ ²⁻ (%)	PuO ₂ ⁺ (%)	Pu(OH) ₄ (aq) (%)
700	PuO ₂ (OH) ₂	5.7E-06	46.29	44.47	8.54		
650	PuO ₂ (OH) ₂	5.8E-06	45.67	43.87	8.42	1.53	
630	Pu(OH) ₄	2.6E-06	44.82	43.06	8.27	3.26	
600	Pu(OH) ₄	2.7E-07	41.50	39.88	7.65	9.71	0.60
550	Pu(OH) ₄	1.0E-08	21.76	20.91	4.01	35.65	16.80
525	Pu(OH) ₄	3.9E-09	8.35	8.02	1.54	36.20	45.14
500	Pu(OH) ₄	2.4E-09	1.93	1.86		22.19	73.22
450	Pu(OH) ₄	1.8E-09				4.14	95.65
400	Pu(OH) ₄	1.8E-09					99.35
300	Pu(OH) ₄	1.7E-09					99.97
250	Pu(OH) ₄	1.7E-09					99.98
200	Pu(OH) ₄	1.7E-09					99.98

Table 12 Uranium solubility and controlling solid phase in two INEEL perched groundwater compositions

Redox (mV)	Low Fluoride, pH 8 Solubility(M)	Phase	High Fluoride, pH 6 Solubility (M)	Phase
800			1.0E-04	UO ₂ CO ₃
700			1.0E-04	
650	1.3 E-04	CaUO ₄	1.0E-04	UO ₂ CO ₃
600	1.3 E-04	CaUO ₄	1.0E-04	UO ₂ CO ₃
500	1.3 E-04	CaUO ₄	1.0E-04	UO ₂ CO ₃
400	1.3 E-04	CaUO ₄	1.0E-04	UO ₂ CO ₃
300	1.1 E-04	CaUO ₄	1.0E-04	UO ₂ CO ₃
200	1.1 E-04	CaUO ₄	1.1E-04	UO ₂ CO ₃
100	1.1 E-04	CaUO ₄	3.4 E-08	Uraninite
0	2.6 E-06	Uraninite	4.1 E-10	Uraninite
-100	1.5E-09	Uraninite	3.9 E-10	Uraninite
-200	3.9E-10	Uraninite	7.9 E-04	Uraninite
-300	4.5E-10	Uraninite		

Table 13 Uranium speciation in low-fluoride pH 8 groundwater

Eh (mV)	Stable Solid	Solubility (M)	UO ₂ (CO ₃) ₃ -4 (%)	UO ₂ (CO ₃) 2-2 (%)	(UO ₂) ₂ CO ₃ (OH) 3- (%)	U(OH) ₄ (aq) (%)
650	CaUO ₄	1.3E-04	77.02	21.07	1.60	
600	CaUO ₄	1.3E-04	77.02	21.07	1.60	
500	CaUO ₄	1.3E-04	77.02	21.07	1.60	
400	CaUO ₄	1.3E-04	76.99	21.10	1.60	
300	CaUO ₄	1.1E-04	74.88	23.09	1.68	
200	CaUO ₄	1.1E-04	74.91	23.07	1.67	
100	CaUO ₄	1.1E-04	74.75	23.22	1.68	
0		2.6E-06	75.63	24.00		26.70
-100		1.5E-09	55.48	17.59		99.89
-200		3.9E-10				100.00
-300		4.5E-10				

APPENDIX H

Silica Flour Partitioning and Ceramic Cell Studies

Silica Flour Partitioning Study

The objective for conducting this partitioning study was to determine if the practice of using silica flour as a packing media for field lysimeters is appropriate for the collection of samples to measure the concentration of strontium and several actinides in groundwater and perched water below the subsurface disposal area at INEEL.

Distribution coefficients were experimentally determined for ^{85}Sr , ^{233}U , ^{241}Am , and $^{239}\text{Pu(IV)}$ in silica flour suspension concentrations of approximately 50,000 mg/L, 100,000 mg/L and 200,000 mg/L in the modified perched water simulant (MPWS). A known activity of each radionuclide was added to replicate 10-ml silica flour suspensions in 14-ml polycarbonate centrifuge tubes and equilibrated by rotating for a period of 10 days. Blank tubes were set for each radionuclide in replicate to determine the extent of sorption to the centrifuge tubes. After equilibration, each tube was centrifuged at 5000 rpm for 30 minutes using a Sorval RCB2 refrigerated centrifuge maintained at $22^{\circ}\text{C} \pm 2^{\circ}\text{C}$. Aqueous phase activity was measured by liquid scintillation and sorbed phase activity was calculated from a comparison of the initial activity and the aqueous phase activity for each of the replicate tubes.

Results of these experiments for each radionuclide are summarized in the attached table and include calculated distribution coefficients for each silica flour suspension concentration. Also included in the table are background corrected initial solution activity (C_0) and aqueous phase activity (C_{aq}) in units of CPM/ml. Distribution coefficients for ^{85}Sr and ^{233}U were 0.493 ± 0.178 and 2.45 ± 0.815 L/Kg respectively. These relatively low Kds suggest that silica flour does not significantly attenuate the mobility of neither strontium nor uranium, indicating that the use of silica flour as packing material for lysimeter cells is acceptable. However, the use of silica flour packing to measure groundwater concentrations of americium and plutonium may be problematic. Distribution coefficients for ^{241}Am and $^{239}\text{Pu(IV)}$ were experimentally measured at 448 ± 42 and 1764 ± 778 L/Kd respectively, suggesting that significant attenuation of these actinides is possible. It is important to note that these measured Kds (i.e. for Am and Pu) are likely confounded due to the chemical behavior of these actinides in the MPWS. Specifically, pH- E_{H} phase diagrams and speciation models predict the predominant solid species for the Am-C-O-H system to be $\text{Am}(\text{CO}_3)$ and PuO_2 for the Pu-C-O-H system. Therefore, measured distribution coefficients for americium are likely a result of sorption onto the silica flour of the cationic species and precipitation of the carbonate solid. Speciation models such as EQ3/6 and Minteq are equilibrium models and most phase diagrams are developed based on thermodynamic equilibrium and even though the PuO_2 solid is predicted for the Pu-C-O-H system, it may not be present in significant amounts due to kinetic limitations. However, if the solid does not predominate, certainly hydrolyzed Pu species ($\text{Pu}(\text{OH})^{3+}$, $\text{Pu}(\text{OH})_2^{2+}$, $\text{Pu}(\text{OH})_3^{1+}$ and $\text{Pu}(\text{OH})_4$) do exist and the latter two species may

predominate at pH 8. Since each of the suspensions were incubated for a period of 10 days, it is possible that some PuO_2 solid was also formed. Therefore, the calculated K_d for plutonium is also confounded by the presence of hydrolyzed plutonium and the solid species.

This discussion to rationalize the behavior of americium and plutonium may be somewhat academic given the objective of the study. Regardless of the mechanism, be it sorption, precipitation of an Am species or formation of true Pu colloids, americium and plutonium are likely to be attenuated by silica flour. Attenuation by the silica flour would only be considered important if sorption of Am and Pu on the natural material surrounding the silica flour is less than sorption onto the silica flour.

Table H.1. Distribution Coefficients (Kd's) for Sr, Am, Pu (IV), and U with silica flour

Bkgd (CPM)		Co 364.9	Co 461	Co 425.40	Co 4.10	Co 570		
		Sr 7.5	Am 0.15	Pu (IV) 0.15	Pu (V) 0.15	U 0.15		
Aqueous Activity (CPM/mL)								
Tube	SS (g/mL)	Gross Cmq	Net Cmq	Net Co/Cmq	Kd (L/kg)	Cs (DPM/g)	Cs/Caq Kd	
Sr	1	0.051040	361.4	353.9	1.01	0.194	69	0.193766
	2	0.057900	354.5	347	1.03	0.518	180	0.517637
	3	0.098880	346.5	339	1.05	0.549	186	0.548921
	4	0.102900	349.6	342.1	1.04	0.435	149	0.434633
	5	0.199050	319	311.5	1.15	0.740	231	0.740274
	6	0.202300	330.7	323.2	1.11	0.523	169	0.523069
	7	0	362	354.5				
	8	0	367.7	360.2				
Am	1	0.049650	20.3	20.15	22.87	440.503	8876	440.5029
	2	0.051060	19.8	19.65	23.45	439.736	8641	439.7361
	3	0.102460	10.5	10.35	44.53	424.815	4397	424.8152
	4	0.099200	9.4	9.25	49.82	492.153	4552	492.1534
	5	0.200610	6.0	5.85	78.78	387.706	2268	387.7064
	6	0.199570	4.7	4.55	101.29	502.509	2286	502.509
	7	0	342.9	342.75				
	8	0	329.9	329.75				
Pu (IV)	1	0.049000	9.9	9.75	43.62	869.702	8480	869.7017
	2	0.050850	9.5	9.35	45.48	874.755	8179	874.7548
	3	0.101190	2.9	2.75	154.64	1518.296	4175	1518.296
	4	0.100730	1.9	1.75	243.00	2402.462	4204	2402.462
	5	0.206380	1.0	0.85	500.29	2419.295	2056	2419.295
	6	0.199630	1.0	0.85	500.29	2501.098	2126	2501.098
	7	0	415.1	414.95				
	8	0	390.5	390.35				
U	1	0.059900	521.1	520.95	1.09	1.551	808	1.551038
	2	0.055400	526.6	526.45	1.08	1.471	774	1.470925
	3	0.102270	446.3	446.15	1.28	2.700	1205	2.700111
	4	0.099460	461.0	460.85	1.24	2.367	1091	2.367128
	5	0.201950	338.5	338.35	1.68	3.381	1144	3.380663
	6	0.203190	343.7	343.55	1.66	3.235	1111	3.234682
	7	0	568.2	568.05				
	8	0	580.0	579.85				

Ceramic Cell Study

Experiments were conducted to determine if the ceramic cells used in suction lysimeters significantly attenuated americium, plutonium, neptunium, or uranium as groundwater permeated the cells during a collection event. A ground water simulant was prepared for each of the actinides at approximately 0.033 $\mu\text{Ci/ml}$ in the modified perched water (MPWS) and transferred to a 250-ml beaker. A ceramic cell was placed in each solution for a period of five hours. The solution flowed into the cell through the ceramic material under the influence of gravity at approximately 0.067 ml/min for the first 2 hours and at 0.041 ml/min for the next 3 hours. Duplicate MPWS samples were collected at time zero and analyzed to determine the solution phase activity of each actinide. A second and third set of samples was collected at 2 and 5 hours analyzed as follows. After the initial 2 hours of exposure all of the solution in each cell was removed and analyzed as follows. A sample of the solution in each beaker (outside the cell) was collected and analyzed by liquid scintillation, filtered at 12 nm and reanalyzed. In addition, a sample of the solution inside the cell was collected and analyzed.

Calculations were made to determine if the actinides were attenuated as the MPWS flowed into the ceramic cell. Results are summarized in Table H-1 and the detailed data are presented in Table H-2. After 2 hours of contact 99.9 %, 81.9 %, 51.9 % and 6.6 % of Am, Pu, Np, and U, respectively, were retained by the ceramic material. After 3 additional hours of contact, 99.9 % and 89.4 % of the initial concentration of Am and Pu was removed from solution. Both Np and U also showed attenuation, but to a lesser extent. Attenuation of Np dropped from 51.9 % to 32.8% and the loss from solution for U dropped from 6.6 % to 2.7%.

Table H-2. Results of Ceramic Cell Study

Time Hr.	Percent Loss to Ceramic Cell			
	Am	Pu(IV)	Np	U
2	99.9	81.8	51.9	6.6
5	99.9	89.4	32.8	2.7

Table H-3. Detailed Data for Ceramic Cell Study

Time Hr.	Sample Type	CPU/mL			
		Am	Pu	Np	U
0	UF	790.6	717.8	700.0	894.1
0	UF	801.2	734.6	700.5	888.7
0	UF _{AVG}	795.9	726.2	700.25	891.4
2	UF	529.0	670.7	661.0	869.0
2	F	489.5	660.7	666.7	861.0
2	Cell	0.6	132.1	336.6	832.2
2	% particle in solution in beaker	7.5%	1.5%	0%	0.9%
2	% loss from original solution	33.5%	7.6%	5.6%	2.5%
2	% loss to cell	99.9%	81.8%	51.9%	6.6%
5	UF	311.3	651.9	667.1	854.2
5	F	275.9	650.2	648.4	877.9
5	Cell	0.5	77.2	470.7	867.1
5	% particle in solution in beaker	11.4%	0.2%	2.8%	0%
5	% loss from original solution	63.8%	10.2%	4.7%	4.1%
5	% loss to cell	99.9%	89.4%	32.8%	2.7%